LBL-6199

MULTIPERIPHERAL RING DYNAMICS AND A DEFINITION OF THE COMPLETE TWISTED REGGEON LOOP

Philip Harrison Lucht

Lawrence Berkeley Laboratory
University of California
Berkeley, California 94720

Ph[illegible]hesis

November 1977

NOTICE

This report was prepared as an account of work sponsored by the United States Government. Neither the United States nor the United States Department of Energy, nor any of their employees, nor any of their contractors, subcontractors, or their employees, makes any warranty, express or implied, or assumes any legal liability or responsibility for the accuracy, completeness or usefulness of any information, apparatus, product or process disclosed, or represents that its use would not infringe privately owned rights.

DISTRIBUTION OF THIS DOCUMENT IS

MULTIPERIPHERAL RING DYNAMICS AND

A DEFINITION OF THE COMPLETE TWISTED REGGEON LOOP

TABLE OF CONTENTS

Abstract 1

(1) Introduction 2

(2) Multi-Regge Production Amplitudes 5

(3) The Vertex: Helicity and Parity Conditions 11

1. Helicity Conservation 11
2. Parity Invariance 12
3. Parity with Reggeons 13
4. Caveats, and the Vertex V 16

(4) The Unitarity Product 17

(5) Frames 21

1. The Vertex 21
2. The Rung 22
3. The Central Level Frames 24
4. Many Rungs 27

(6) The Helicity Pole Expansion 29

(7) Naturality Condition for the Kernel 34

(8) The Multiperipheral Chain and Phase Space 37

(9) The Diagonalization of Angular Momentum 41

(10) The Planar Bootstrap 44

1. Form of the Integral Equation 44
2. The Projected Helicity Pole Propagator P_λ 46
3. The Projected Kernel and Its Threshold Behavior 47
4. The Naturality Diagonalization 50
5. The Bootstrap Problem 54
6. Counting 55

(11) The Cylinder 56

1. Diagonalization of the Charge Conjugation 58
2. The Cylinder in Rapidity 59
3. The One-Twist Term of the Cylinder as a Helicity Pole Expansion 63
4. Angular Momentum Versus Helicity 65
5. Regge Cuts and Nonsense Zeros 66
6. The Complete Twisted Reggeon Loop 67
7. The Full Cylinder 70

(12) Fixed Poles, Nonsense Zeros, and the Helicity Contour Problem 71

Appendix A: Some Useful Functions 76

Appendix B: Toller M-Functions 80

Appendix C: The Helicity Pole Expansion Formula 84

Appendix D: Threshold Kinematics 87

Appendix E: The Cross-Channel Continuation 89

Appendix F: Reattachment of the End-Rungs 95

Acknowledgments 98

References 99

Figures 102

Table 124

ABSTRACT

The $t<0$ multiperipheral formalism of Ciafaloni, DeTar, Misheloff, Mueller, Muzinich and Yesian is reviewed, extended, and applied to the ordered S-matrix whose ring amplitudes comprise the zeroth level of the topological expansion. Toller M-function notation is used throughout. The bootstrap and cylinder problems are formulated in terms of a well-defined helicity pole propagator; a definition of the complete twisted Reggeon loop, which appears in the one-twist term of the cylinder, is given as a helicity pole expansion. Some consideration is given to the following subjects: diagonalization, naturality, threshold behavior, Regge cuts, and complex helicity.

(1) INTRODUCTION

During the year 1969-1970, after a period of vigorous activity in the field of multiperipheral dynamics, Ciafaloni, DeTar, Misheloff, Mueller, Muzinich and Yesian presented, in five heavily overlapping papers, the exact kinematic analysis of the multiperipheral model.[1-5] These papers were, in our opinion, extremely complicated in part due to the nature of the subject, and in part due to the fact that they incorporated mathematical ideas which were simultaneously being invented by the mathematicians, notably Mukunda.[6] Possibly, the relative obscurity of these papers has discouraged people from attempting an exact multiperipheral calculation, leading them instead to rely upon the approximate Mellin analysis and thereby to relinquish the capability of handling the true angular momentum which is central to Regge physics.

Since the invention of the S-matrix topological expansion in 1973-74 by Veneziano, there has been some renewed interest in multiperipheral calculations, in particular as they pertain to planar amplitudes. In a recent review,[7] Chew and Rosenzweig have partially reformulated these planar ideas in terms of the so-called Ordered S-Matrix, the connected parts of which are called ring functions. Although the concept of ordered ring amplitudes has not yet been convincingly extended to the baryonic sector, it seems likely that efforts now in progress will soon succeed.[8]

In this paper we have attempted to review, elaborate upon, and consolidate the ideas of Ciafaloni et al, and to adapt these ideas to the ordered S-matrix framework.

A reader familiar with the above-mentioned multiperipheral papers would find, upon comparison of our descriptions with theirs, many differences in presentation, some of which we now enumerate. First of all, we feel we have greatly simplified the group-theoretic aspect of the multiperipheral analysis by identifying, as the agent which performs the diagonalization of the multiperipheral equations, an almost trivial addition theorem involving the same Legendre Q_j-type functions which appear in the Froissart-Gribov projection of Regge theory. These Legendre functions are generalized in that they carry complex helicity indices whose role we continually stress. The reader is referred to Ref. 9 for an extensive discussion of this group theoretic business.

Another difference one will notice is our attempt to isolate and identify an object called the helicity pole propagator which connects cluster discontinuities along the multiperipheral chain. Strangely enough, this propagator owes its existence to a factorization condition which results from the same Legendre addition theorem mentioned above.

Obviously spin is an important concept in a multiperipheral analysis which purports to compute Regge trajectories. We have attempted to include spin in full generality (i.e., on external particles as well as internal poles) by making use of the Toller M-function formalism. To our knowledge, no one has written unitarity equations in this formalism which seems so well suited to the presentation of multiperipheral kinematics.

Interlaced with the discussion on the following pages one will find a sort of running commentary on parity and naturality, leading to a naturality diagonalization of the planar bootstrap which is,

we feel, an improvement on the original discussion by Ciafaloni and Yesian.

Generally speaking, the exact kinematic analysis allows one to think about things which simply do not exist in the rapidity framework which more or less ignores helicity. We have extracted the threshold behavior of the ring functions and have made a start at examining the nonsense zeros which are presumed to remove Regge cuts.

In Section (5) we describe in a rather different manner than that of Refs. 2 and 4 the construction of the standard frames of the multiperipheral ladder. By continuing the ladder kinematics to the center-of-mass cross channel, we show in Appendix (E) how the peculiar boost parameters which link the standard frames are the continuations of variables familiar from center-of-mass kinematics.

The "planar" bootstrap and cylinder problems are both set up — the cylinder in more detail because it lacks the counting problem — but no detailed calculation is attempted because we are stymied by a problem involving the correct method of shifting the helicity contour. We have isolated this problem in the last section of the paper; it must be solved before the machinery described herein can be put to work.

Nevertheless, we do obtain an exact formal expression for the complete twisted Reggeon loop k(t) which controls the cylinder shifts of the planar trajectories in the phenomenology of Chew and Rosenzweig.[10]

For a detailed outline of the paper we refer to the Table of Contents preceding this Introduction. In general, the first eight sections describe the multiperipheral construction, Section (9) gives the angular momentum diagonalization, and Sections (10) and (11) apply the analysis to the bootstrap and cylinder problems.

(2) MULTI-REGGE PRODUCTION AMPLITUDES

To motivate the specific form we use for the multi-particle production amplitudes, we appeal to the notion of a particle pole in the S-matrix. Figure 1 shows a particle pole term known to be present in the ℓ-point function (repeated indices are implicitly summed),

$$M_{m_1 m_2 m_3 m_4 m_5 m_6}(a_1, a_2, a_3, a_4, a_5, a_6) \doteq$$
$$M_{m_7 m_3 m_4 m_5}(a_7, a_3, a_4, a_5) \left[\frac{c\, D^{s_7}_{m_7 m_7'}(g)}{s_7 - m_7^2 + i\epsilon} \right] M_{m_1 m_2 m_7' m_6}(a_1, a_2, a_7', a_6) \; . \tag{2.1}$$

This pole has a residue which factorizes into two pieces, each piece being a 4-point function normalized in the same way as the original 6-point function.

Each × in Fig. 1 marks a particular standard rest frame for the particle on whose line the × appears. (When the pole is reggeized below, some ×'s must denote spacelike rest frames.) The notation is approximately that of Toller:[11] the s_i are the spins of various particles, m_i are helicities (component of spin along the z-axis in the standard frame marked by an ×). The same symbols s_i and m_i are also used to denote certain Mandelstam invariants and masses of particles; the usage should be clear from the context. The meaning of a dot *under* a helicity index is explained in Appendix (B).

The a_i appearing in Eq. (2.1) and Fig. 1 are, for each particle, the parameters of a (possibly complex) Lorentz transformation which connects the particle standard rest frame to an arbitrary "lab" frame as indicated in the figure. The variable g appearing in $D^{s_7}_{m_7 m_7'}(g)$ denotes the rotation $g = a_7^{-1} a_7'$; the standard D-function [see Appendix (A)] is generated by covariation from the M-function on

the left according to the simple rule given in Eq. (8.3). s_7 is the spin of the particle pole, and m_7, m_7' are the helicities of that particle in two different reference frames.

It is perhaps worth noting that, although they carry spin and helicity indices, the M-functions appearing in Eq. (2.1) are Lorentz scalars, unlike the momentum space M-functions of Stapp[12] and Taylor.[13] Secondly, we have been careful to properly order the particles consistently around the connected parts so that all our equations apply equally well to the ordered amplitudes (ring functions) in the ordered S-matrix framework associated with the topological expansion.[7]

The factor $(s_7 - m_7^2 + i\epsilon)^{-1}$ in (2.1) is of course the actual pole; the numerical constant c is discussed below in Section (4), and can be arranged to equal unity.

Equation (2.1) is, for the pole term, an exact statement. We now assume that this particle pole is in fact one of many poles which occur on a Regge trajectory α_7. The contribution of α_7 to the 6-point function shown in Fig. 1 should be given by the above expression with s_7 continued to α_7 and with the various group arguments and invariants continued so that the equation is in a useful Regge region. Accounting for signature, the usual Regge machinery* may be implemented to give

---

*Regge theory for n-point functions with $n > 4$ is much more complicated than we make it sound.[37,38] Rigorously,[38] both the physical and ordered S-matrix n-point functions must be decomposed into a sum of "spectral components" by means of an $(n-3)$-variable dispersion relation (Bargmann-Weil). Each spectral term contains only Steinmann-allowed multiple discontinuities, a fact which implies the existence of a Lehmann ellipse of convergence for each z_i variable in an appropriate physical cross channel (hexagraph). As a result, the infinite angular momentum and helicity sums are convergent at least somewhere, and this allows the Sommerfeld-Watson continuations to be defined. So, rigorously one does a Regge analysis on each spectral component and then adds the results, or one sticks with a single component and diagonalizes unitarity onto the spectral components. We feel that the form of our results will be the same in either the rigorous Regge theory or Ref. 38, or the naive Regge theory presented in Section (2).

the following result (see Fig. 2):

$$M^{s_1 \cdots s_6}_{m_1 \cdots m_6} \doteq M^{\alpha_7 s_3 s_4 s_5}_{m_7 m_3 m_4 m_5} \; [\text{factor}]^{\alpha_7 \tau_7}_{m_7 m_7} \; M^{s_1 s_2 \alpha_7 s_6}_{m_1 m_2 m_7 m_6} \quad , \tag{2.2}$$

where we have suppressed the a_i arguments, and where

$$[\text{factor}]^{\alpha\tau}_{mm'} = e^{-im\phi} \; e^{-im'\phi'} \; c\alpha'\pi \times \left\{ \frac{d^{\alpha}_{m,-m'}(-z) + \tau(-1)^{m+\epsilon} \; d^{\alpha}_{mm'}(z)}{2 \sin\pi(\alpha + m)} \right\} \quad . \tag{2.3}$$

The variables $g = (\phi, z = \cos\theta, \phi')$ which appear in Fig. 1 are now O(2,1) variables $(\phi, z = \cosh\xi, \phi')$. The signature of Reggeon α_7 is τ_7 (a spin-½ particle has positive signature), and $\epsilon_7 = 0$ or ½ depending on whether α_7 is a boson or fermion trajectory. Using Eq. (A.8) one may show by taking $\alpha_7 \to s_7$ that the Regge form (2.2) duplicates the particle pole term of Eq. (2.1).

The final step in obtaining the Regge form we shall use is to perform a "Mandelstam trick" operation[14] which causes the first-kind functions in $[\text{factor}]_{mm'}$ to be replaced by second-kind functions which have simpler asymptotic behavior. Performing this operation we find

$$[\text{factor}]^{\alpha\tau}_{mm'} = \gamma \, \xi \, E^{-\alpha-1}_{mm'}(g) \quad , \tag{2.4}$$

where

$$E^{-\alpha-1}_{mm'}(g) = e^{-im\phi} \; e^{-\alpha-1}_{mm'}(z) \; e^{-im'\phi'} \quad , \tag{2.5}$$

$$\gamma = -c\alpha' \tan\pi(\alpha - \epsilon) \quad , \tag{2.6}$$

and

$$\xi = \left[\frac{e^{-i\pi(\alpha - \epsilon)} + \tau}{2 \sin\pi(\alpha - \epsilon)} \right] . \tag{2.7}$$

The function $e^{-\alpha-1}_{mm'}(z)$, defined in Eq. (A.10), has the expected Regge behavior z^{α} for large z, ξ is a standard signature factor, and γ contains the leftover factors. In particular, γ contains α' and therefore has dimensions E^{-2}. In Eq. (2.1) these dimensions are generated by the pole itself. Realizing that the n-point Toller M-function has dimensions E^{4-n}, one may verify the dimensional correctness of (2.1) or (2.2).

The Regge residues appearing in (2.2) are three-particle/one-Reggeon amplitudes normalized in the correct way so as to become physical four-particle amplitudes when the Reggeon is taken to the appropriate value of mass and spin (and signature, if M is not an ordered amplitude). Since the physical helicity amplitudes must vanish when the helicity is out of range (has a nonsense value), the residues must contain factors to knock out the unphysical poles, since this ghost-killing function is not being performed by $[\text{factor}]_{mm'}$. For example, one might take*

$$M^{\alpha_7 s_3 s_4 s_5}_{m_7 m_3 m_4 m_5} = \quad \text{[diagram: 5, 7, 4, 3]} \quad = \frac{M'}{[\Gamma(\alpha_7+1+m_7)\Gamma(\alpha_7+1-m_7)]^{\frac{1}{2}}} \; . \tag{2.8}$$

So far we have considered the Reggeization of a single-pole term in unitarity. Had we started with the appropriate multiple pole term, we could have obtained a multiple Regge residue or four-Reggeon amplitude which, were all Reggeons continued to particle points, would be normalized so as to yield a physical four-particle helicity amplitude. We feel that this is a useful way to normalize Regge

*In the sense-nonsense region, additional square-root zeros are provided by the d-functions. See, for example, Fig. 8e of Ref. 9.

residues, and is ultimately necessary if one attempts a complete bootstrap of, say, the triple-Regge vertex. We shall mention this later in Section (10) (but will not attempt such a bootstrap).

Although three-particle scattering amplitudes have no place in a stable-particle S-matrix theory, unstable particles may be called upon to give meaning to the following equations. Figure 3 shows a particle pole term in the 4-point function. In analogy to (2.1) we write

$$M^{s_1 s_2 s_3 s_4}_{m_1 m_2 m_3 m_4}(a_1, a_2, a_3, a_4) \doteq$$

$$M^{s_5 s_3 s_4}_{m_5 m_3 m_4}(a_5, a_3, a_4) \left[\frac{c \Pi^{s_5}_{m_5 m_5'}(g)}{s_5 - m_5^2 + i\epsilon} \right] M^{s_1 s_2 s_5}_{m_1 m_2 m_5'}(a_1, a_2, a_5') \quad . \tag{2.9}$$

Reggeization in the same way as before yields this expression for the Regge pole term shown in Fig. 4:

$$M^{s_1 \cdots s_4}_{m_1 \cdots m_4} \doteq M^{\alpha_5 s_3 s_4}_{m_5 m_3 m_4} \cdot \left[\gamma_5 \xi_5 \, E^{-\alpha_5 - 1}_{m_5 m_5'}(g) \right] M^{s_1 s_2 \alpha_5}_{m_1 m_2 m_5'} \quad . \tag{2.10}$$

Again, the Regge residues (pieces of the factorizing residue of the Regge pole in the Froissart-Gribov projection) appearing in Eq. (2.10) are normalized so that, as $\alpha_5 \to s_5$, these two-particle/one-Reggeon amplitudes approach the standard three-particle Toller M-functions appearing in Eq. (2.9). The helicity nonsense-zero structure of these standardized "Regge couplings" is presumably similar to (2.8) above. Notice from the rule E^{4-n} that these Regge couplings have the dimensions of energy.

By reggeizing a double pole unitarity term, one may obtain the following Regge contribution for the two-to-three production amplitude shown in Fig. 5:

$$M^{s_1 \cdots s_5}_{m_1 \cdots m_5} \doteq M^{s_2 s_3 \alpha_6}_{m_2 m_3 m_6} \left[\gamma_6 \xi_6 \, E^{-\alpha_6 - 1}_{m_6 m_6'} (g_6) \right]$$

$$\times \; M^{\alpha_6 s_4 \alpha_7}_{m_6' m_4 m_7} \left[\gamma_7 \xi_7 \, E^{-\alpha_7 - 1}_{m_7 m_7'} (g_7) \right] M^{\alpha_7 s_5 s_1}_{m_7' m_5 m_1} \quad . \tag{2.11}$$

The object $M^{\alpha_6 s_4 \alpha_7}$ is the two-Reggeon/one-particle amplitude which continues to the Toller 3-point function when $\alpha_6 \to s_6$ and $\alpha_7 \to s_7$. Again, this "double Regge vertex" has dimensions of energy, as does the triple Regge vertex which we have not shown. These vertices differ considerably from the phenomenological Regge couplings (dimensionless) and triple-Regge couplings (GeV^{-2}).

The form of the general multi-Regge production amplitude should be clear from Eq. (2.11). Each Reggeon gets a bracketed "propagator" factor with linking helicity sums on both sides. All vertices are standard Toller 3-point functions continued in the appropriate way.

We conclude this section by observing that, in the ordered S-matrix framework where the M-functions in (2.11) are replaced by ordered ring amplitudes, the multi-Regge-pole expansion should be, in the peripheral region, a very good approximation since there are (presumably) no Regge cuts in the ring functions. The theoretical accuracy of (2.11), when summed on α_6 and α_7, is thus limited only by peripherality and the convergence rate of the Regge asymptotic series, i.e., duality.

(3) THE VERTEX: HELICITY AND PARITY CONDITIONS

We have been writing the triple vertex in the form $M_{m_1m_2m_3}(a_1,a_2,a_3)$ to stress the fact that the vertex is like any other n-point Toller M-function. As we now show, however, this notation is extremely redundant. Using the freedom allowed by the Toller invariance condition [see Eq. (B.3)], one can choose to superpose the external "lab" reference frame — with respect to which the various a_i are defined, as in Fig. 1 — onto one of the standard reference frames associated with the vertex. Since the vertex standard frames are connected by certain z-boosts σ_1, σ_2, and q which are functions only of the invariants entering the vertex [see Eq. (5.1)], one may conclude that $M_{m_1m_2m_3}(a_1,a_2,a_3)$ is itself a function only of these invariants. This situation is illustrated in Fig. 6a where we have placed the reference frame onto the standard frame of particle 1 to get $M_{m_1m_2m_3}(e,q^{-1},\sigma_1^{-1})$, where e is the identity transformation.

1. Helicity Conservation

Consider now this series of operations in which ϕ represents the z rotation $R_z(\phi)$:

$$
\begin{aligned}
&M_{m_1m_2m_3}(a_1,a_2,a_3)\\
&\quad = M_{m_1m_2m_3}(e,\ q^{-1},\ \sigma_1^{-1})\\
&\quad = M_{m_1m_2m_3}(\phi e,\ \phi q^{-1},\ \phi\sigma_1^{-1})\\
&\quad = M_{m_1m_2m_3}(e\phi,\ q^{-1}\phi,\ \sigma_1^{-1}\phi)\\
&\quad = e^{-im_1\phi}\ e^{-im_2\phi}\ e^{-im_3\phi}\ M_{m_1m_2m_3}(e,\ q^{-1},\ \sigma_1^{-1})\\
&\quad = e^{-i\phi(m_1+m_2+m_3)}\ M_{m_1m_2m_3}(a_1,a_2,a_3)\quad . \qquad (3.1)
\end{aligned}
$$

In line 1 the reference frame is identified with the rest frame of particle 1, as already noted. In line 2 the ϕ's are made to appear via the invariance condition of Eq. (B.2). In line 3 these rotations are commuted through the z boosts $q^{-1} = B_z(-q)$ and σ_1^{-1}, and then in line 4 the ϕ's are separately covariated to the right according to Eq. (B.3). Comparison of the last line with the first then shows that

$$m_1 + m_2 + m_3 = 0 \quad , \tag{3.2}$$

i.e., helicity is conserved at the vertex.*

One does not find such a condition for the higher n-point functions because the rotation ϕ does not commute through all the a_i no matter how they are chosen.

2. Parity Invariance

If parity is an invariance of the theory, we may use an argument similar to that of Section 3.1 to state parity invariance in terms of the vertex. Since the parity operation, which Toller[15] calls s , is an element of the little group H_+ of the 4-vector $(*,0,0,0)$, the rotational covariance conditions [shown in Eq. (B.3)] may be extended to read, e.g.,

$$M_{m_1m_2m_3}(a_1,a_2,a_3;s) = M_{m_1m_2m_3}; D^{s_3\Pi_3}_{m_3;m_3}(s) = \Pi_3 M_{m_1m_2m_3}(a_1,a_2,a_3), \tag{3.3}$$

where Π_3 is the intrinsic parity of particle 3. Since the operation s fails to commute through the z boosts [see Eq. (7.6)], it is more convenient to use Toller's parity operator s' defined by

$$s' = R_y(\pi)s \tag{3.4}$$

*But see Section 3.4 for qualifications on this and subsequent equations of this section.

for which the covariance condition on particle 2 reads, according to Eqs. (3.3) and (A.8),

$$M_{m_1 m_2 m_3}(a_1,a_2,a_3 s') = \left[\Pi_3 (-1)^{s_3 - m_3}\right] M_{m_1 m_2, -m_3}(a_1,a_2,a_3) . \quad (3.5)$$

Operator s' brings out the intrinsic parity and negates the helicity of the affected particle. Since s' *does* commute with the z boosts, one may repeat the argument (3.1) to find this vertex parity condition:

$$M_{m_1 m_2 m_3}(a_1,a_2,a_3) = M_{-m_1,-m_2,-m_3}(a_1,a_2,a_3) \prod_{i=1}^{3}\left(\Pi_i (-1)^{s_i - m_i}\right) . \quad (3.6)$$

As a corollary to Eq. (3.6) one has either

$$\prod_{i=1}^{3}\left(\Pi_i (-1)^{s_i}\right) = 1 , \qquad \text{or} \qquad M^{s_1 s_2 s_3}_{000}(a_1,a_2,a_3) = 0 . \quad (3.7)$$

For example, if $s_1 = s_2 = 0$ then all three helicities must vanish and *one concludes from the above that the vertex vanishes if* $\Pi_1\Pi_2\Pi_3 \neq (-1)^{s_3}$, as one would expect from a more conventional angular momentum argument.

3. Parity with Reggeons

Another convenient property of the parity operator s' is that s', unlike s, belongs also to the little group H_- of the spacelike rest vector $(0,0,0,*)$, as does $R_z(\phi)$. Therefore, if one or more of the particles at a vertex is replaced by a Reggeon — which may be *spacelike so that* H_- *is the appropriate little group — one shall find* that the helicity and parity conditions still exist. The helicity conservation condition of Eq. (3.2) is unchanged, except as noted below. The Reggeon parity covariance condition is

$$M^{s_1 s_2 \alpha_3}_{m_1 m_2 m_3}(a_1,a_2,a_3 s') = \left[\sigma_3 e^{-i\pi m_3}\right] M^{s_1 s_2 \alpha_3}_{m_1 m_2, -m_3}(a_1,a_2,a_3) \quad (3.8)$$

where

$$\sigma_i = \Pi_i \; e^{+i\pi s_i} \tag{3.9}$$

with s_i a physical point on α_i, and Π_i the intrinsic parity of that physical point.

The quantity σ_i appearing in (3.9) is what we shall call the Reggeon naturality, and is a constant along an ordered Regge trajectory. Another way to say this is that the exchange degenerate partners which together compose an ordered (planar) Regge trajectory have the same naturality σ_i, even though the intrinsic parity Π_i and spin parity $(-1)^{s_i-\epsilon_i}$ alternate at the physical points. One sees that, as $\alpha_3 \to s_3$, Eq. (3.8) reproduces (3.5).

For fermions, the physical point parities Π_i and naturalities σ_i are, according to Eq. (3.9), out of phase by 90°. In the M-function formalism one can prove[16] from crossing and TCP that

$$\Pi_i \Pi_{\bar{i}} = (-1)^{2s_i} \quad . \tag{3.10}$$

A purist, allowing for the possible existence of self-conjugate fermions, would have to accept imaginary parities for those fermions. As emphasized by Stapp[17] the most reasonable convention is to give all fermions imaginary intrinsic parities. (Toller too uses this convention.[11]) In this case, naturality $\sigma = \pm 1$ for fermions as well as bosons.

We leave to the reader a comparison of Eq. (3.9) with the more common definition of naturality

$$\eta_i = P_i(-1)^{s_i-\epsilon_i} \tag{3.11}$$

where intrinsic parity $P_i = \pm 1$ for both bosons and fermions, and $\epsilon_i = 0$ for bosons and one-half for fermions. Certainly for bosons, $\eta_i = \sigma_i$.

Once Eq. (3.8) has been established, the argument of Eq. (3.1) may be applied to give a parity condition for the single Regge vertex shown in Fig. 6b:

$$M^{s_1 s_2 \alpha_3}_{m_1 m_2 m_3}(a_1,a_2,a_3) = M^{s_1\ s_2\ \alpha_3}_{-m_1,-m_2,-m_3}(a_1,a_2,a_3) \times \left[\Pi_1(-1)^{s_1-m_1}\right]\left[\Pi_2(-1)^{s_2-m_2}\right]\left[\sigma_3\, e^{-i\pi m_3}\right] . \tag{3.12}$$

This says, e.g., that two pions cannot couple to an η trajectory, even though such a coupling is allowed by G-parity.

For the two-Reggon/one-particle vertex a condition similar to Eq. (3.12) results (see Fig. 6c):

$$M^{\alpha_1\alpha_2 s_3}_{m_1 m_2 m_3}(a_1,a_2,a_3) = \left[\sigma_1\, e^{-i\pi m_1}\right]\left[\sigma_2\, e^{-i\pi m_2}\right]\left[\Pi_3(-1)^{s_3-m_3}\right] \times M^{\alpha_1\ \alpha_2\ s_3}_{-m_1-m_2-m_3}(a_1,a_2,a_3) . \tag{3.13}$$

The triple-Regge vertex is more complicated because one cannot always link the three standard frames with z-boosts. In particular, when $\Delta(t_1,t_2,t_3)$ is negative, the three frames are connected by y-rotations[18] (see Fig. 16). Conveniently, the parity operator s' also commutes with y-rotations; the parity argument then goes through to yield

$$M^{\alpha_1\alpha_2\alpha_3}_{m_1 m_2 m_3}(a_1,a_2,a_3) = \left[\sigma_1\, e^{-i\pi m_1}\right]\left[\sigma_2\, e^{-i\pi m_2}\right]\left[\sigma_3\, e^{-i\pi m_3}\right] \times M^{\alpha_1\ \alpha_2\ \alpha_3}_{-m_1-m_2-m_3}(a_1,a_2,a_3) , \tag{3.14}$$

so that negating the Reggeon helicities is equivalent, for $\Delta > 0$, to multiplying by the product of the Reggeon naturalities, since the helicities cancel by Eq. (3.2). However, since y- and z-rotations

do not commute, the helicity condition of Eq. (3.2) is broken for the spacelike triple-Regge vertex, $\Delta < 0$.

4. Caveats, and the Vertex V

We must now add two important qualifications to the preceding equations of this section. As written, they apply to Toller 3-point M-functions with all particles and Reggeons being in the initial "state" and with all spinor indices of the undotted upper type (see Appendix B).

To be consistent, certain particles and Reggeons must be put into the final "state" of each vertex. We choose to let this convention be determined by the direction of the arrows in, say, Fig. 15. Whenever a particle or Reggeon is in the final state, the relevant bracketed factor in Eqs. (3.5) → (3.8) and (3.12) → (3.14) must be complex-conjugated.

Secondly, we must face the fact that inevitably some of the helicity indices we are dealing with are of the undotted lower type. These indices, marked underneath by dots as in Eq. (2.1), are necessarily lower in order to preserve the spinor covariance of the equations. When an amplitude with a lower undotted helicity index is covariated as in Eq. (B.3), the D function must be replaced by D^*. The net result is that helicities in Eq. (3.2) corresponding to lowered indices will enter with minus signs. However, the parity conditions are the same, regardless of whether indices are upper or lower.

The vertices in which we are mainly interested have the form of the central vertex of Eq. (2.11). In the notation of Appendix B and with the conventions made above (and, as always, maintaining the cyclic ring ordering) we write this vertex as

$$M^{\alpha_6 s_4 \alpha_7}_{m_6' m_4 m_7} = \tilde{M}^{m_7 + m_4}_{m_6'}(a_7; a_6', a_4) \equiv V^{\alpha_6 s_4 \alpha_7}_{m_6' m_4 m_7} \quad . \tag{3.15}$$

The helicity and parity conditions for this vertex are then found from Eqs. (3.2) and (3.13) and the above conventions:

$$m_7 - m_6' + m_4 = 0 \quad , \tag{3.16}$$

$$V^{\alpha_6 s_4 \alpha_7}_{m_6' m_4 m_7} = \left[\sigma_6 \, e^{-i\pi m_6'}\right]^* \left[\Pi_4 (-1)^{s_4 - m_4}\right]^* \left[\sigma_7 \, e^{-i\pi m_7}\right] V^{\alpha_6 s_4 \alpha_7}_{-m_6' -m_4 -m_7} . \tag{3.17}$$

Once again it should be stressed that this vertex V has the standard normalization of a Toller M-function, has dimensions of energy, and (in addition to the labels shown) is a function only of the invariants entering the vertex.

(4) THE UNITARITY PRODUCT

Even when all particles carry spin,[13] the unitarity equations for the momentum-space M-functions are completely characterized by the usual bubble diagrams[19] together with a set of "Olive's rules,"

$$\text{internal line} = -2\pi i c \, \delta^+(p^2 - z^2)$$

$$\text{independent loop} = d^4p/(-2\pi i c f)$$

$$\text{pole} = c/(s - m^2 + i\epsilon) \quad .$$

One needs also the relation between the M-function bubbles and the raw connected parts:

$$(S_c) = (-2\pi i c f) \, \delta^4(\text{ext}) \, M^{(+)}$$

$$(S_c^+) = (-2\pi i c f)^* \, \delta^4(\text{ext}) \, M^{(-)}$$

In these relations, the constant f determines the normalization of the single-particle states,

$$\langle p,m'|p',m'\rangle = 2Ef\delta^3(p-p')\delta_{m,m'} \quad ,$$

and c gives the pole residue, as in Eq. (2.1). Authors naturally differ in their conventions, e.g.,

ELOP:[19]	$c = 1$	$f = (2\pi)^3$
Stapp:[12]	$c = i$	$f = (2\pi)^3$
Taylor:[13]	$c = -1$	$f = 1/2$.

We favor the convention of ELOP, but shall always give results in terms of c and f.

Once a unitarity equation is expressed in terms of the Stapp-Taylor M-functions $M_{m_1\ldots}(p_1,p_2\ldots)$, it may be converted to Toller M-functions via the inverse of Eq. (B.4). Details of this conversion process with attention paid to the spinor indices will be given elsewhere.[16]

Before tackling the general multiperipheral unitarity product, we first illustrate the form unitarity takes in terms of the Toller M-functions by writing down elastic unitarity as sketched in Fig. 7. The formula is

$$\begin{aligned}\frac{1}{2i}\,\mathrm{disc}\;\; & M_{m_1m_2\dot{m}_3\dot{m}_4}(a_1,a_2,a_3,a_4) \\ &= -cf\pi\int dQ_2\,[M_{m_3m_4m_5m_6}(a_3,a_4,a_5,a_6)]^* \\ &\quad\times\; d^{s_5}_{m_5m_5'}(X_5)\;\; d^{s_6}_{m_6m_6'}(X_6)\;\; M_{m_1m_2m_5'm_6'}(a_1,a_2,a_5',a_6') \quad ,\end{aligned} \tag{4.1}$$

where

$$dQ_2 = \delta^4(p_1+p_2-p_5-p_6)\;\frac{d^4p_5\;\delta^+(p_5^2-m_5^2)}{f}\;\;\frac{d^4p_6\;\delta^+(p_6^2-m_6^2)}{f} \quad .$$

As usual, we are maintaining the ring function ordering conventions.[7] The dots over the m_a and m_b indices on the left side of Eq. (4.1) are necessary to maintain the spinor covariance. The rotation functions arise in the same way as the $D(g)$ in Eq. (2.1), namely, from the Toller covariance condition shown in Eq. (B.3). We are anticipating a system of standard reference frames to be reviewed shortly in which it will turn out that these rotations will be pure y-rotations, χ_i, whose presence was first noticed by Misheloff.[4] At $t = 0$ the rotations all vanish, but for $t < 0$ they do not vanish and are determined up to a sign by the peripheral invariants t_i [see Section (5)].

From Eq. (4.1) it should be clear how the general n-body unitarity product appears. Each intermediate particle gets a Misheloff rotation, and the helicity indices are summed over systematically. The n-body phase space is

$$dQ_n = \delta^4(\text{ext}) \prod_{i=1}^{n} \left(\frac{d^4p_i \; \delta^+(p_i^2 - m_i^2)}{f} \right) \tag{4.2}$$

where, as in Eq. (B.1), $p_i = L(a_i)\tilde{p}_i$. Sometimes it is useful to visualize each produced particle as a cluster of variable mass and spin, in which case Eq. (4.2) can be adjusted by replacing $\delta^+(p_i^2 - m_i^2) \to \delta^+(p_i^2 - s_i)ds_i$ and adding spin sums Σ_{s_i}.

We are now ready to insert into the general n-body unitarity product a model for the production amplitudes, namely, the multi-Regge production amplitudes developed in Section 2, which we now write as

$$\begin{aligned} M_{m_a p_o p_1 p_2 \cdots p_n m_b}^{s_a s_o s_1 s_2 \cdots s_n s_b} &= V_{m_a p_o m_1}^{s_a s_o \alpha_1} \cdot \left[\gamma_1 \xi_1 \, E_{m_1 r_1}^{-\alpha_1 - 1}(g_1) \right] \\ &\cdot V_{r_1 p_1 m_2}^{\alpha_1 s_1 \alpha_2} \cdot \left[\gamma_2 \xi_2 \, E_{m_2 r_2}^{-\alpha_2 - 1}(g_2) \right] \cdots \cdot V_{r_n p_n m_b}^{\alpha_n s_n s_b} . \end{aligned} \tag{4.3}$$

This amplitude is shown in Fig. 8; the V's are the standard vertices described in Section (3), and we are now using m,r,p as helicity labels.

It is perhaps useful to observe that the bracketed factors in Eq. (4.3) have three sources of phase when α is real:

i) the azimuthal phase $\exp[-i(m_i\phi_i + r_i\phi_i')]$ from $E(g_i)$;

ii) the phase $(\pm i)^{m_i - n_i}$ from the e-functions at $z > 1$ arising from the kinematic spin cuts (half angle factors) in the amplitude;

iii) the Regge phase of the signature factor ξ_i.

Of these three phases, only the Regge phase will be incorporated into the helicity pole propagator to be defined below.

Suppressing the Toller a_i arguments, we now state the n-body multiperipheral unitarity product as

$$\frac{1}{2i}\,\mathrm{disc}\; M^{s_b s_a s_a' s_b'}_{m_b p_a p_a' m_b'} = -c f \pi \int dQ_n \cdot \left[M^{s_b' s_n \cdots s_1 s_0 s_a'}_{m_b' p_n' \cdots p_1' p_0' m_a'}\right]^* \times \prod_{i=1}^{n} \left(d^{s_i}_{p_i' p_i}(\chi_i)\right) \left[M^{s_a s_0 s_1 \cdots s_n s_b}_{m_a p_0 p_1 \cdots p_n m_b}\right] , \quad (4.4)$$

where each M-function on the right has a form as in Eq. (4.3), and where dQ_n is given by Eq. (4.2). In (4.4) the only variables *not* summed over are those with subscripts a and b. The spins and helicities appearing in (4.4) are labeled in Fig. 9 which shows the n-body unitarity product with the multi-Regge amplitudes inserted. Our notational plan is always to use primed variables for the upper side of the ladder and unprimed for the lower side. The reader is again cautioned about our multiple usage of the symbols s_i (spin, *invariants*), p_i (*momentum*, helicity), and m_i (helicity, mass).

The next step in the program is to actually insert the production amplitudes of Eq. (4.3) into (4.4) and make some sense out of the resultant expression. We wish to show that Regge poles in the upper and lower amplitudes are converted into helicity poles in the central kinematic level, and that it is these helicity poles which determine the Reggeon loop which lies at the heart of all bootstrap and cylinder calculations. Before we do this, however, we must make some comments about the frames in the various kinematic levels.

(5) FRAMES

The study of the reference frames associated with the multiperipheral ladder is at best a tedious and unpleasant business. We propose only to outline the development of these frames and to provide a few interpretations where useful. The ends of the multiperipheral ladder, where the frames are slightly different, will be completely ignored. Usually in multiperipheral analysis the end-rungs (or at least one end-rung) are amputated, the physics is done, and then later the end-rungs are reattached (see Appendix F); Regge physics *does not* require the end-rungs and this is our justification for ignoring them.

In the description which follows we have for no particular reason adopted the notation of Ciafaloni, DeTar and Misheloff[3] rather than that of Mueller and Muzinich.[2]

1. The Vertex

The frame analysis begins with the simple vertex shown in Fig. 10, where two spacelike momenta k_1 and k_2 meet a future timelike momentum p_1. Frame c is a rest frame of p_1 in which the 3-momentum

$\vec{k}_1 = \vec{k}_2$ points in the positive z direction. Obviously, frame c is only defined up to a z-rotation, a fact we shall make use of later. Frame b (d) is obtained from frame c by a z-boost v_1 (σ_2^{-1}) which brings k_1 (k_2) to spacelike rest [$k_i = (0,0,0,\sqrt{-t_i})$]. Clearly, frames b and d are linked by the z-boost $q_1 = v_1 + \sigma_2$. From momentum conservation it is easy to compute these boosts in terms of the invariants t_1, t_2 and s_1:

$$
\begin{aligned}
\mathrm{sh}v_1 &= (s_1 + t_1 - t_2) / 2\sqrt{s_1}\,\sqrt{-t_1} \quad , \\
\mathrm{sh}\sigma_2 &= (s_1 - t_1 + t_2) / 2\sqrt{s_1}\,\sqrt{-t_2} \quad , \qquad (5.1) \\
\mathrm{ch}q_1 &= (s_1 - t_1 - t_2) / 2\sqrt{-t_1}\,\sqrt{-t_2} \quad .
\end{aligned}
$$

The variable q_1 may be interpreted as sensing the mass^2 s_1 flowing up the cluster p_1. By computing $(k_2 - k_1)$ in frame b, one finds that q_1 is positive because p_1 is *future* timelike.

The frames b,c,d defined above are the usual BCP frames[20] associated with a production vertex.

2. The Rung

We now combine two vertices to make one multiperipheral rung, shown in Fig. 11. The triad of frames (b,c,d) just discussed appears on the lower vertex, and a new triad (b',c',d') appears on the upper vertex. The primed boosts connecting the upper frames are given by Eq. (5.1) with $t_i \to t_i'$.

Frames c and c' are both rest frames of p_1 and must therefore be connected by some rotation $g = R_z(\phi_1)R_y(\chi_1)R_z(\phi_1')$. We now use up the z-rotation degree of freedom in defining each vertex frame triad to set $\phi_1 = \phi_1' = 0$ so that the frames c and c' are linked by a pure

y-rotation X_1. This is the Misheloff rotation mentioned in Section (4). In Appendix E we interpret this variable as a cross channel ($t \to \infty$) Regge variable $z = \cos(X)$; an expression for $\cos(X)$ will be given below.

The six frames shown in Fig. 11 are now interlocked, and all 3-momenta are confined to the x-z plane.

Next, four new frames a, a', e, e' are added as shown in Fig. 12. For example, frame a is obtained from frame b by an x-boost h_1. This boost of course does nothing to momentum $k_1^{(b)} = (0,0,0,\sqrt{-t_1})$, but is chosen so that $k_1'^{(a)}$ is x-z like; i.e., the boost h_1 clears out the energy component of $k_1'^{(b)}$. Boost h_1' is chosen similarly so that $k_1^{(a')}$ is x-z like. These statements may be summarized as follows:

$$\begin{aligned} k_1^{(a)} &= (0,0,0,*) & k_1^{(a')} &= (0,*,0,*) \\ k_1'^{(a)} &= (0,*,0,*) & k_1'^{(a')} &= (0,0,0,*) \ . \end{aligned} \tag{5.2}$$

It should be clear from Eq. (5.2) and the lack of y-boosts in the problem (so far) that frames a and a' are connected by a y-rotation, which we label $\theta_{11'}$. From the fact that $t = (k_1 + k_1')^2$ one quickly shows this rotation to be given in magnitude by

$$\cos\theta_{11'} = (t_1 + t_1' - t) / 2\sqrt{-t_1}\ \sqrt{-t_1'} \ . \tag{5.3}$$

Then, from the loop equation on the left side of Fig. 12,

$$X_1 = v_1'(h_1')^{-1}\ \theta_{11'} h_1\ v_1 \ , \tag{5.4}$$

one finds the magnitude of the Misheloff rotation

$$\cos X_1 = (\cos\theta_{11'} - \mathrm{sh}v_1' \mathrm{sh}v_1) / \mathrm{ch}v_1' \mathrm{ch}v_1 \ . \tag{5.5}$$

Reordering the same loop equation one may then compute the boosts h_1 and h_1':

$$\begin{aligned} \mathrm{ch}\, h_1 &= \mathrm{ch}\, v_1' \sin\chi_1 / \sin\theta_{11'} \quad , \\ \mathrm{ch}\, h_1' &= \mathrm{ch}\, v_1 \sin\chi_1 / \sin\theta_{11'} \quad . \end{aligned} \tag{5.6}$$

We have now described the frames a and a', and the new transformations h_1, h_1' and $\theta_{11'}$. In exact analogy one defines the frames e and e' and transformations f_2, f_2' and $\theta_{22'}$. Equations similar to those above are then obtained by comparing Eq. (5.4) to the right-side loop equation $\chi_1 = (\sigma_2')^{-1} f_2' \theta_{22'} f_2^{-1} \sigma_2^{-1}$.

3. The Central Level Frames

To the set of ten frames so far defined with respect to this one multiperipheral rung, two final frames f and g are now added, as shown in Fig. 13. We shall refer to frames like a,b,d,e as being lower level frames, those like a',b',d',e' as being upper level, and f and g as being frames in the central level. These central level frames are in fact brick wall systems (bws) or Breit frames. We define a bws frame for the system (k_i, k_i') to be any frame in which $\underset{\sim}{k}_i + \underset{\sim}{k}_i' = 0$, where $\underset{\sim}{k}_i$ represents the *first* three components of the 4-vector k_i. We shall refer to such (t,x,y) objects as *versors*[21] to distinguish them from the normal 3-vectors (x,y,z) like $\vec{k}_i$. Since $\underset{\sim}{k}_i + \underset{\sim}{k}_i' = 0$ in a bws frame, the overall momentum transfer $Q = k_i + k_i'$ is at spacelike rest, $Q = (0,0,0,\sqrt{-t})$. In Appendix E we perform a complex Lorentz transformation which converts bws frames to cms frames in which $\vec{k}_i + \vec{k}_i' = 0$ and $Q = (\sqrt{t}, 0,0,0)$.

Now, frame f in Fig. 13 is that particular bws frame in which versor $\underset{\sim}{k}_1$ points in the positive x direction, and versor $\underset{\sim}{k}_2$ is t-x like. Similarly, frame g is defined to put versor $\underset{\sim}{k}_2$ in the positive x direction and to make $\underset{\sim}{k}_1$ t-x like. These two frames f and g are

thus linked by an x-boost ν_1 whose magnitude we shall compute in a moment.

In all bws frames for the system of momenta (k_i, k_i') the z-components and versor magnitudes are the same, just as in all cms frames the energy components and vector magnitudes are the same. We find

$$(\underset{\sim}{k_i})^2 = (k_i^t)^2 - (k_i^x)^2 - (k_i^y)^2$$

$$= \Delta(t_i, t_i', t) / 4(-t) \equiv -k_i^2 \quad , \tag{5.7}$$

$$k_i^z = (-t - t_i + t_i') / 2\sqrt{-t} \equiv z_i \ , \tag{5.8}$$

$$(k_i')^z = (-t - t_i' + t_i) / 2\sqrt{-t} \equiv z_i' \ . \tag{5.9}$$

Because our interest is limited to the interior runs of the $t < 0$ multiperipheral chain where the kinematics requires $\Delta(t, t_i, t_i') < 0$, we have defined $-k_i^2$ as above. When the symbol κ_i appears below as a scalar, it refers to this versor magnitude $(-\underset{\sim}{k_i^2})^{1/2}$ and should not be confused with the 4-vector k_i.

We wish to stress the similarity of Eqs. (5.7) through (5.9) to the normal cms kinematics. If k_i and k_i' were future timelike 4-vectors with masses $(t_i)^{1/2}$ and $(t_i')^{1/2}$, then in any cms frame where $Q = (\sqrt{t}, 0, 0, 0)$, $t > 0$, one would have

$$(\vec{k}_i)^2 = \Delta(t_i, t_i', t) / 4t \quad , \tag{5.10}$$

$$E_i = (t + t_i - t_i') / 2\sqrt{t} \quad , \tag{5.11}$$

$$E_i' = (t + t_i' - t_i) / 2\sqrt{t} \quad , \tag{5.12}$$

so that the versor magnitude k_i is the analytic continuation of the cross-channel cms momentum.

Sometimes the variables z_i and z_i' shown above are written in this way:

$$z_i = \tfrac{1}{2}(-t)^{\frac{1}{2}} - w_i \quad , \qquad z_i' = \tfrac{1}{2}(-t)^{\frac{1}{2}} + w_i \quad , \tag{5.13}$$

where

$$w_i = \left(\frac{t_i - t_i'}{2\sqrt{-t}}\right) \quad . \tag{5.14}$$

The variables k_i and w_i are useful replacements for the Regge mass^2 variables t_i and t_i'.

$$t_i = \tfrac{1}{2}t - (k_i^2 + w_i^2) - w_i(-t)^{\frac{1}{2}} \qquad t_i' = \tfrac{1}{2}t - (k_i^2 + w_i^2) + w_i(-t)^{\frac{1}{2}} \ . \tag{5.15}$$

In particular,

$$dk_i dw_i = \frac{1}{2}\ \frac{dt_i dt_i'}{[-\Delta(t,t_i,t_i')]^{\frac{1}{2}}} \quad . \tag{5.16}$$

Applying the above definitions to frame f of Fig. 13 we have

$$k_1^{(f)} = (0,k_1,0,z_1) \qquad k_2^{(f)} = (k_2 sh\nu_1,\ k_2 ch\nu_1,\ 0,\ z_2)$$
$$k_1'^{(f)} = (0,-k_1,0,z_1') \qquad k_2'^{(f)} = (-k_2 sh\nu_1,\ -k_2 ch\nu_1,\ 0,\ z_2') \ . \tag{5.17}$$

Comparison of $k_1^{(f)}$ to $k_1^{(a)}$ then shows these frames to be linked by a very simple y-rotation θ_1:

$$k_1^{(a)} = (0,0,0,\sqrt{-t_1}) \qquad k_1^{(f)} = (0,k_1,0,z_1)$$
$$\Rightarrow \sin\theta_1 = k_1/\sqrt{-t_1} \qquad \cos\theta_1 = z_1/\sqrt{-t_1} \quad . \tag{5.18}$$

Thus, the new frames f and g are interlocked with the previous ten frames to give a total of twelve frames associated with this single rung of the multiperipheral ladder. Computing $\underset{\sim}{p}_1^2 = (\underset{\sim}{k}_2 - \underset{\sim}{k}_1)^2$ in frame f we find that the boost ν_1 is given by

$$\mathrm{ch}\nu_1 = (k_1^2 + k_2^2 + p_1^2) / 2k_1k_2 \quad , \tag{5.19}$$

where

$$p_1^2 = s_1 + (w_1 - w_2)^2 \tag{5.20}$$

and all symbols on the right of Eq. (5.19) refer to versor magnitudes. With t and all t_i fixed, ν_1 measures the mass^2 s_1 of the particle or cluster p_1; in this sense the variable ν_1 is similar to the BCP variables q_1 and q_1' appearing in Fig. 11.

The complete set of twelve frames associated with the rung p_1 is shown in Fig. 14.

4. Many Rungs

We are now ready to juxtapose two rungs of the multiperipheral ladder, as shown in Fig. 15. In this figure one sees that the twelve-frame systems associated with each rung are linked by a very important y-boost called ξ_2. This variable measures the separation of the two rungs in a quantity which would be called the gap rapidity in a one-dimensional model. Notice that the same variable ξ_2 appears in the upper, lower, and central levels. The frames on the central level are linked to the upper and lower levels by y-rotations like θ_1 of Fig. 13. These rotations are given by the formulas one would guess looking at Eq. (5.18) above, e.g.,

$$\sin\theta_2' = k_2 / \sqrt{-t_2'} \quad , \qquad \cos\theta_2' = z_2' / \sqrt{-t_2'} \quad . \tag{5.21}$$

The only transformations not shown in Fig. 15 are the y-rotations like $\theta_{11'}$, appearing in Fig. 14. Obviously $\theta_{11'} = \theta_1 + \theta_1'$.

We now make some remarks concerning the frames of Fig. 15. First of all, most of the frames on the lower level are the usual BCP frames referred to earlier. Since the tranformation labeled g_2 connects two frames in which k_2 is at spacelike rest, g_2 must be an O(2,1) transformation. In BCP this g_2 is written as

$$g_2 = R_z(\mu_2)\, B_x(\tilde{\xi}_2)\, R_z(\nu_2) \quad .$$

This form, known as the discrete-basis parametrization, goes all the way back to Bargmann, but we have put a twiddle over the x-boost parameter in order not to confuse that variable with our y-boost variable ξ_2. The azimuthal rotations μ_2 and ν_2 are conjugate to the Reggeon helicities in the sense discussed back in Section (2), and are connected with the so-called Toller angles $\omega_i = \mu_i + \nu_{i+1}$. Variable $\tilde{\xi}_2$ is the Regge variable, i.e., $z = \cosh(\tilde{\xi}_2)$, and is conjugate to the angular momentum associated with the link k_2, which is to say, α_2 (see Fig. 8).

Although the same BCP O(2,1) transformation g_2 appears in Fig. 15, it is parametrized differently, namely,

$$g_2 = B_x(f_2)\, B_y(\xi_2)\, B_x(h_2) \quad ,$$

the so-called continuous-basis[6] parametrization of O(2,1). As already noted, the same variable ξ_2 appears also in g_2', the O(2,1) transformation appropriate to the *upper* production amplitude of Fig. 15.

Prior to leaving this section on frames, we wish to add one more observation concerning the frames connected with the single rung shown in Figs. 13 and 14. If one were to imagine the multiperipheral

ladder on the right as generating a Reggeon in the central level, one might draw the figure shown in Fig. 16, where we have redrawn the frames a,a' and f, and their connecting y-rotations. We just want to remark that these three frames are the usual standard frames one associates with the triple Regge vertex[18] in the configuration $\Delta < 0$, and the thetas are the standard y-rotations. A similar remark applies to the frame triad, g,e,e'.

We are now ready to convert the Regge poles of the upper and lower amplitudes into helicity poles in the central level.

(6) THE HELICITY POLE EXPANSION

Consider once again Fig. 15. In order to motivate the next technical maneuver, we anticipate a diagonalization procedure which will be explained in Section (9). The frames on the central level of Fig. 15 are linked by alternating x-boosts ν_i and y-boosts ξ_i. It will turn out that these frames and variables are the relevant ones for the diagonalized (or even undiagonalized) consideration of the multi-peripheral ladder, the reason being that these are the bws frames in which the overall 4-momentum Q is at spacelike rest. We will show that certain groupings of the ν and ξ variables form convenient O(2,1) transformations. For example, the combination

$$B_y(\xi_2)B_x(\nu_2)B_y(\xi_3)$$

is an O(2,1) transformation in the continuous-basis mentioned earlier which in a certain sense surrounds the cluster p_2 in the central level of Fig. 15. In the diagonalization process it will be shown that the variable ν_2 is conjugate to angular momentum j in the central level,

while the boosts ξ_2 and ξ_3 are conjugate to complex helicity variables λ_2 and λ_3. Helicity poles in the complex helicity plane λ will correspond to powers of $e^{|\xi|}$ since these variables are Fourier conjugates. It is for this reason that we shall now expand the upper and lower Regge propagator functions $E^{-\alpha-1}(g)$ and $E^{-\alpha'-1}(g')$ into powers of $e^{|\xi|}$. These functions appear in Fig. 17, which represents a portion of the multiperipheral chain, i.e., a portion of the unitarity product of Eq. (4.4) with the model amplitudes of (4.3).

We shall refer to the form $e^{|\xi|\alpha}$ as a helicity-pole term in the same way one speaks of z^{α} as a Regge pole term, with the understanding that the actual pole occurs in the plane of the conjugate variable, be it helicity or angular momentum. Also, the square-bracketed expressions in Fig. 17 will be called Reggeon propagators.

In Appendix C we give a derivation of the following (convergent) helicity-pole expansion of the lower propagator E-function:

$$E^{-\alpha_2-1}_{m_2 r_2}(g_2) = (+i)^{m_2-r_2} \sum_{\kappa_2=\pm} \sum_{n_2=0}^{\infty} \theta(\kappa_2\xi_2) \times F^{\alpha_2}_{n_2,\kappa_2 m_2}(f_2)\; e^{|\xi_2|(\alpha_2-n_2)}\; F^{\alpha_2}_{n_2,\kappa_2 r_2}(-h_2)\,. \tag{6.1}$$

Recall that $g_2 = (f_2, \xi_2, h_2)$, and that f_2 and h_2 are x-boost parameters fixed by the t_i [see Eq (5.6)]. The quantity $[\alpha_2 - n_2]$ is the *helicity* of the Reggeon whose spin is α_2. When α_2 takes some general non-*integral value, the Reggeon helicity takes the values* α_2, α_2-1, $\alpha_2-2, \ldots$ in an infinite sequence. Were α_2 to approach a physical value s_2 (which does not happen in the multiperipheral region of course), we would expect this sequence to truncate at helicity equal to $-s_2$. This truncation is affected by the interaction of the functions F

appearing in Eq. (6.1) with the helicity nonsense-zeros present in the standard Toller vertices discussed in Section (3), the V of Fig. 17. These functions F are given in Eq. (C.5). The new index κ_2 appearing in Eq. (6.1) will be connected with parity in Section (7). Basically, $\kappa_2 = \mathrm{sign}(\xi_2)$.

The important point to be made about Eq. (6.1) is that each helicity term *factorizes*. It is not obvious that an expression like (6.1) had to exist. A similar situation is encountered in a much more complicated mathematical environment with the Regge pole expansion of a single Toller/Lorentz pole. Regge poles there are the factorizing daughters of a Toller pole, and helicity poles here are the factorizing daughters of a Regge pole.

The fact that each helicity pole factorizes is the fact which allows us to momentarily define a helicity pole propagator. This concept will greatly reduce the bulge of complexity with which we are now confronted. Had the helicity poles not factorized, we would be in real trouble.

When all the Reggeon propagators [...] in the unitarity product of Fig. 17 are helicity-pole expanded according to Eq. (6.1), certain factors may be grouped to the vertices, leaving a very simple helicity pole propagator. The new rung with these regrouped factors is shown in Fig. 18, and the helicity pole propagator is shown in Fig. 19 and has the form

$$P_2(\xi_2) = \gamma_2\overline{\gamma_2'}\,\xi_2\overline{\xi_2'}\,\theta(\kappa_2\xi_2)\;e^{|\xi_2|[(\alpha_2-n_2)+(\overline{\alpha_2'}-n_2')]} \tag{6.2}$$

The power to which $e^{|\xi_2|}$ is raised in Eq. (6.2) is the sum of the helicities of the Reggeons in the (2,2') channel. Notice that each of the helicities is in general a complex number, whereas the Reggeon

helicities discussed in Section (2) were always integers or half-integers. The reason is that here the Reggeon helicities are eigenvalues of the (non-Hermitian) y-boost generator K_2 which is generating the boosts $B_y(\xi)$. In Appendix E it is shown that, when the structure of Fig. 15 is continued to the $t > 0$ case via a complex Lorentz transformation, the generator K_2 is turned into a normal rotation generator and the helicities become the normal (discrete valued) helicities mentioned in Section (2). The variable ξ_2 becomes a rotation ($\phi_2 = i\xi_2$) which again measures the sum of the helicities in the (2,2') channel, namely, $m_2 + m_2'$.

The other important point to be made about the helicity-pole propagator is that it still contains the physical (planar) poles in the signature factor denominators, e.g.,

$$\xi_2 = \left[\frac{e^{-i\pi(\alpha_2 - \epsilon_2)} + \tau_2}{2\sin\pi(\alpha_2 - \epsilon_2)} \right] . \tag{2.7}$$

These poles generate the normal thresholds in the cross channel when t is continued to $t > 0$.

Turning now to the rung or kernel of Fig. 18, the helicity summations r_1, r_1', p_1, p_1', and m_2, m_2' can be performed since they are now detached from the rest of the chain by helicity-independent (in this sense) helicity-pole propagators. We might first sum over the upper and lower (discrete) helicities to go from Fig. 18 to Fig. 20a, renormalizing for the first time our standard vertices V. The new vertex $\tilde{V}$ is given by

$$\tilde{V}_{p_1}(\alpha_1, n_1; \alpha_2, n_2; \kappa_1, \kappa_2; s_1) \equiv \sum_{r_1, m_2 = -\infty}^{\infty} (i)^{-r_1} F^{\alpha_1}_{n_1, \kappa_1 r_1}(-h_1)$$

$$\times V^{\alpha_1 s_1 \alpha_2}_{r_1 p_1 m_2} F^{\alpha_2}_{n_2, \kappa_2 m_2}(f_2) (i)^{m_2} \equiv \tilde{V}_{p_1} . \tag{6.3}$$

(Group-theoretically, this corresponds to a conversion from the discrete to the continuous helicity basis.)

Finally, we sum over the Misheloff rotation helicities p_1, p_1' to go from Fig. 20a to Fig. 20b, which shows the final kernel

$$K(\alpha_1, n_1, t_1;\ \alpha_1', n_1', t_1';\ \alpha_2, n_2, t_2;\ \alpha_2', n_2', t_2';\ \kappa_1, \kappa_2;\ s_1,\ t)$$

$$\equiv \sum_{p_1, p_1' = -s_1}^{s_1} [\tilde{v}_{p_1'}]^* \ d^{s_1}_{p_1' p_1}(\chi_1) \ [\tilde{v}_{p_1}] \ \equiv \ \kappa_{12} \quad . \qquad (6.4)$$

This kernel is a function of the four Reggeon spins α_j, helicities $\alpha_i - n_i$, and masses t_i. Due to the kappa indices appearing in Eq. (6.1), the kernel is also a function of the kappa label on each side. This particular kernel is a single particle kernel and thus depends on the spin s_i of that single particle. We could just as well have defined p_1 (the produced object) to be a cluster, in which case, as noted earlier, Eq. (6.4) should be summed over s_1.

Before concluding this section we wish to make a few additional remarks about the critical helicity-pole expansion formula (6.1). This formula, or something close to it, has been derived by other workers[2,4] as only an asymptotic expansion. We wish to emphasize that (6.1) as derived in Appendix C is an exact and very convergent equality based on an elementary addition theorem of the second-kind Legendre functions. In other approaches, the step in the argument represented by (6.1) has been to some extent obscured by complicated group theoretic arguments. For example, (6.1) can be interpreted in terms of O(2,1) mixed-basis matrix elements in the continuous series, in which case the discrete index κ has a certain mathematical meaning. Alternatively, Eq. (6.1) can be related to the O(2,1) analytically

continued Clebsch-Gordon coefficients which couple angular momenta between the upper, lower, and central kinematic levels in Fig. 15. These approaches are no doubt correct, but introduce so much complication that one cannot tell for sure whether or not a formula is correct without expending much effort. Our approach has been to consolidate this group theory into a few easily verifiable addition theorems[9] which are then used to derive various results.

(7) NATURALITY CONDITION FOR THE KERNEL

In Section (3) it was shown that, after accounting for the correct Toller M-function notation for the vertex

$$V^{\alpha_i s_j \alpha_k}_{m_i m_j m_k} = M_{m_k m_i m_j}(a_k : a_i, a_j) \quad , \tag{7.1}$$

the statement of parity invariance for the vertex in Fig. 18 is

$$V^{\alpha_1 s_1 \alpha_2}_{r_1 p_1 m_2} = [\sigma_1 (-i)^{2r_1}]^* \, [\Pi_1 (-1)^{s_1 - p_1}]^* \, [\sigma_2 (-i)^{2m_2}] \times V^{\alpha_1 \, s_1 \, \alpha_2}_{-r_1 - p_1 - m_2} \quad , \tag{7.2}$$

where σ_i is the Reggeon naturality of Eq. (3.9) and Π_1 the intrinsic parity of the produced particle.

Insertion of the parity condition (7.2) into the definition (6.3) of the renormalized vertex $\tilde{V}$ then yields

$$\tilde{V}_{p_1}(\kappa_1, \kappa_2) = \bar{\sigma}_1 \sigma_2 \, \bar{\Pi}_1 (-1)^{s_1 - p_1} \, \tilde{V}_{-p_1}(-\kappa_1, -\kappa_2) \quad . \tag{7.3}$$

When this result is in turn substituted into the definition (6.4) of the kernel K, one finds

$$K(\kappa_1, \kappa_2) = \bar{\sigma}_1 \sigma_1' \, \sigma_2 \bar{\sigma}_2' \, K(-\kappa_1, -\kappa_2) \tag{7.4}$$

which is the desired naturality condition for the kernel.*

We may now interpret Eq. (7.4) as saying: a parity transformation on the kernel is equivalent to multiplication by the product of the naturalities of the four attached Reggeons. To see why a parity transformation negates κ_1 and κ_2 we refer to Fig. 21 which shows a segment of the multiperipheral chain with its central level boost ξ. The figure also shows the same chain segment in a parity-inverted world where the two frames are connected by some boost ξ'. These inverted-world frames are connected to their non-inverted-world counterparts by Toller's parity transformation s' defined in Eq. (3.4). Since

$$(s')^{-1}\, B_y(\xi)s' = B_y(-\xi) \quad , \tag{7.5}$$

one concludes that $\xi' = -\xi$. This is what is meant by saying that parity negates all the ξ-boosts in the chain, and therefore the $\kappa_i = \mathrm{sign}(\xi_i)$.

Equation (7.5) is one entry in the following table which shows how the parity operators s and s' affect the signs of rotation and boost parameters:

	R_x	R_y	R_z	B_x	B_y	B_z
s	+	+	+	-	-	-
s'	-	+	-	+	-	+

(7.6)

Notice that of all the variables listed in Fig. 15 and relating to the multiperipheral chain, only the y-boosts ξ_i are negated by parity s'.

---

*This condition is derived in Ref. 5, Eq. (2.8), for the production of spinless particles only; see also Eqs. (2.7) and (2.10) of that paper for a Toller angle discussion, and Eq. (2.16) which relates to our comments at the end of Section (6).

If there were z-rotations somewhere, these would also be negated by s', as the table shows, and this fact has a bearing on the Toller angle which we mention here as a digression.

In the usual BCP analysis of the production amplitude shown, e.g., in Fig. 8, one uses for the O(2,1) transformations g the discrete basis parameters $R_z(\mu)B_x(\tilde{\xi})R_z(\nu)$, which we mentioned at the end of Section (5), and in terms of which the lower Reggeon propagator function may be written

$$E_{mr}^{-\alpha-1}(g) = e^{-im\mu}\ e_{mr}^{-\alpha-1}(ch\tilde{\xi})\ e^{-ir\nu} \quad . \tag{7.7}$$

If the asymptotic limit of this E function is taken [see Eqs. (A.15) and (A.16)] to get $(ch\tilde{\xi})^{\alpha}$ times helicity-factorizing factors, and if these factors and the azimuthal exponentials are absorbed into renormalized vertices β and the helicity sums done, one obtains for the production amplitudes the form

$$\ldots\ \beta_{p_1}(\nu_1,\mu_2)\ (ch\tilde{\xi}_2)^{\alpha_2}\ \beta_{p_2}(\nu_2,\mu_3)\ (ch\tilde{\xi}_3)^{\alpha_3}\ \ldots \quad , \tag{7.8}$$

where the p_i are the helicities of the produced particles. Then from Eq. (7.2), the parity condition for these renormalized vertices β may be shown to be similar to Eq. (7.3),

$$\beta_{p_1}(\nu_1,\mu_2) = \bar{\sigma}_1\sigma_2\ \bar{\Pi}_1(-1)^{s_1-p_1}\ \beta_{-p_1}(-\nu_1,-\mu_2) \quad . \tag{7.9}$$

In the case of spinless produced particles, the vertex β is a function only of the Toller angle $\omega_1 = \nu_1 + \mu_2$ and Eq. (7.9) becomes

$$\beta(\omega_1) = \bar{\sigma}_1\sigma_2\ \bar{\Pi}_1\ \beta(-\omega_1) \quad . \tag{7.10}$$

Finally, slightly renormalizing the vertices once again, we end up with the asymptotic or phenomenological multi-Regge amplitude for the production of spinless particles along the chain

$$\ldots \quad \widetilde{\beta}(\omega_1)(s_2)^{\alpha_2} \quad \widetilde{\beta}(\omega_2)(s_3)^{\alpha_3} \quad \ldots \tag{7.11}$$

Multiplying two such amplitudes together to get the unitarity product, one would identify the kernel as

$$\widetilde{K}(\omega_1,\omega_1') \quad = \quad [\widetilde{B}(\omega_1)] \; [\widetilde{B}(\omega_1')]^* \quad , \tag{7.12}$$

and this kernel would then have a naturality condition

$$\widetilde{K}(\omega_1,\omega_1') \quad = \quad \overline{\sigma}_1\sigma_1' \quad \sigma_2\overline{\sigma}_2' \quad \widetilde{K}(-\omega_1,-\omega_1') \quad . \tag{7.13}$$

This condition is, however, just a special case of Eq. (7.4) which was derived without any approximations. Therefore, a parity transformation can be regarded either as negating the ξ_i variables in the exact kinematic scheme, or as negating the Toller angles in the asymptotic production of spinless particles.

(8) THE MULTIPERIPHERAL CHAIN AND PHASE SPACE

In Section (6) the helicity-pole propagator P_i and kernel K_{ij} were defined. Figure 22 shows how these quantities alternate to compose the multiperipheral chain

$$\ldots \quad K_{12}(\nu_1)P_2(\xi_2)K_{23}(\nu_2)P_3(\xi_3)K_{34}(\nu_4) \quad \ldots \quad . \tag{8.1}$$

The figure also shows the central level frames with their connecting boosts. The ν variables measure the "rapidity width" of the kernels (clusters or single particles), whereas the ξ boosts measure the rapidity width of the helicity-pole propagators. Since these alternating boosts are not collinear ($\nu_i = B_x$ and $\xi_i = B_y$), the notion of additive rapidities arises only in the extreme relativistic limit where

$$\mathrm{ch}\nu = \mathrm{ch}\nu_1\,\mathrm{ch}\nu_2 + \mathrm{sh}\nu_1\,\mathrm{sh}\nu_2\,\mathrm{ch}\xi_2 \tag{8.2}$$

becomes

$$\nu = \nu_1 + \xi_2 + \nu_2 \quad . \tag{8.3}$$

The sums which are implicit in the chain (8.1) will be discussed in a moment.

First, something must be said about the phase space. Each particle or cluster (here K will be regarded as a cluster) gets a momentum phase-space factor d^4p_i, where p_i is the momentum flowing up the cluster $K_{i,i+1}$. Replacing d^4p_i with d^4k_i, where k_i is the 4-momentum of the lower Reggeon of the system (i,i'), and simply evaluating this 4-momentum in one of the central level frames a few removed from the frames nearest p_i, one may express d^4k_i in terms of the group variables appearing in Fig. 22. Recalling the meaning of the central level frames, we have, e.g.,

$$k_1^{(d)} = (0, k_3, 0, z_3) \quad ,$$

$$k_3^{(c)} = (k_3\mathrm{sh}\nu_2, k_3\mathrm{ch}\nu_2, 0, z_3) \quad ,$$

$$k_3^{(b)} = (k_3\mathrm{sh}\nu_2\mathrm{ch}\xi_2,\ k_3\mathrm{ch}\nu_2,\ k_3\mathrm{sh}\nu_2\mathrm{sh}\xi_2,\ z_3)\ , \tag{8.4}$$

where k_3 (the versor magnitude) and z_3 were defined in Eqs. (5.7) and (5.13). From the last line of Eq. (8.4) we find that

$$\begin{aligned} d^4k_3 &= [d^3\underset{\sim}{k}_3]dz_3 = [k_3^2 dk_3 d\xi_2\ d(\mathrm{ch}\nu_2)]dz_3 \\ &= 2\pi k_3^2 dk_3 dw_3 \cdot \left[\frac{d\xi_2}{2\pi} \cdot d(\mathrm{ch}\nu_2)\right] \quad , \end{aligned} \tag{8.5}$$

where z_3 has been replaced by the w_3 of Eq. (5.14). The portion dk_3dw_3 of the phase space is the so-called transverse integration because it can be expressed in terms of $d^2p_3^t$ where p_3^t is the

transverse momentum of the cluster 3 whose parallel momentum component $p_3^{\parallel}$ is related to the standard rapidity variable. In terms of the invariants t_3 and t_3' one can show, as in Eq. (5.16), that

$$dk_3 dw_3 = \frac{1}{2} \frac{dt_3 dt_3'}{\sqrt{-\Delta(t,t_3,t_3')}} . \tag{8.6}$$

The second factor in the last line of Eq. (8.5) shows the O(2,1) equivalent of the $d\Omega = d\phi\, d(\cos\theta)$ one finds in cms kinematics, e.g., elastic unitarity. The fact that $d\xi_2\, d(ch\nu_2)/2\pi \equiv d\mathcal{G}_2$ is a piece of the O(2,1) invariant measure (in continuous-basis parameters) is what allows the exact diagonalization of the multiperipheral chain onto central level angular momentum, as is done in the next section.

The reader familiar with the Chew-Goldberger-Low approximation[22] to the multiperipheral phase space will recognize the expression in Eq. (8.6) as a portion of the asymptotic form of the quasi-cms phase space of two clusters,

$$d^4p_1 d^4p_2\, \delta^4(P - p_1 - p_2) \approx \frac{ds_1 ds_2}{s} \left[\frac{1}{2} \frac{dt_2 dt_2'}{\sqrt{-\Delta(t,t_2,t_2')}} \right], \tag{8.7}$$

where $(s_1)^{1/2}$ and $(s_2)^{1/2}$ are the masses flowing up the two adjacent clusters. In order to compare Eq. (8.5) with (8.7) we write, shifting to the left one rung,

$$d\mathcal{G}_1 = \frac{d\xi_1}{2\pi} \cdot d(ch\nu_1) = \frac{d(ch\nu_1)d(ch\nu_2)\theta(\nu - \nu_1 - \nu_2)}{\pi[k(ch\nu, ch\nu_1, ch\nu_2)]^{1/2}} , \tag{8.8}$$

where $k(x,y,z) = x^2 + y^2 + z^2 - 2xyz - 1$. *If it were true that* $\nu \gg \nu_1, \nu_2$ throughout the entire phase space, one could approximate

$$k(ch\nu,\, ch\nu_1,\, ch\nu_2) \approx (ch\nu)^2 .$$

Then from formulas like Eq. (5.19),

$$\mathrm{ch}\nu_1 = \frac{s_1 + k_1^2 + k_2^2 + (w_1 - w_2)^2}{2k_1k_2} ,$$

one finds that

$$d\mathcal{G}_1 = \frac{ds_1 ds_2}{2\pi k_2^2 s} ,$$

and then

$$d^4k_2 = \frac{dk_2 dw_2 ds_1 ds_2}{s} = \left[\frac{1}{2} \frac{dt_2 dt_2'}{\sqrt{-\Delta(t,t_2,t_2')}}\right] \frac{ds_1 ds_2}{s} ,$$

which is the CGL approximation (8.7). Since the approximation $s \gg s_1, s_2$ is not particularly valid except in special cases like double diffractive dissociation, one would expect a more accurate result to be obtained in any related calculation (like the cylinder) by using the exact phase space. Naturally, an exact angular momentum diagonalization only works if this correct group phase space is retained.

We now consider the sums implicit in (8.1) and Fig. 22. For each segment or propagator of the multiperipheral chain there is a sum of the form (e.g., for segment 2,2')

$$\int d\mathcal{G}_1 \sum_2 .$$

where

$$\sum_2 \equiv \int d\phi_2 \sum_{\kappa_2=\pm} \sum_{\alpha_2,\alpha_2'} \sum_{n_2,n_2'=0}^{\infty} \tag{8.9}$$

and

$$\int d\phi_2 = \frac{2\pi}{f}\int_{-\infty}^{\infty} dw_2 \int_{L}^{\infty} dk_2 \cdot k_2^2 \quad , \tag{8.10}$$

with f being the normalization factor of Section (4). For each fixed value of t_2 and t_2' [see Eq. (5.15)] and the discrete index κ_2, and for each pair of Reggeons α_2, α_2', we sum over all of the helicity poles labeled by n_2, n_2', these being the helicity daughters of the Reggeons. Next, we sum over all possible upper and lower Reggeon combinations. Finally, we sum over κ_2 and do the transverse integration. The group integrations dg_i will be removed in the next section.

(9) THE DIAGONALIZATION OF ANGULAR MOMENTUM

To avoid confusing the mathematics with the physics, we briefly discuss our diagonalization procedure; a fuller explanation may be found elsewhere.[9]

Consider the following mathematical relation among four functions A, B, C, and D, each a function of three variables:

$$A(\xi,\nu,\xi') = \int_{-\infty}^{\infty} \frac{d\xi_1}{2\pi} \int_{1}^{\infty} d(\mathrm{ch}\nu_1) \int_{-\infty}^{\infty} \frac{d\xi_2}{2\pi} \int_{1}^{\infty} d(\mathrm{ch}\nu_2)\, B(\xi_1,\nu_1,0)\, C(\xi_2,\nu_2,0)$$
$$\times\, D(\xi_3,\nu_3,\xi_3') \quad . \tag{9.1}$$

Schematically, this equation is represented in Fig. 23. If the variables are in the range $-\infty < \xi_i < \infty$ and $0 \leq \nu_i < \infty$, we may interpret the functions A, B, C, D as being defined on a certain sector of the group $SU(1,1) \sim O(2,1)$, and we write the same equation in group theoretic notation as follows:

$$A(g) = \int dg_1 \int dg_2 \int dg_3\, \delta(g - g_1 g_2 g_3)\, B(g_1)\, C(g_2)\, D(g_3) \quad , \tag{9.2}$$

where $g = (\xi,\nu,\xi')$, $\mathbf{g}_1 = (\xi_1,\nu_1,0)$, etc. The variables $g_3 = (\xi_3,\nu_3,\xi_3')$ in Eq. (9.1) are functions of the other variables according to the SU(1,1) group multiplication $g_3 = g_2^{-1}g_1^{-1}g$. In Eq. (9.2) this fact is made more explicit by use of an invariant delta function.

Equation (9.1) or (9.2) can be diagonalized exactly by projecting the functions onto the continuous-basis representation functions of SU(1,1). These functions are the second-kind generalized Legendre functions $\mathcal{Q}^j_{\mu\nu}(z)$ discussed briefly in Appendix A and at great length in Refs. 9 and 23. The diagonalization of (9.1) is given by

$$A^j_{\mu\mu'} = \int \frac{d\lambda}{i\pi} \int \frac{d\lambda'}{i\pi} \; B^j_{\mu\lambda} \; \mathcal{C}^j_{\lambda\lambda'} \; D^j_{\lambda'\mu'} \quad , \tag{9.3}$$

where

$$A^j_{\mu\mu'} = \int dg \; \mathcal{Q}^j_{\mu\mu'}(g) \; A(g) \quad , \tag{9.4}$$

$$B^j_{\mu\lambda} = \int d\mathbf{g}_1 \; \mathcal{Q}^j_{\mu\lambda}(\mathbf{g}_1) \; B(\mathbf{g}_1) \quad , \tag{9.5}$$

and the projection of C is like that of B; D like that of A. The invariant measures are

$$dg = \frac{d\xi}{2\pi} \, d(\mathrm{ch}\nu) \, \frac{d\xi'}{2\pi} \quad , \tag{9.6}$$

$$d\mathbf{g}_1 = \frac{d\xi_1}{2\pi} \, d(\mathrm{ch}\nu_1) \quad , \tag{9.7}$$

and the function $\mathcal{Q}(g)$ is defined as

$$\mathcal{Q}^j_{\mu\mu'}(g) = e^{-u\xi} \; \mathcal{Q}^j_{\mu\mu'}(\mathrm{ch}\nu) \; e^{-u'\xi'} \quad , \tag{9.8}$$

with $\mathcal{Q}(z)$ given in Eq. (A.2).

In the diagonalized equation (9.3), each group integration has been replaced by a helicity contour integration running up the

imaginary helicity axis. The source of this contour is the second-kind addition theorem which, for convenience, we compare to the first-kind addition theorem:

$$P^j_{mm'}(g_1 g_2) = \sum_{n=-\infty}^{\infty} P^j_{mn}(g_1)\, P^j_{nm'}(g_2) \quad ; \tag{9.9}$$

$$\mathcal{P}^j_{\mu\mu'}(g_1 g_2) = \int \frac{d\lambda}{i\pi}\, \mathcal{P}^j_{\mu\lambda}(g_1)\, \mathcal{P}^j_{\lambda\mu'}(g_2) \quad . \tag{9.10}$$

The familiar helicity sum of the first-kind theorem (P functions are essentially the rotation D functions) appears as a helicity integration in the second-kind formula. In Ref. 9, Eq. (9.10) is derived from (9.9) and interpreted group-theoretically.

When all the functions appearing in Eq. (9.1) are independent of the ξ_i variables, the diagonalized equation simplifies somewhat,

$$a^j = b^j\, c^j\, d^j \quad , \tag{9.11}$$

where

$$f^j = \frac{1}{\pi}\int_1^{\infty} d(ch\nu)\; Q_j(ch\nu)\; F(\nu) \quad . \tag{9.12}$$

More generally this is not the case and the helicity contours appearing in Eq. (9.3) are shifted sideways to pick up helicity pole contributions of the integrand. The λ are the complex helicity variables to which we referred earlier.

In the particular mathematical example considered above, we diagonalized a chain of three functions B, C, D. Hopefully it is clear that a chain of any length may be similarly diagonalized. Each projected function contains the diagonal angular momentum projection label j along with two helicity labels which are systematically tied to neighboring helicities by the "summations" $\int d\lambda$.

We are, by the way, referring to j as angular momentum because, in the Regge language, Eq. (9.4) is a true Foissart-Gribov projection so that j is the analytic continuation of the true angular momentum. In Eq. (F.5) we show how to recover a function $\tilde{A}(g)$ from its projections $\tilde{A}^j_{\mu\mu'}$, i.e., we give the inversion of formula (9.4).

(10) THE PLANAR BOOTSTRAP

1. Form of the Integral Equation

The basic multiperipheral chain was illustrated in Fig. 22, and we shall now be more specific. The contribution from three particles or clusters to the 4-Reggeon ring discontinuity is given by*

$$^{(3)}\tilde{A}_{14}(\xi,\nu,\xi') = \sum_{2,3} \int d\mathbf{k}_1 \int d\mathbf{k}_2 \; P_1(\xi_1)K_{12}(\nu_1)P_2(\xi_2)K_{23}(\nu_2) \times P_3(\xi_3)K_{34}(\nu_3)P_4(\xi_3') \quad , \tag{10.1}$$

where the notations P, K, $d\mathbf{k}$ and Σ were defined in Eqs. (6.2), (6.4), (9.7), and (8.9). Since (10.1) is of the form (9.1), the diagonalization may be read from (9.3) to be

$$^{(3)}\tilde{A}^j_{\mu\mu'}(1,4) = \sum_{2,3} \int \frac{d\lambda}{i\pi} \int \frac{d\lambda'}{i\pi} \; P_\mu(1)K^j_{\mu\lambda}(1,2)P_\lambda(2)K^j_{\lambda\lambda'}(2,3) \times P_{\lambda'}(3)K^j_{\lambda'\mu'}(3,4)P_{\mu'}(4) \quad , \tag{10.2}$$

where

---

*We have tried very hard to keep track of the normalization of amplitudes, but, alas, have lost the battle. Strictly speaking, if A is a discontinuity, equations like (10.1) should contain the overall factor $-c/\pi$ shown in Eq. (4.4), $2\pi/f$ for each $d\mathbf{k}$, and an extra $1/f$ because $\delta^{(4)}(\text{ext})$ removes one d^4k_i. However, as we mention in Section 10.8, and show in Fig. 29, A is not Toller-normalized, so we omit these overall factors. There is always a question of how many π's and 2's appear in the phase space $d\Phi$ of the planar bootstrap or Eq. (11.24), and we have therefore lost track of these factors.

$$K^j_{\mu\lambda}(1,2) = \int_1^\infty d(ch\nu)\, Q^j_{\mu\lambda}(ch\nu)\, K_{12}(\nu) \quad , \tag{10.3}$$

$$P_\mu(1) = \int_{-\infty}^{\infty} \frac{d\xi}{2\pi}\, e^{-\mu\xi}\, P_1(\xi) \quad . \tag{10.4}$$

Therefore, defining ${}^{(3)}\tilde{A}^j_{\mu\mu'}$ *by*

$${}^{(3)}\tilde{A}^j_{\mu\mu'}(1,4) = P_\mu(1)\, {}^{(3)}A^j_{\mu\mu'}(1,4)\, P_{\mu'}(4) \quad , \tag{10.5}$$

Eq. (10.2) may be re-expressed as

$${}^{(3)}A^j_{\mu\mu'}(1,4) = \sum_{2,3} \int \frac{d\lambda}{i\pi} \int \frac{d\lambda'}{i\pi}\, K^j_{\mu\lambda}(1,2)P_\lambda(2)K^j_{\lambda\lambda'}(2,3)P_{\lambda'}(3)K^j_{\lambda'\mu'}(3,4) \tag{10.6}$$

which is schematized in Fig. 24.

In the usual way one may write an integral equation for the complete 4-Reggeon ring discontinuity which will be solved by a sum of terms of the form (10.1). This integral equation reads

$$\tilde{A}_{13}(\xi,\nu,\xi') = P_1(\xi)K_{13}(\nu)P_3(\xi') + \sum_2 \int d\xi_1 P_1(\xi_1)K_{12}(\nu_1)\tilde{A}_{23}(\xi_2,\nu_2,\xi_2') \tag{10.7}$$

which may once again be diagonalized by inspection to give, together with the definition (10.5),

$$A^j_{\mu\mu'}(1,3) = K^j_{\mu\mu'}(1,3) + \sum_2 \int \frac{d\lambda}{i\pi}\, K^j_{\mu\lambda}(1,2)P_\lambda(2)A^j_{\lambda\mu'}(2,3) \quad , \tag{10.8}$$

which is represented by Fig. 25. The problem of obtaining the 4-particle discontinuity from the 4-Reggeon solution of (10.8) is illustrated in Fig. 26 and discussed in Appendix F.

Near a Regge pole, the projected ring discontinuity A factorizes (see Fig. 27):

$$A^{j}_{\mu\mu'}(1,3)\Big|^{j\approx\alpha} \doteq \frac{\pi}{\Gamma(\alpha)} \; \frac{G^{\alpha}_{\mu}(1;\alpha)\; G^{\alpha}_{\mu'}(3;\alpha)}{j-\alpha} \quad . \qquad (10.9)$$

Taking the residue of the pole on both sides of (10.8) then yields the vertex bootstrap

$$G^{\alpha}_{\mu}(1;\alpha) \;=\; \sum_{2} \int \frac{d\lambda}{i\pi} \; K^{\alpha}_{u\lambda}(1,2) P_{\lambda}(2) C^{\alpha}_{\lambda}(2;\alpha) \quad , \qquad (10.10)$$

as shown in Fig. 28. The normalization of the triple-Regge couplings G is described in Section 10.5 below.

2. The Projected Helicity-Pole Propagator P_{λ}

The helicity-pole propagator was defined in Eq. (6.2) to be

$$P_i(\xi) \;=\; 2\pi\, H(i)\theta(\xi\kappa_i)\, \exp[h_i|\xi|], \qquad (10.11)$$

where

$$H(i) \;\equiv\; (2\pi)^{-1} * (\gamma_i\bar{\gamma}'_i) * (\xi_i\bar{\xi}'_i) \quad , \qquad (10.12)$$

$$h_i \;\equiv\; (\alpha_i - n_i) * (\bar{\alpha}'_i - n'_i) \quad . \qquad (10.13)$$

According to (10.4), the projected propagator takes the form

$$P_{\lambda}(i) \;=\; H(i) \,/\, (\kappa_i\lambda - h_i) \quad , \qquad (10.14)$$

where we now see the actual helicity pole at $\lambda = \kappa_i h_i$.

In the ordered S-matrix, Regge trajectories must occur in strongly exchange degenerate pairs. When the upper and lower signature factors are summed over signature taking into account the exchange degeneracy, one finds for the regular (untwisted) propagator P,

$$\xi_i\bar{\xi}'_i \rightarrow \sum_{\gamma_i\gamma'_i} \xi_i\bar{\xi}'_i \;=\; \frac{\exp\left\{-i\pi[(\alpha_i - \epsilon_i) - (\bar{\alpha}'_i - \epsilon'_i)]\right\}}{\sin\pi(\alpha_i - \epsilon_i)\; \sin\pi(\bar{\alpha}'_j - \epsilon'_i)} \quad . \qquad (10.15)$$

For the twisted propagator ^{x}P used later in the cylinder discussion,

$$\xi_i\tilde{\xi}_i' \to \sum_{\tau_i\tau_i'}(\tau_i\xi_i)(\tau_i'\xi_i') = \frac{1}{\sin\pi(\alpha_i - e_i)\ \sin\pi(\tilde{\alpha}_i' - e_i')} \ . \quad (10.16)$$

3. The Projected Kernel and Its Threshold Behavior

In the kernel, shown schematically in Fig. 18, there are seven quantities each of which depends on the kernel mass s_1 and therefore on the variable ν_1 of Eq. (5.19), so that computation of the projected kernel (10.3),

$$K^j_{\mu\lambda}(1,2) = \int_1^\infty d(\mathrm{ch}\nu)\ \mathcal{K}^j_{\mu\lambda}(\mathrm{ch}\nu)\ K_{12}(\nu) \quad , \qquad (10.3)$$

in terms of the standardized vertex V is an unpleasant numerical task which we shall not attempt. This task is, however, a necessary aspect of the functional bootstrap to be mentioned below.

Lacking an analytic expression for $K^j_{\mu\lambda}$, we search for any potentially useful information buried in formula (10.3). One such piece of information is the threshold behavior which we now extract.

Since $K^j_{\mu\lambda}(1,2)$ is a Froissart-Gribov projection, we are reminded that it should be possible to find its threshold behavior in the usual way. First, however, one must identify the threshold behavior of the unprojected kernel.

In expanded notation one has

$$K_{12}(\nu) = K_{12}(t_1,t_1';\ t_2,t_2';\ \nu) = K_{12}(k_1,w_1;\ k_2,w_2;\ \nu) \ ,$$

where k_i is the versor magnitude (continued cms momenta) of the channel (i,i'),

$$k_i = [-\Delta(t,t_i,t_i')]^{\frac{1}{2}} / 2(-t)^{\frac{1}{2}} \quad ,$$

and

$$w_i = (t_i - t_i') / 2(-t)^{\frac{1}{2}} \quad .$$

We shall define "threshold behavior in the (i,i') channel" to be any approach to the kinematic boundary $\Delta(t,t_i,t_i') = 0$ as shown, e.g., in Fig. 40, so that at the (1,1') threshold $k_1 \to 0$. (Variables t, t_i, t_i' here are negative.)

To determine, then, the behavior of K_{12} as k_1 or k_2 vanishes, we examine the functional and kinematic structures of K as shown in Figs. 18 and 14. As demonstrated in Appendix D, as $k_1 \to 0$, one has

$$\mathrm{ch}(h_1) \to \mathrm{const} \times (k_1)^{-1} \qquad \mathrm{ch}(f_2) \to \mathrm{const} \quad ,$$

but when $k_2 \to 0$ the situation is reversed

$$\mathrm{ch}(h_1) \to \mathrm{const} \qquad \mathrm{ch}(f_2) \to \mathrm{const} \times (k_2)^{-1} .$$

In Eq. (C.5) the function $F(-h_1)$, which appears as part of the kernel in Fig. 18, is given roughly as

$$F^{\alpha_1}_{n_1,\kappa_1 r_1}(-h_1) \doteq Q^{-\alpha_1-1}_{\alpha_1-n_1,\kappa_1 r_1}(-i\,\mathrm{sh}\, h_1) \quad .$$

Since $-i\,\mathrm{sh}(h_1) \to \infty$ as $k_1 \to 0$, one finds from the large z behavior z^{α} of $q^{-\alpha-1}_{\mu\nu}(z)$ that

$$k_1 \to 0 \Rightarrow F^{\alpha_1}(-h_1) \sim (k_1)^{-\alpha_1} \quad .$$

Similarly,

$$k_2 \to 0 \Rightarrow F^{\alpha_2}(+f_2) \sim (k_2)^{-\alpha_2} \quad .$$

Collecting similar factors from the upper vertex $\tilde{V}$ of Fig. 18, one may conclude that

$$K_{12}(\nu) = (k_1)^{-(\alpha_1+\overline{\alpha_1'})}(k_2)^{-(\alpha_2+\overline{\alpha_2'})} K'_{12}(\nu) \quad , \qquad (10.17)$$

where K' is a reduced amplitude, real on the uncut portion of the real t axis.

The threshold behavior of the projected kernel $K^j_{\mu\lambda}$ may now be found from the Froissart-Gribov projection (10.3). Equation (5.19) which expresses $ch(\nu_1)$ in terms of s_1 shows that

$$ch\nu_1 \to s_1/2k_1k_2$$

as either k_1 or $k_2 \to 0$. Therefore, using once again the large z behavior of $Q^j_{\mu\nu}(z) \sim z^{-j-1}$ and remembering that the integration in Eq. (10.3) actually begins above $z = 1$ at the lowest production threshold of the kernel, we pick up the usual extra factor $(k_1k_2)^j$, so that the complete threshold behavior of the projected kernel is given by

$$K^j_{\mu\lambda}(1,2) = (k_1)^{j-(\alpha_1+\overline{\alpha_1'})}(k_2)^{j-(\alpha_2+\overline{\alpha_2'})}(K')^j_{\mu\lambda}(1,2) \; . \qquad (10.18)$$

When this kernel is continued to the physical cross channel $t > 0$ and the four Reggeons taken to their physical points, we regain the usual threshold behavior given, e.g., by Jackson and Hite,[24]

$$(k_1)^{L_1(\min)}(k_2)^{L_2(\min)} \quad ,$$

where $L_i(\min) = J - S_i(\max)$ and $S_i(\max) = s_i + s_i'$.*

*In deriving this threshold condition we have ignored parity which causes the distinction between threshold and pseudothreshold and which may raise some $L(\min)$ by one unit.

Since the above analysis used only the kinematic structure of Fig. 18, one may conclude that this threshold behavior is equally applicable to the single-particle or clusterized kernels as well as to the full amplitude.

4. The Naturality Diagonalization

In Section (7) it was shown that in a parity-conserving theory the kernel $K_{12}(\nu)$ has the parity condition

$$K(\kappa_1,\kappa_2) = \sigma_1\sigma_1' \sigma_2\sigma_2' K(-\kappa_1,-\kappa_2) \quad , \tag{10.19}$$

where the σ_i are the naturalities — as defined in Eq. (3.9) — of the Reggeons attached to the kernel. The property (10.19) passes immediately to the projected kernel $K^j_{\mu\lambda}$ via (10.3).

At this juncture it is convenient to convert all Froissart projections like $K^j_{\mu\lambda}$ of (10.3) to lower-case projections $k^j_{\mu\lambda}$ defined by

$$k^j_{\mu\lambda}(1,2) \equiv \int_1 d(ch\nu)\, q^j_{\mu\lambda}(ch\nu)\, K_{12}(\nu) \quad , \tag{10.20}$$

where q is simply related to Q as in Eq. (A.13). The reason for this change is that q has a simpler helicity-negation symmetry than Q, a symmetry which of course is carried over into $k^j_{\mu\lambda}$,

$$k^j_{\mu\lambda}(1,2) = k^j_{-\mu,-\lambda}(1,2) \quad . \tag{10.21}$$

Combining (10.19) through (10.21) we find

$$k^j_{\mu\lambda}(\kappa_1,\kappa_2) = \sigma_1\sigma_1' \sigma_2\sigma_2' k^j_{-\mu,-\lambda}(-\kappa_1,-\kappa_2) \quad . \tag{10.22}$$

One may now study the effect of this symmetry on the ring

discontinuity components. Converting the ${}^{(2)}A$ equation to lower-case projections as in Eq. (10.20), one finds

$$ {}^{(2)}a^{j}_{\mu\mu'}(1,3) = \sum_{2}\sum_{\kappa_2}\int \frac{d\lambda}{i\pi}\; H^{j}_{\lambda}\; k^{j}_{\mu\lambda}(1,2)\; P_{\lambda}(2)\; k^{j}_{\lambda\mu'}(2,3)\;, \qquad (10.23) $$

where the κ_2 sum has been removed from Σ_2 and explicitly displayed, and where

$$ H^{j}_{\lambda} \equiv \Gamma(j+1+\lambda)\;\Gamma(j+1-\lambda) \quad . \qquad (10.24) $$

From the symmetry of (10.22), and the obvious fact [see Eq. (10.14)] that

$$ P_{\lambda}(\kappa_2) = P_{-\lambda}(-\kappa_2) \quad , \qquad (10.25) $$

one may easily show from (10.23) — using the symmetry of the λ contour — that the symmetry of (10.22) propagates into ${}^{(2)}a$,

$$ {}^{(2)}a^{j}_{\mu\mu'}(\kappa_1,\kappa_3) = \sigma_1\sigma_1'\;\sigma_3\sigma_3'\;{}^{(2)}a^{j}_{-\mu,-\mu'}(-\kappa_1,-\kappa_3) \quad , \qquad (10.26) $$

and similarly into all ${}^{(n)}a$ and the full a. The persistence of this symmetry means that all our projected equations can be diagonalized in the 2×2 space of the kappa indices; this is the naturality diagonalization discussed by Ciafaloni and Yesian.[5]

We now perform this diagonalization on the following prototype equation

$$ a^{j}_{\mu\mu'}(\kappa_1,\kappa_3) = \sum_{\kappa_2}\int \frac{d\lambda}{i\pi}\; H^{j}_{\lambda}\; b^{j}_{\mu\lambda}(\kappa_1,\kappa_2)\; p(\kappa_2\lambda)\; c^{j}_{\lambda\mu'}(\kappa_2,\kappa_3) \qquad (10.27) $$

where p is any function, and a,b,c are any functions having the symmetry of Eq. (10.26). Define

$$ a_{\kappa_1\kappa_3} \equiv a^{j}_{\kappa_1\mu,\kappa_3\mu'}(\kappa_1,\kappa_3) \qquad (10.28) $$

and similarly for b and c, and notice that

$$a_{-\kappa_1,-\kappa_3} = \sigma_1\sigma_1'\,\sigma_3\sigma_3'\,a_{\kappa_1\kappa_3} \quad . \tag{10.29}$$

Taking $\mu \to \kappa_1\mu$, $\lambda \to \kappa_2\lambda$, $\mu' \to \kappa_3\mu'$ in Eq. (10.27) yields

$$a_{\kappa_1\kappa_2} = \sum_{\kappa_2} \int \frac{d\lambda}{i\pi}\, H^j_\lambda\, b_{\kappa_1\kappa_2}\, p(\lambda)\, c_{\kappa_2\kappa_3} \tag{10.30}$$

since $H^j_{\kappa\lambda} = H^j_\lambda$. In terms of the projections of definite naturality*

$$a^\sigma \equiv \frac{1}{\sqrt{2}}\left[a_{++} + \sigma\sigma_1\sigma_1'\, a_{-+}\right] \quad . \tag{10.31}$$

Eq. (10.30) takes the diagonal form

$$a^\sigma = \int \frac{d\lambda}{i\pi}\, H^j_\lambda\, b^\sigma\, p(\lambda)\, c^\sigma \quad . \tag{10.32}$$

Thus, the naturality diagonalization of (10.27) is given by

$$a^{j\sigma}_{\mu\mu'} = \int \frac{d\lambda}{i\pi}\, H^j_\lambda\, b^{j\sigma}_{\mu\lambda}\, p(\lambda)\, c^{j\sigma}_{\lambda\mu'} \tag{10.33}$$

where

$$a^{j\sigma}_{\mu\mu'} = \frac{1}{\sqrt{2}}\left[a^j_{\mu\mu'}(+,+) + \sigma\sigma_1\sigma_1'\, a^j_{-\mu,\mu'}(-,+)\right] \quad . \tag{10.34}$$

In terms of upper-case projections like (10.3), Eq. (10.27) becomes

$$A^j_{\mu\mu'}(\kappa_1,\kappa_2) = \sum_{\kappa_2} \int \frac{d\lambda}{i\pi}\, B^j_{\mu\lambda}(\kappa_1,\kappa_2)\, p(\kappa_2\lambda)\, C^j_{\lambda\mu'}(\kappa_2,\kappa_3) \tag{10.35}$$

---

*For a discussion of why σ is identified with naturality, the reader is referred to page 438, equation (9.59) of the textbook of Martin and Spearman, Ref. 32.

and its naturality diagonalization is given by

$$A^{j\sigma}_{\mu\mu'} = \int^{\uparrow} \frac{d\lambda}{i\pi} \; B^{j\sigma}_{\mu\lambda} \, p(\lambda) \; C^{j\sigma}_{\lambda\mu'} \tag{10.36}$$

with projections of the form

$$A^{j\sigma}_{\mu\mu'} = \frac{1}{\sqrt{2}} \left[A^{j}_{\mu\mu'}(+,+) + \sigma\sigma_1\sigma_1' \, \frac{\Gamma(j+1+\mu)}{\Gamma(j+1-\mu')} \; A^{j}_{-\mu,\mu'}(-,+) \right] . \tag{10.37}$$

Now, since (10.8) is of the form (10.35), the naturality-diagonal bootstrap equation can be read from (10.33),

$$a^{j\sigma}_{\mu\mu'}(1,3) = k^{j\sigma}_{\mu\mu'}(1,3) + \sum_{\substack{\alpha_2\alpha_2' \\ n_2 n_2'}} \int d\phi_2 \int^{\uparrow} \frac{d\lambda}{i\pi} \; H^{j}_{\lambda} \; k^{j\sigma}_{\mu\lambda}(1,2)$$

$$\times \; \frac{H(2)}{\lambda - h_2} \; a^{j\sigma}_{\lambda\mu'}(2,3) \quad , \tag{10.38}$$

where

$$\left.\begin{aligned} H(2) &= (2\pi)^{-1} \, \gamma_2 \overline{\gamma}_2' \times \text{Eq. (10.15)} \\ H^{j}_{\lambda} &= \Gamma(j+1+\lambda) \, \Gamma(j+1-\lambda) \\ \int d\phi_2 &= \text{Eq. (8.10)} \end{aligned}\right\} \tag{10.39}$$

and

$$a^{j\sigma}_{\mu\mu'}(1,2) = \frac{1}{\sqrt{2}} \left[a^{j}_{\mu\mu'}(1,+;\, 2,+) + \sigma\sigma_1\sigma_1' \; a^{j}_{-\mu,-\mu'}(1,-;\, 2,+) \right], \tag{10.40}$$

where $\pm$ refers to the κ values, and similarly for $k^{j\sigma}_{\mu\mu'}$.

Left-shifting the helicity contour as suggested in Eq. (12.12) yields this final form for the planar bootstrap equation:

$$a^{j\sigma}_{\mu\mu'}(1,3) = k^{j\sigma}_{\mu\mu'}(1,3) + 2 \sum_{\substack{\alpha_2\alpha_2' \\ n_2 n_2'}} \int d\phi_2 \, H(2) \; H^{j}_{h_2} \; \hat{k}^{j\sigma}_{\mu h_2}(1,2) \; \hat{a}^{j\sigma}_{h_2\mu'}(2,3), \tag{10.41}$$

where $\hat{k}$ is a projection onto $\hat{q}$ of (A.20). All that remains is the transverse integration $d\phi_2$ and the sum over all upper and lower loop Reggeons and their associated helicity pole daughters. With $\mu = h_1$ and $\mu' = h_3$, Eq. (10.41) is a matrix (lattice) equation in the space of the helicity indices.

In passing, we note that the apparent Regge cuts in (10.41) due to poles of $H^j_{h_2}$ should be cancelled by the nonsense zeros of the product $\hat{k}\,\hat{a}$.

5. The Bootstrap Problem

Equation (10.41) states the integral equation which *is* the planar bootstrap for the four-Reggeon *ing discontinuity*. Assuming the existence of a family of Regge trajectories $\{\alpha_i\}$, and given a knowledge of the standard vertex V_{ijk}, one can in principle compute the single-particle kernel K and its projection $K^j_{\mu\lambda}$. Since the propagator is trivially known as in Eq. (10.14), one can then search for solutions A of the integral equation. The existence of a solution depends functionally on the Reggeon set $\{\alpha_i\}$ and the form of the vertex V.

The residue of the bootstrap equation at any Regge pole $j = \alpha$, where $\alpha \in \{\alpha_i\}$, yields the vertex bootstrap (10.10) which is perhaps more interesting than the original equation because it contains only one unknown function $V(t_1, t_2, t_3)$, given the Reggeon set $\{\alpha_i\}$. We return to the vertex bootstrap in a moment.

First we must note a certain inconvenient property of the functions A of Eq. (10.8) and the vertex G of (10.9). A side effect of doing the helicity pole expansion is that these functions are not

normalized in the sense of the standard Toller M-function discussed in Section (2). Figures 29 and 30 show schematically how A and G are related to the normalized ring amplitudes (ordered M-functions). The functions F and F' are like the F's appearing in Fig. 18 and Eq. (C.5). As noted earlier, the approximate role of these functions is to convert the Reggeon helicity from the discrete values m, r, p, ... as in Fig. 18 to the complex values $(\alpha - n)$.

Accounting for these normalization factors, we now rewrite the vertex bootstrap in the extremely schematic form of Fig. 31 which shows the bootstrap as a nonlinear functional integral equation of the 3-point ring amplitude and the Reggeon set $\{\alpha_i\}$. In principle, this equation should allow the computation of the ordered triple-Regge vertex as a function of all three arguments. To our knowledge, this calculation has never been done.

6. Counting

Approximate bootstrap calculations using a very small leading Reggeon set $\{\alpha_i\}$ have often indicated that the single-particle kernel, with experimentally determined couplings, does not have the strength necessary to elevate the generated output trajectories to their experimentally observed intercepts. Assuming that this result is not an artifact of the approximations made, one must conclude that the peripherality and/or the Regge-expansion convergence assumptions which go into the multiperipheral model are simply not viable for single-particle production, and one turns instead to cluster production. One replaces the single-particle kernel with a cluster of limited maximum width, but sufficiently broad so as to approximately

Regge-factorize, even though there is no Regge pole in such a kernel. This is the concept of the dotted Reggeon, and the program of Fig. 31 is then replaced with that of Fig. 32 which, when the left coupling is boldly cancelled on both sides, gives the famous equation " 1 = gNg " of Ref. 25, where N = N (flavor).

In going to the multi-particle kernel, however, one encounters certain counting problems which invalidate the diagonalization procedure which led to the simple equation (10.8). The necessary alterations involve pre-convoluting the cluster/kernel with a propagator on one side.[26,27] To avoid this counting problem, we have chosen to concentrate instead on the cylinder calculation where there is no counting difficulty.

(11) THE CYLINDER

The ordered or planar bootstrap discussed in the preceding section consists of sewing together two ordered amplitudes (zero handles, one boundary) in an ordered manner so as to obtain the discontinuity of another ordered amplitude. By sewing together ordered amplitudes (h=0, b=1) with a certain well-defined disorder, one may construct the cylinder component (h=0, b=2) of the physical 4-point function. Figure 33 shows parts of this cylinder component in several different notations. Figure 33a depicts, in quark diagram notation, a particular contribution to the two-twist-pair piece $C^{(2)}$ of the cylinder resulting from the unitarity product of two 9-point ordered amplitudes. Figure 33b shows the complete $C^{(2)}$, but the figure only has meaning in terms of discontinuities after

the upper and lower Regge expansions have been inserted. These are shown in Fig. 33c which is now drawn in the ring notation. Finally, Figs. 33d and 33e display the topological meaning of the twists in the absence of quark notation. To conform with the kinematic diagrams like Fig. 15, we shall continue to use the notation of Fig. 33c.

The full cylinder is defined as the sum of all its twist-pair components,

$$C = \sum_{i=1}^{\infty} C^{(n)} \quad . \tag{11.1}$$

When the $C^{(2)}$ component shown in Fig. 33c is diagonalized onto angular momentum j, charge conjugation* τ, and naturality σ, one obtains the triple pole configuration shown in Fig. 34 (when the simplest assumptions are made for the j and flavor dependence of the various elements, and when only the leading helicity pole of the leading Reggeon pair is kept in each Reggeon loop)

$$^{(2)}C^{\tau} \doteq g \frac{1}{j-\alpha} (\tau k) \frac{1}{j-\alpha} (\tau k) \frac{1}{j-\alpha} g \quad , \tag{11.2}$$

where

$$k = k(t) = k(j,t) = \int d\phi_1 \cdot g(t,t_1,t_1')^2 \times \{\text{other factors}\}. \tag{11.3}$$

In the phenomenology of Chew and Rosenzweig[10] the cylinder-shifts of the f, f', ω, and ϕ trajectories are simple functions of k, which is sometimes approximated by setting $j = \alpha$. Roughly, the

*We are relieving τ from its tradition duty of representing signature since signature seems to play such a small role in the ordered S-matrix, and also because there are already too many C's floating around in Section (11).

shifted f = pomeron has the intercept [in SU(1)]

$$\alpha_p(0) \doteq \alpha(0) + k(\alpha,0) \quad . \tag{11.4}$$

We wish to discuss the technique used to arrive at the expression (11.3) for k and to suggest how k might more accurately be calculated as a helicity-pole expansion. After first diagonalizing the charge conjugation, we review a one-dimensional cylinder calculation and then proceed to the three-dimensional helicity pole analysis.

1. Diagonalization of the Charge Conjugation

Since the cylinder terms $C^{(n)}$ carry zero additive quantum numbers, it is desirable to diagonalize the charge conjugation in addition to the naturality so that cylinder poles can be identified with physical particles. This procedure is very simple, as we now show.

The ordered ring discontinuities carry orientation indices which have been suppressed throughout this paper. One might write $\langle 1,\sigma_1|A|2,\sigma_2\rangle$ where $\sigma_i = \pm 1$ depending on whether the ordered channel i lies in the clockwise or counterclockwise Hilbert space.[7] As a 2×2 matrix in this orientation space, A is diagonal with equal diagonal elements, $\langle 1,\sigma_1|A|2,\sigma_2\rangle = A\,\delta_{\sigma_1,\sigma_2}$. Changing to the charge-conjugation basis $|1,\tau\rangle = [|1,\sigma_1=+\rangle + \tau|1,\sigma_1=-\rangle]/\sqrt{2}$, one finds that $\langle 1,\tau_1|A|2,\tau_2\rangle = A\,\delta_{\tau_1,\tau_2}$, so there is no need for A itself to carry a τ label.

In contrast, the twisted Reggeon propagator ${}^xP$ always connects states of opposite orientation, $\langle 1,\sigma_1|{}^xP|2,\sigma_2\rangle = \delta_{\sigma_1,-\sigma_2}\,{}^xP$. In the τ basis ${}^xP$ is again diagonal but the elements have opposite sign, so

${}^{x}P$ must carry a trivial τ label,

$$(1,\tau|{}^{x}P|2,\tau') = \delta_{\tau,\tau'}\,{}^{x}P^{\tau} \qquad \text{where} \qquad {}^{x}P^{\tau} = \tau\,{}^{x}P \ . \qquad (11.5)$$

Therefore, the only effect of charge conjugation diagonalization is to add a τ label to the $C^{(n)}$ and to replace ${}^{x}P \to \tau\,{}^{x}P$ everywhere.

By comparison, the untwisted Reggeon propagator P which appears in the planar bootstrap does not mix orientations, so all contributions $A^{(n)}$ to the ring discontinuity A are diagonal with equal diagonal elements in the orientation space and therefore also in the τ basis, assuming the special case of zero additive quantum numbers along the chain.

2. The Cylinder in Rapidity

For comparison with the kinematically accurate (though still physically slippery) cylinder calculation presented in the next sections, we review here a "typical" rapidity analysis of the cylinder. For simplicity, only one flavor is assumed instead of the three flavors (with $1 \approx 2 \neq 3$ symmetry breaking) used by Chew and Rosenzweig.[10]

In terms of the usual rapidity or Chew-Pignotti[28] variables, and with the CGL phase-space approximation discussed earlier in Section (8), one writes in the energy plane the one-twist term of the cylinder as follows (see Fig. 35):

$$\begin{aligned} {}^{(1)}C^{\tau}(t_1^{\pm},y,t_3^{\pm}) &= \int_0^y dx_1 \int_0^y dg \int_0^y dx_2\ \delta(y - x_1 - g - x_2) \\ &\quad \times \int d\phi_2\ A(t_1^{\pm},x_1,t_2^{\pm})\ {}^{x}P^{\tau}(g,t_2^{\pm})\ A(t_2^{\pm},x_2,t_3^{\pm}) \ , \end{aligned} \qquad (11.6)$$

with $d\phi_2$ as given in Eq. (8.10). Here, A is the absorptive part of a four-Reggeon ring amplitude of rapidity width x_i, and ${}^{x}P^{\tau}$ is the twisted (no cosine) Reggeon propagator of gap width g to be given below. The label τ indicates that the equation has been diagonalized in the charge conjugation, $\tau = \pm 1$.

Incorporating the Neveu-Schwarz shift $\alpha \to \alpha - 1$, we normalize our triple-Regge couplings in the usual way,

$$R(t_1^{\pm},s,t_2^{\pm}) \doteq g_1 g_2 \, \Gamma(1-\alpha)(-s)^{\alpha} \tag{11.7}$$

$$A(t_1^{\pm},s,t_2^{\pm}) = \frac{\pi}{\Gamma(\alpha)} \, g_1 g_2 \, (+s)^{\alpha} \quad , \tag{11.8}$$

and take for the Mellin-projected ring discontinuity a form exhibiting symmetric nonsense zeros,

$$A(t_1^{\pm},j,t_2^{\pm}) \approx \frac{\pi}{\Gamma(\alpha)} \left[g_1\left(\frac{j-\alpha_{c_1}}{\alpha-\alpha_{c_1}}\right)\right] \frac{1}{j-\alpha} \left[g_3\left(\frac{j-\alpha_{c_3}}{\alpha-\alpha_{c_3}}\right)\right] . \tag{11.9}$$

The presence of nonsense-zeros in a Mellin projection is equivalent to the absence of fixed-poles in the Froissart-Gribov projection; we want such fixed-poles to be absent because we assume there to be no fixed powers in the ring amplitude $R(t_1^{\pm},s,t_2^{\pm})$.

The assumption of the first nonsense-zero in a Mellin projection corresponds to the absence of a constant term on the right-hand side of a FMSR over $A(t_1^{\pm},s,t_2^{\pm})$. By attempting to respect the analytic structure of multi-Regge amplitudes, several authors[29] have used somewhat controversial asymmetric FMSR to argue that, in effect, the amplitude shown in Eq. (11.9) should have a nonsense-zero on one side or the other (depending on which external overlapping invariant is held fixed), but not on both sides; i.e., that the form of (11. ,

should be asymmetric. We feel, however, that the four-Reggeon amplitude should be left/right symmetric, even if asymmetric NMC is used in its generation, and this is our motivation for the form (11.9), though we have no rigorous argument to support this conjecture.

One of the physical weaknesses of the cylinder calculation is that small changes in the smooth (i.e., non-singular) j-dependence of the projected planar amplitude, such as nonsense zeros, can cause violent changes in the output pomeron location,[30] so no calculation can be trusted until the low-energy/smooth-j behavior of the planar amplitude has been determined from the planar bootstrap. Hopefully, such behavior might be computed from the helicity pole formalism. Meanwhile, we shall use the form (11.9) only as a prototype and continue our calculation.*

The twisted Reggeon propagator appearing in (11.6) is

$$ {}^{x}P^{T}(g,t_2^{\pm}) = \tau\tilde{H}(t_2^{\pm})\,\exp(g\alpha_{c_2}) \quad . \tag{11.10}$$

In Mellin projection this becomes

$$ {}^{x}P^{T}(j,t_2^{\pm}) = \frac{\tau\tilde{H}(t_2^{\pm})}{j-\alpha_{c_2}} \tag{11.11}$$

with

$$ \tilde{H}(t_2^{\pm}) = \Gamma(1-\alpha_2^{+})\,\Gamma(1-\alpha_2^{-}) \quad , \tag{11.12}$$

which may be compared to (10.12) with (10.16).

Now, the $C^{(1)}$ equation (11.6) may be trivially Mellin diagonalized to yield

$$ {}^{(1)}C^{T}(t_1^{\pm},j,t_3^{\pm}) = \int d\phi_2\; A(t_1^{\pm},j,t_2^{\pm})\left[\frac{\tau\tilde{H}(2)}{j-\alpha_{c_2}}\right]A(t_2^{\pm},j,t_3^{\pm}). \tag{11.13}$$

*Low energy *data* are, of course, helpful on this point.

Inserting the expression (11.9) we find

$$^{(1)}C^{\tau}(t_1^{\pm},j,t_3^{\pm}) = \frac{\pi}{\Gamma(\alpha)}\left[g_1\left(\frac{j-\alpha_{c_1}}{\alpha-\alpha_{c_1}}\right)\right]\frac{[\tau k(j)]}{(j-\alpha)^2}\left[g_3\left(\frac{j-\alpha_{c_3}}{\alpha-\alpha_{c_3}}\right)\right] \qquad (11.14)$$

with

$$k(j) = \frac{\pi}{\Gamma(\alpha)}\int d\phi_2\; g_2^2\,\tilde{H}(t_2^{\pm})\,\frac{(j-\alpha_{c_2})}{(\alpha-\alpha_{c_2})^2} \quad . \qquad (11.15)$$

By employing symmetric nonsense zeros in (11.9), we have removed the Regge-cut generating factor of the propagator (11.11), and have added another factor $(j-\alpha_{c_2})$ in the numerator; $k(j)$ is j-dependent.

From the diagonalized integral equation for the full cylinder,

$$C^{\tau}(1,j,3) = {}^{(1)}C^{\tau}(1,j,3) + \int d\phi_2\; A(1,j,2)\;{}^{x}p^{\tau}(j,2)\;C^{\tau}(2,j,3), \qquad (11.16)$$

or by simply summing the geometric series the first term of which is given by (11.14), one finds that

$$C^{\tau}(1,j,3) = \frac{\pi}{\Gamma(\alpha)}\left[g_1\left(\frac{j-\alpha_{c_1}}{\alpha-\alpha_{c_1}}\right)\right]\frac{\tau k(j)}{(j-\alpha)(j-\alpha-\tau k(j))}\left[g_3\left(\frac{j-\alpha_{c_3}}{\alpha-\alpha_{c_3}}\right)\right], \qquad (11.17)$$

which shows the pomeron ($\tau = +$) at the solution of

$$j = \alpha + k(j) \quad . \qquad (11.18)$$

Finally, adding C to the planar term A extinguishes the unshifted pole in the manner of Ref. 10,

$$A(1,j,3) + C^{\tau}(1,j,3) = \frac{\pi}{\Gamma(\alpha)}\left[g_1\left(\frac{j-\alpha_{c_1}}{\alpha-\alpha_{c_1}}\right)\right]\frac{1}{j-(\alpha+\tau k)}\left[g_3\left(\frac{j-\alpha_{c_3}}{\alpha-\alpha_{c_3}}\right)\right], \qquad (11.19)$$

and the symmetric nonsense zeros appear also in the cylindrically corrected amplitude.

3. The One-Twist Cylinder Term as a Helicity Pole Expansion

The typical multi-cluster contribution ${}^{(3)}\tilde{A}(\xi,\nu,\xi')$ to the four-Reggeon ring discontinuity was given in (10.1) and illustrated in Fig. 22. The sum of all such terms defines the complete *four-Reggeon ring discontinuity* in the "energy plane." Of necessity, the object $\tilde{A}$ contains the propagators on both ends of the multiperipheral ladder. It is important to realize that $\tilde{A}$ contains these end-propagators *in convolution*, so that, unlike the kernel, $\tilde{A}(\xi,\nu,\xi')$ *cannot* be written in the form

$$\tilde{A}_{12}(\xi,\nu,\xi') = P_1(\xi)\, A_{12}(\nu)\, P_2(\xi') \quad .$$

Only after diagonalization can the end-propagators be removed as in (10.5). For this reason, it is difficult to write cylinder terms — in particular $C^{(1)}$ — in the energy plane, but very easy to write these terms in projection, as we now show.

Let us define an extremely condensed notation so that, for example, Eq. (10.1) or its diagonalization (10.2) both read:

$${}^{(3)}\tilde{A} = PKPKPKP \quad .$$

Similarly, the planar bootstrap reads

$$\begin{aligned} \tilde{A} &= PKP + PK\tilde{A} && \text{[energy plane, see (10.7)]} \ , \\ A &= K + KPA && \text{[j-plane, see (10.8)]} \ . \end{aligned} \qquad (11.20)$$

In this notation, the $C^{(1)}$ cylinder term may be written in the energy plane as

$$\tilde{C}^{(1)} = \tilde{A}KP_xK\tilde{A} + PKP_xK\tilde{A} + \tilde{A}KP_xKP + PKP_xKP \quad , \qquad (11.21)$$

where P_x is the twisted helicity pole propagator (see below). The

diagonalization of (11.21) is, in our condensed notation, again (11.21). Once (11.21) has been diagonalized, we may use (10.5) to expose the propagators so that

$$\tilde{C}^{(1)} = P[APK + K]\, P_x[KPA + K]P \qquad \text{(j-plane)}. \quad (11.22)$$

Inserting the planar bootstrap (11.20) twice yields

$$\tilde{C}^{(1)} = PAP_xAP \qquad \text{(j-plane)}. \quad (11.23)$$

Finally, in analogy to (10.5), we define $C^{(1)}$ in terms of $\tilde{C}^{(1)}$ to get

$$C^{(1)} = AP_xA \qquad \text{(j-plane)},$$

which, in full j-plane notation, reads

$$^{(1)}C^{j}_{\mu\mu'}(1,3) = \sum_2 \int \frac{d\lambda}{i\pi}\, A^{j}_{\mu\lambda}(1,2)\; {}^{x}P_{\lambda}(2)\; A^{j}_{\lambda\mu'}(2,3) \quad . \quad (11.24)$$

This equation, illustrated in Fig. 36, gives the projected one-twist cylinder term in terms of the projected ring discontinuity A which solves the bootstrap (10.8).* From (10.14),

$$^{x}P_{\lambda}(2) = \frac{H(2)}{\kappa_2\lambda_2 - h_2} \quad , \quad (11.25)$$

where H(2) is given by (10.12) with the signature-factor product replaced this time by (10.16).

Adding the naturality and charge conjugation labels [see Sections (10.4) and (11.1)], (11.24) becomes

$$^{(1)}C^{j\sigma\tau}_{\mu\mu'}(1,3) = \sum_2 \int \frac{d\lambda}{i\pi}\, H(2)\; A^{j\sigma}_{\mu\lambda}(1,2)\left[\frac{\tau}{\lambda - h_2}\right] A^{j\sigma}_{\lambda\mu'}(2,3) \quad , \quad (11.26)$$

---

*Notice that Eq. (11.24) does not say $C^{(1)} = KP_xK$.

or, in terms of the lower-case projections of (10.20),

$$ {}^{(1)}C^{j\sigma\tau}_{\mu\mu'}(1,3) = \sum_{\lambda} \int \frac{d\lambda}{i\pi} H(\lambda)\, H^{j}_{\lambda}\, \mathcal{A}^{j\tau}_{\mu\lambda}(1,2)\, \frac{\tau}{\lambda - h_2}\, \mathcal{A}^{j\sigma}_{\lambda\mu'}(2,3) \ , \tag{11.27} $$

with $H^{j}_{\lambda} = \Gamma(j+1+\lambda)\Gamma(j+1-\lambda)$.

4. Angular Momentum vs. Helicity

We pause to make a few observations about Eq. (11.27). First, it should be clear that the "Reggeon propagator" (11.25) is not directly related to the angular momentum j, in contrast to the feeling one gets from the rapidity approximation. That is, the leading helicity-pole propagator has the form $1/(\lambda - h_2)$, not $1/(j - \alpha_c)$ as in Eq. (11.13). As emphasized in Appendix E, the variable ξ which measures the energy dependence of the object we loosely call a Reggeon propagator is the analytic continuation of an azimuthal Euler angle, not a central Euler angle like θ of (ϕ,θ,ϕ'). Therefore, the correctly projected propagator is a function of the variable conjugate to that continued azimuth ξ, namely, the continued helicity λ, and not the angular momentum j. The rapidity formalism with its collinear boosts is incapable of distinguishing angular momentum from helicity, and projects everything onto a hybridized Mellin projection index "J". One feels that asymptotically - i.e., near singularities in the projection index - this hybridization is acceptable. Even so, it seems unlikely that the low-energy behavior of a planar discontinuity could be determined from a planar bootstrap which uses such an approximation, and the same goes for the cylinder. For example, it is just this distinction between j and the variable λ (which is forced to the value $h_2 = \alpha_{c_2} + 1$) which gives rise to the threshold factor appearing in Eq. (11.38) below.

5. Regge Cuts and Nonsense Zeros

The λ-plane for Eq. (11.27) is shown in Fig. 37. As j is varied, the helicity contour is repeatedly pinched between the helicity pole at $\lambda = h_2$ and the poles of $\Gamma(j + 1 - \lambda)$. Each pinch generates a pole in j which is in turn converted to a Regge cut by the transverse integration $d\phi_2$. These j-plane poles are, of course, explicit when the helicity contour in (11.27) is left-shifted as per (12.12) to give

$$
{}^{(1)}C^{j\sigma\tau}_{\mu\mu'}(1,3) = 2\pi \sum_{\substack{\alpha_2\alpha_2' \\ n_2 n_2'}} \int d\phi_2 \; H(2) \; \Gamma(j + 1 + h_2) \; \Gamma(j + 1 - h_2)
$$

$$
\times \; \hat{a}^{j\sigma}_{\mu h_2}(1,2) \; \hat{a}^{j\sigma}_{h_2\mu'}(2,3) \quad . \tag{11.28}
$$

Keeping only the leading helicity poles of the leading Reggeons so that

$$
h_2 = \alpha_2 + \tilde{\alpha}_2' \equiv \alpha_{c_2} + 1 \tag{11.29}
$$

and setting $\mu = \mu' = 0$, (11.28) becomes

$$
{}^{(1)}C^{j\sigma\tau}_{00}(1,3) = \tau \int d\phi_2 \, [2H(2)] \; \Gamma(j + \alpha_{c_2} + 1) \; \Gamma(j - \alpha_{c_2})
$$

$$
\times \; \hat{a}^{j\sigma}_{0h_2}(1,2) \; \hat{a}^{j\sigma}_{h_2 0}(2,3) \tag{11.30}
$$

which may be compared to the rapidity result (11.13),

$$
{}^{(1)}C^{j\tau}(1,3) = \tau \int d\phi_2 \; [\tilde{H}(2)] \; (j - \alpha_{c_2})^{-1} \cdot a^j(1,2) \; a^j(2,3) \; . \tag{11.31}
$$

Whereas (11.31) shows only the first Regge cut, (11.30) exhibits the complete family of Regge cuts associated with the Reggeon pair α_2, α_2'. Recall, however, that if the upper-case projections $A^j_{\mu\mu'}$

lack fixed poles at the nonsense points, the lower case $a^j_{\mu\mu'}$ have nonsense zeros. We presume, then, that these amplitudes in fact have a string of nonsense zeros which cancel all the gamma function poles and thereby eliminate all Regge cuts from the cylinder, just as we contrived to do in the rapidity model. More significantly, the same mechanism should remove Regge cuts from the planar bootstrap. Unfortunately, we have been unable to pursue this question due to a technical difficulty which we discuss in Section (12).

6. The Complete Twisted Reggeon Loop

Since the A's appearing in (11.26) are the projections of ring discontinuities, their j-plane singularity structure contains, hopefully, only Regge poles. We then write as an asymptotic series,

$$A^j_{\mu\lambda}(1,2) = \sum_\alpha \frac{\left[\sqrt{\frac{\pi}{\Gamma(\alpha)}}\, G^{j\sigma}_\mu(1;\alpha)\right]\left[\sqrt{\frac{\pi}{\Gamma(\alpha)}}\, G^{j\sigma}_\lambda(2;\alpha)\right]}{(j-\alpha)} , \tag{11.32}$$

where the G are triple-Regge couplings,

$$G^{j\sigma}_\mu(i;\alpha) = G^{j\sigma}_\mu(\alpha_i,\alpha_i';\ t_i,t_i';\ \alpha,t) \quad ,$$

whose normalization was discussed in Section (10.5) and shown in Fig. 30. Near a particular Regge-pole, Eq. (11.32) reduces to the form (10.9) given earlier, but in general we wish to maintain the j-dependence in the triple-Regge couplings, as discussed below.

Since $G^j(1;\alpha)$ couples two Reggeons (α_1,α_1') to a third Reggeon α, it is clear that the coupling vanishes if α has the wrong naturality, so we now drop the naturality label, keeping in mind that (11.32) represents a sum only over trajectories of the proper naturality.

Inserting the pure Regge pole expansion (11.32) twice into (11.26), we find for the projected one-twist cylinder term

$$
{}^{(1)}C^{j\tau}_{\mu\mu'}(1,3) = \sum_{\alpha,\alpha'} \left[\sqrt{\frac{\pi}{\Gamma(\alpha)}}\; G^j_\mu(1;\alpha)\right] \frac{1}{j-\alpha} \left\{\tau k^j_{\alpha\alpha'}(t)\right\} \frac{1}{j-\alpha'}
$$

$$
\times \left[\sqrt{\frac{\pi}{\Gamma(\alpha')}}\; G^j_{\mu'}(3;\alpha')\right] \quad , \tag{11.33}
$$

where

$$
k^j_{\alpha\alpha'}(t) = \frac{\pi}{\sqrt{\Gamma(\alpha)\Gamma(\alpha')}} \sum_2 \int \frac{d\lambda}{i\pi} H(2) \left[G^j_\lambda(2;\alpha) \frac{1}{j-h_2} G^j_\lambda(2;\alpha')\right] . \tag{11.34}
$$

When the helicity contour is shifted to the left as suggested in Section (12), the resultant k is

$$
k^j_{\alpha\alpha'}(t) = \frac{2\pi}{\sqrt{\Gamma(\alpha)\Gamma(\alpha')}} \sum_2 H(2)\; [\hat{G}(2;\alpha)]^j_{h_2}\; [\hat{G}(2;\alpha')]^j_{h_2} . \tag{11.35}
$$

In our Regge pole expansion (11.32) for the ordered four-Reggeon discontinuity $A^j_{\mu\lambda}(1,2)$, we have exhibited the triple-Regge couplings as being j-dependent, just as in the rapidity version (11.9). Usually Regge couplings are presumed to be independent of j, e.g.,

$$
A_{ab}(j) = \frac{\gamma_a\gamma_b}{(j-\alpha)} \quad ,
$$

so we wish to comment on this point. The Regge expansion given in (11.32) is supposed to be a reasonable approximation to the exact partial wave amplitude $A^j_{\mu\lambda}(1,2)$. However, we know from (10.18) that when $k_1 \to 0$ or $k_2 \to 0$ [k_i are the continued cms momenta, see Eq. (5.7)], the partial wave amplitude $A^j_{\mu\lambda}(1,2)$ must exhibit the characteristic threshold behavior,

$$
[A(1,2)]^j_{\mu\lambda} \to (k_1)^{j-\alpha_{c_1}-1} (k_2)^{j-\alpha_{c_2}-1} [A'(1,2)]^j_{\mu\lambda} . \tag{11.36}
$$

Therefore, in order that the (finite) Regge expansion (11.32) be accurate, we must assume that the couplings also exhibit this threshold behavior,

$$[G(2;\alpha)]^j_\lambda = (k_2)^{j-\alpha_{c_2}-1} [G'(2;\alpha)]^j_\lambda \quad . \tag{11.37}$$

We might then ignore the j-dependence of the *residual coupling* G'. In particular, we have already noted that G' should have no fixed poles in j.

Therefore, a model for the complete twisted Reggeon loop k accounting for this threshold behavior and lack of fixed poles is

$$k^j_{\alpha\alpha'}(t) = \frac{2\pi}{[\Gamma(\alpha)\Gamma(\alpha')]^{\frac{1}{2}}} \sum_{\alpha_2,\alpha_2'} \sum_{n_2 n_2'} \frac{2\pi}{f} \int_{-\infty}^{\infty} dw_2 \int_0^{\infty} dk_2 (k_2^2)^{j-\alpha_{c_2}} H(2)$$

$$\times [\hat{G}'(2;\alpha)]^j_{h_2} [\hat{G}'(2;\alpha')]^j_{h_2} \quad , \tag{11.38}$$

where we have used $d\phi_2 = (2\pi/f)\, k^2 dk dw$ as given in Eq. (8.10), and where H(2) is Eq. (10.12) with (10.16). In the past, expressions for k have not shown this threshold behavior because the projected triple-Regge coupling has been identified with the j-independent dual coupling

$$g(t,t_2,t_2') = \frac{\Gamma(\alpha+1)}{\Gamma(\alpha-\alpha_{c_2})} \quad .$$

The complete twisted Reggeon loop and its relation to $C^{(1)}$ are shown in Fig. 38. There, the loop is cross-hatched to indicate that it is a *complete* twisted Reggeon loop incorporating the effects of all the helicity poles of all Reggeon pairs.

We may now compare this precise Reggeon loop to its approximation in the rapidity model as given in Eq. (11.15). First, since we have included more than one Regge pole in our approximation to A^j, the k of (11.38) is a matrix in the space of the Reggeon set $\{\alpha_i\}$, whereas (11.15) shows only the leading diagonal element of this matrix. Secondly, the usual numerator gamma functions of (11.12) which contain the physical poles of the propagator, now appear as sines in the denominator of the factor $H(2)$, with the job of ghost removal now incumbant upon the couplings G in the sense of Eq. (2.8). We have retained the ϵ_2, ϵ_2' factors in $H(2)$ to allow for fermions on the top and/or bottom of the Reggeon loop. For example, the upper and lower Reggeons must both be baryons in the contribution to the cylinder which mixes regular mesons with baryonium states,[31] (see Fig. 39). Finally, the k appearing in (11.15) contains only the leading pair of Reggeons (α_2, α_2'), and only the leading helicity pole corresponding to that pair, i.e., $n_2 = n_2' = 0$.

7. The Full Cylinder

So far we have discussed the zero and one-loop contributions to the full cylinder, Eqs. (11.32) and (11.33), which we now rewrite in an abbreviated notation

$$C^{(0)}(1,3) = g(1)_i \, P_i \, g(3)_i$$

$$C^{(1)}(1,3) = g(1)_i \, P_i \, K_{ij} \, P_j \, g(3)_j \quad ,$$

where now $P_i = (j - \alpha_i)^{-1}$ and $K_{ij} = \tau k_{\alpha_i \alpha_j}$. To compute the full cylinder including the planar part,

$$\overline{C}(1,3) = \sum_{n=0}^{\infty} C^{(n)}(1,3) \quad ,$$

we remove the external couplings on the ends to make matrices of the $C^{(n)}$, and we replace the P_i with diagonal matrices

$$P_{ij} = \delta_{ij} P_i = \delta_{ij}(j - \alpha_i)^{-1} \quad .$$

Then $\overline{C}$ is a geometric matrix series which one sums to get

$$[\overline{C}(1,3)]_{ij} = [P + PKP + \ldots]_{ij} = [P^{-1} - K]^{-1}_{ij} = \frac{[\mathrm{cof}^T(P^{-1} - K)]_{ij}}{\det(P^{-1} - K)} \; .$$

The locations of the poles of the full cylinder are then determined by

$$\det D(j,t) = 0 \tag{11.39}$$

where

$$[D(j,t)]_{ij} = \big(j - \alpha_i(t)\big)\delta_{ij} - \tau k^j_{ij}(t) \quad , \tag{11.40}$$

with k_{ij} as given in Eq. (11.34). In practice, one can restrict to a small number of leading planar trajectories and include symmetry breaking. If the matrix space is crudely limited to one dimension, Eq. (11.40) shows that k recovers its simple significance as the shift between the pomeron and planar Reggeon in the one-flavor model, as in Eq. (11.18).

(12) FIXED POLES, NONSENSE ZEROS, AND THE HELICITY CONTOUR PROBLEM

Whereas the diagonalization procedure described in Section (9) is straightforward, the problem of shifting the helicity contour in the diagonalized equation is still, we feel, an unresolved question. Rather than bury this discussion in the cylinder calculation above, we thought it best to expose the problem clearly in the hope that someone will solve it, and to show the drastic assumption we make in the end. The problem described here in effect blocks the completion

of the helicity pole expansion program.

Consider a simpler version of Eq. (9.1),

$$A(g) = \int d\mathbf{g}_1\, B(\mathbf{g}_1)\, C(g_2) \qquad , \tag{12.1}$$

or its diagonalization

$$A^j_{\mu\mu'} = \int_1^\infty \frac{d\lambda}{2\pi}\, B^j_{\mu\lambda}\, C^j_{\lambda\mu'} \qquad , \tag{12.2}$$

with projections as given in Eqs. (9.4) and (9.5), which we now write as

$$C^j_{\lambda\mu'} = \int_1^\infty dz\, Q^j_{\lambda\mu'}(z)\, C_{\lambda\mu'}(\nu) \qquad (z = \mathrm{ch}\,\nu) \tag{12.3}$$

$$C_{\lambda\mu'}(\nu) = \int_{-\infty}^{\infty} \frac{d\xi}{2\pi}\, e^{-\lambda\xi} \int_{-\infty}^{\infty} \frac{d\xi'}{2\pi}\, e^{-\mu'\xi'}\, C(\xi,\nu,\xi') \tag{12.4}$$

and similarly for $A^j_{\mu\mu'}$, out for $B^j_{\mu\lambda}$ we have

$$B^j_{\mu\lambda} = \int_1^\infty dz\, Q^j_{\mu\lambda}(z)\, B_\mu(\nu) \tag{12.5}$$

$$B_\mu(\nu) = \int_{-\infty}^{\infty} \frac{d\xi}{2\pi}\, e^{-\mu\xi}\, B(\xi,\nu,0) \qquad . \tag{12.6}$$

The functions $Q^j_{\lambda\mu'}(z)$, like the regular $Q_j(z)$, have poles in j and therefore (it turns out) in λ and μ', and this certainly suggests *that the projections like* $C^j_{\lambda\mu'}$ of Eq. (12.3) might also have these "fixed poles," although this is not necessarily the case. Nevertheless, it is useful to convert from the functions $Q^j_{\lambda\mu'}$ to the $q^j_{\lambda\mu'}$ of Eq. (A.13) which are analytic in j, λ, μ' and have no zeros, at least for $\mathrm{Re}(j) > -1$. Defining new, lower-case projections as in Section (10),

$$c^j_{\lambda\mu'} = \int_1^\infty dz\, q^j_{\lambda\mu'}(z)\, C_{\lambda\mu'}(\nu) \qquad , \tag{12.7}$$

we can say that if $C^j_{\lambda\mu'}$ has no "fixed poles," then $c^j_{\lambda\mu'}$ must have zeros (nonsense zeros), since c is the residue of the pole in C. (In this sense, c is closer to the Mellin projection than C.)

In terms of the lower-case projections, (12.2) becomes

$$a^j_{\mu\mu'} = \int \frac{d\lambda}{i\pi} H^j_\lambda \, g^j_{\mu\lambda} \, c^j_{\lambda\mu'} \quad , \tag{12.8}$$

where $H^j_\lambda = \Gamma(j+1+\lambda)\Gamma(j+1-\lambda)$. As $\lambda \to i\infty$, $H^j_\lambda \to \exp(-\pi|\lambda|)$, providing the excellent apparent convergence for the helicity integration. One pays a price to get this exponential damping, however: H^j_λ has poles going off in both real directions in the λ-plane (see Fig. 37). Suppose $g^j_{\mu\lambda}$ is analytic in λ and $c^j_{\lambda\mu'}$ has a simple pole at, say, $\lambda = h = -1+i$. One would like to say that, when the contour is shifted to the left, this pole makes a contribution to $a^j_{\mu\mu'}$. However, the poles of H^j_λ also make contributions, and to make matters worse, the poles of $c^j_{\lambda\mu'}$ at $\lambda = h$ can pinch the contour against all the poles of $\Gamma(j+1-\lambda)$ causing $a^j_{\mu\mu'}$ to have poles in j ("Regge cuts"). Since Regge cuts are unwanted in the cylinder or planar bootstrap, we would like to claim that the poles of $\Gamma(j+1-\lambda)$ are cancelled by nonsense zeros in the projections like $c^j_{\lambda\mu'}$, which is to say, the Froissart-Gribov projection $C^j_{\lambda\mu'}$ has no fixed poles. This sounds reasonable if $C^j_{\lambda\mu'}$ is the projection of an ordered (planar) amplitude where fixed poles must be absent so that the Regge cut discontinuity formulas give zero discontinuity, circularly speaking.

Granting that the product $g^j_{\mu\lambda} \, c^j_{\lambda\mu'}$ has full nonsense zeros to cancel the poles of $\Gamma(j+1-\lambda)$ and remove Regge cuts, one must still consider the problem of shifting the contour. It must be impossible to shift to the right because then one gets $a^j_{\mu\mu'} = 0$, certainly not

desirable. Shifting to the left yields a contribution from the pole at $\lambda = h$, but still there are all the poles of $\Gamma(j+1+\lambda)$. The conjectured form of the helicity nonsense zeros of Eq. (2.8) suggests that the zeros in the λ-plane should be symmetric and therefore the poles of $\Gamma(j+1+\lambda)$ are also killed (although the $d\lambda$ convergence is now jeopardized by the removal of H^j_λ).

Now, presumably, the integrand of Eq. (12.8) is analytic in λ except for the pole at $\lambda = h$ (the "helicity pole") and we would like to say: shift the contour to the left pick up the helicity pole contribution, and hope the contour integration vanishes as it is shifted off to $Re(\lambda) = -\infty$.

However, in the $C^{(1)}$ cylinder calculation of Section (11) we found that, aside from the helicity pole, the integrand was symmetric in λ, so that if we disallow a shift to the right, we must also disallow a shift to the left.

The situation is analogous to the problem of the Sommerfeld Watson representation which is resolved by the "Mandlestam trick" of replacing the poorly behaved functions P^j with j-decaying functions like Q_j. In Ref. 3 it is suggested that a similar procedure be applied in the present context. Presumably the projections $c^j_{\lambda\mu'}$ are badly behaved as $Re(\lambda) \to \pm\infty$ because the $q^j_{\lambda\mu'}$ are badly behaved. As shown in Appendix A, one can decompose

$$q^j_{\lambda\mu'} = \hat{q}^j_{\lambda\mu'} + \hat{q}^j_{-\lambda,-\mu'} \tag{12.9}$$

where $\hat{q}^j_{\lambda\mu'}$ has poles only on the right, those of $\Gamma(j+1-\lambda)$, and is well behaved as $Re(\lambda) \to -\infty$, as can be shown by applying Watson's Lemma to the integral representation, Eq. (A.18). Defining projections $\hat{\beta}$ and $\hat{c}$ in the obvious way, (12.8) becomes

$$a^j_{\mu\mu'} = \int \frac{d\lambda}{i\pi} H^j_\lambda \left[\hat{\mathcal{B}}^j_{\mu\lambda} + \hat{\mathcal{B}}^j_{-\mu,-\lambda}\right]\left[\hat{c}^j_{\lambda\mu'} + \hat{c}^j_{-\lambda,-\mu'}\right]. \quad (12.10)$$

Now, sadly, one does not really know the large λ behavior of the various projections because, looking at (12.7): (a) infinite range integrations can change asymptotic behavior; and (b) $C_{\lambda\mu'}(\nu)$ *also* depends on λ via the Fourier projection (12.6).

At this point one throws up one's hands and makes a guess. Of the four terms on the right side of (12.10), the fourth term may be harmlessly shifted off to the right where the projections $\hat{\mathcal{B}}^j_{-\mu,-\lambda}$ and $\hat{c}^j_{-\lambda,-\mu'}$ have at least power decay. The two cross terms either cancel, or may also be shifted off to the right, also yielding no contribution to $a^j_{\mu\mu'}$. The first term *must* be shifted to the left, in the direction that $\hat{\mathcal{B}}^j_{\mu\lambda}$ and $\hat{c}^j_{\lambda\mu'}$ are at worst power behaved. This term picks up the helicity pole at $\lambda = h$, giving the final result

$$a^j_{\mu\mu'} = 2H^j_h \cdot \hat{\mathcal{B}}^j_{\mu h} \operatorname{Res}\left[\hat{c}^j_{h\mu'}\right] , \quad (12.11)$$

or, *in terms of the original equation,*

$$A^j_{\mu\mu'} = 2\hat{\mathcal{B}}^j_{\mu h} \cdot \operatorname{Res}\left[\hat{C}^j_{h\mu'}\right] . \quad (12.12)$$

In this paper, we have made the assumption that (12.2) can be replaced with (12.11) or (12.12) in the following locations: (10.41), (11.28), (11.30), (11.35), and (11.38).

APPENDIX A

SOME USEFUL FUNCTIONS

References 9 and 23 describe at length the properties of the generalized Legendre functions $P^j_{\mu\nu}$ and $Q^j_{\mu\nu}$. Here we reproduce only their definitions and basic symmetry properties:

$$P^j_{\mu\nu}(z) = \left(\frac{z-1}{2}\right)^{\frac{1}{2}(\nu-\mu)} \left(\frac{z+1}{2}\right)^{\frac{1}{2}(\nu+\mu)} \frac{F\left(j+1+\nu,\ -j+\nu;\ \nu-\mu+1;\ \frac{1-z}{2}\right)}{\Gamma(\nu-\mu+1)} , \tag{A.1}$$

$$Q^j_{\mu\nu}(z) = \tfrac{1}{2}\,\Gamma(j+1+\mu)\Gamma(j+1-\nu) \left(\frac{z+1}{z-1}\right)^{\frac{1}{2}(\mu+\nu)} \left(\frac{z-1}{2}\right)^{-j-1} \times \frac{F\left(j+1+\mu,\ j+1+\nu;\ 2j+2;\ \frac{2}{1-z}\right)}{\Gamma(2j+2)} , \tag{A.2}$$

$$\begin{aligned} P^j_{\mu\nu} &= P^j_{-\nu,-\mu} , & P^j_{\mu\nu} &= P^{-j-1}_{\mu\nu} , \\ Q^j_{\mu\nu} &= Q^j_{-\nu,-\mu} , & Q^j_{\mu\nu} &= G^j_{\mu\nu}\, Q^j_{\nu\mu} , \end{aligned} \tag{A.3}$$

where

$$G^j_{\mu\nu} = \frac{\Gamma(j+1+\mu)\Gamma(j+1-\nu)}{\Gamma(j+1-\mu)\Gamma(j+1+\nu)} . \tag{A.4}$$

All variables are general complex numbers. Sometimes we make use of the following combination:

$$Q^j_{\mu\mu'}(g) = Q^j_{\mu\mu'}(\xi,\nu,\xi') = e^{-\mu\xi}\, Q^j_{\mu\mu'}(ch\nu)\, e^{-\mu'\xi'} . \tag{A.5}$$

The usual rotation d-functions[32] are given by [± for $\mathrm{Im}(z) \gtrless 0$]

$$d^j_{mm'}(z) = (\pm i)^{m-m'} \left(G^j_{m'm}\right)^{\frac{1}{2}} P^j_{mm'}(z) , \tag{A.6}$$

or

$$d^j_{mm'}(\theta) = \left(G^j_{m',m}\right)^{\frac{1}{2}} \left(+\sin\frac{\theta}{2}\right)^{m'-m} \left(\cos\frac{\theta}{2}\right)^{m'+m}$$

$$\times \frac{F\left(j+1+m',\ -j+m';\ m'-m+1;\ \sin^2\frac{\theta}{2}\right)}{\Gamma(m'-m+1)} \quad . \qquad (A.7)$$

When j,m,m' are all integers or half-integers, one has

$$d^j_{m,-m'}(-z) = (-1)^{j+m}\ d^j_{mm'}(z) \quad ,$$

$$d^j_{mm'}(\theta=\pi) = (-1)^{j-m'}\ \delta_{m,-m'} \quad . \qquad (A.8)$$

As usual, the complete rotation-group matrix element is given by

$$D^j_{mm'}(g) = D^j_{mm'}(\phi,\theta,\phi') = e^{-im\phi}\ d^j_{mm'}(\theta)\ e^{-im'\phi'} \quad . \qquad (A.9)$$

The accompanying second-kind e-functions[33] are defined by

$$e^j_{mm'}(z) = (\pm i)^{m-m'}\ \left(G^j_{m',m}\right)^{\frac{1}{2}}\ \mathcal{E}^j_{mm'}(z) \quad , \qquad (A.10)$$

with

$$E^j_{mm'}(g) = E^j_{mm'}(\mu,\tilde{\xi},\nu) = e^{-im\mu}\ e^j_{mm'}(\mathrm{ch}\tilde{\xi})\ e^{-im'\nu} \ . \qquad (A.11)$$

The d and e functions have these helicity symmetries:

$$(-1)^{m-m'}\ d^j_{mm'} = d^j_{m'm} = d^j_{-m,-m'} \quad ,$$

$$(-1)^{m-m'}\ e^j_{mm'} = e^j_{m'm} = e^j_{-m,-m'} \quad . \qquad (A.12)$$

Sometimes it is convenient to use still another version of the second-kind function,

$$q^j_{\mu\nu}(z) = \frac{\mathcal{E}^j_{\mu\nu}(z)}{\Gamma(j+1+\mu)\Gamma(j+1-\nu)} \quad . \qquad (A.13)$$

This q-function has the advantages of being analytic in j, μ, ν, and

having very simple symmetries:

$$q^j_{\mu\nu} = q^j_{\nu\mu} = q^j_{-\mu-\nu} = q^j_{-\nu-\mu} \quad . \tag{A.14}$$

The asymptotic behavior is given by

$$\lim_{z\to\infty} q^j_{\mu\nu}(z) = \frac{2^j z^{-j-1}}{\Gamma(2j+2)} \quad , \tag{A.15}$$

and the relation between q and e is

$$e^j_{mm'}(z) = (\pm i)^{m-m'} [H^j_{mm'}]^{\frac{1}{2}} q^j_{mm'}(z) \quad , \tag{A.16}$$

where $H^j_{mm'} = H^j_m H^j_{m'}$, and $H^j_\mu = \Gamma(j+1+\mu)\Gamma(j+1-\mu)$. An integral representation for q is given by[34]

$$H^j_\mu \, q^j_{\mu\lambda}(\mathrm{ch}\nu) = \tfrac{1}{2}\int_{-\infty}^{\infty} d\alpha \; f(\alpha) \tag{A.17}$$

where

$$f(\alpha) = e^{-\mu\alpha} (\mathrm{ch}\nu + \mathrm{sh}\nu \, \mathrm{ch}\alpha)^{-j-1} \left[\frac{e^\alpha + \mathrm{th}(\nu/2)}{1 + e^\alpha \mathrm{th}(\nu/2)}\right]^\lambda .$$

Since $q^j_{\mu\lambda}$ is analytic in μ, and has no identical zeros, the function on the left-hand side of Eq. (A.17) has poles going off in both directions in the μ-plane. By decomposing the integral into two parts, it is possible to produce a function which has poles only on the right,

$$H^j_\mu \; \hat{q}^j_{\mu\lambda}(\mathrm{ch}\nu) \equiv \tfrac{1}{2}\int_{-\infty}^{0} d\alpha \; f(\alpha) \quad , \tag{A.18}$$

and is well behaved as $\mathrm{Re}(\mu) \to -\infty$. Comparing (A.18) with (A.17), we find

$$q^j_{\mu\lambda} = \hat{q}^j_{\mu\lambda} + \hat{q}^j_{-\mu,-\lambda} \quad . \tag{A.19}$$

Letting $e^{-\alpha} = \mu$ in (A.18) and using Bateman's[35] formula [5.8.2(5)], $\hat{q}$ may be shown to be a two-variable hypergeometric function

$$H^j_\mu \, \hat{q}^j_{\mu\lambda}(\mathrm{ch}\nu) = \tfrac{1}{2}\,\Gamma(j+1-\mu) \left(\mathrm{ch}\,\frac{\nu}{2}\right)^{-\beta} \left(\mathrm{sh}\,\frac{\nu}{2}\right)^{-\beta'} \times \frac{F_1\left(\alpha,\beta,\beta',\gamma;\ -\mathrm{th}\,\frac{\nu}{2}\ ,-\mathrm{cth}\,\frac{\nu}{2}\right)}{\Gamma(\gamma)} ,$$

where

$$\begin{aligned} \gamma &= \alpha + 1 = j + 2 - \mu , \\ \beta &= j + 1 + \lambda , \\ \beta' &= j + 1 - \lambda . \end{aligned} \tag{A.20}$$

The poles mentioned above are now evident. Our functions q and $\hat{q}$ appear in Ref. 3 as d-functions [no connection to Eq. (A.6) above]:

$$\begin{aligned} H^j_\mu \, q^j_{\mu\mu'} &= \pi d^j_{\mu\mu'} , \\ H^j_\mu \, \hat{q}^j_{\mu\mu'} &= \pi \hat{d}^j_{\mu\mu'} . \end{aligned} \tag{A.21}$$

APPENDIX B
TOLLER M-FUNCTIONS

We present here the definition and some basic properties of the Toller M-functions used in Section (2). Our conventions differ somewhat from Toller's[11] and will be presented in detail elsewhere.[16] As noted earlier, the M-function formalism applies equally well to the physical or ordered S-matrix connected parts.[7]

A Toller M-function representing a 2-to-3 amplitude may be defined as follows:

$$\tilde{M}^{m_1 m_2 m_3 m_4 m_5}(1,a_1;\ 2,a_2;\ 3,a_3;\ 4,a_4;\ 5,a_5)\ A\ \delta^4(\text{ext})$$

$$\equiv \Big([\tilde{p}_5^{\,m_5}|U^\dagger(a_5) \otimes [\tilde{p}_4^{\,m_4}|U^\dagger(a_4) \otimes [\tilde{p}_3^{\,m_3}|U^\dagger(a_3)\Big|$$

$$S_C\Big|U(a_1)|\tilde{p}_1^{\,m_1}\rangle \otimes U(a_2)|\tilde{p}_2^{\,m_2}\rangle\Big)\Big), \qquad (B.1)$$

where

$$\delta^4(\text{ext}) = \delta^4(p_1 + p_2 - p_3 - p_4 - p_5) \quad ,$$

$$p_i = L(a_i)\tilde{p}_i \quad ,$$

$$\tilde{p}_i = (m_i, 0, 0, 0) \ ,$$

and the constant $A = -2\pi icf$ is discussed at the start of Section (4). The $L(a_i)$ are the 4×4 Lorentz matrices which act on 4-vectors, whereas the $U(a_i)$ are unitary operators which represent the elements $(0,a_i)$ of the Poincare group in the single-particle Hilbert space. The states $|\ )$ and $|\ ]$ are defined and discussed in Ref. 13; basically they are linear combinations of the usual $|\ \rangle$ states which are designed to transform as undotted and dotted spinor representations of the Lorentz group. In Eq. (B.1) all helicity (spinor) indices are

of the undotted upper (contravariant) type. Generally there are four kinds of spinor indices: x^{m}, x_{m}, $x^{\dot{m}}$, and $x_{\dot{m}}$, which can be raised (G acts on the left) or lowered (G acts on the right) by an anti-symmetric metric spinor

$$G_{mm'} = G^{mm'} = G_{\dot{m}\dot{m}'} = G^{\dot{m}\dot{m}'} = d^{s}_{mm'}(-\pi) \quad ,$$

where s is the spin of the particle involved. Except on a few occasions we use only the x^{m} and x_{m} index types. However, in order to allow room for explicit spin labels like s, we have adopted the following notation:

$$M_{\underset{\cdot}{m}_1 m_2 m_3 \underset{\cdot}{m}_4 m_5} = M^{s_1 s_2 s_3 s_4 s_5}_{\underset{\cdot}{m}_1 m_2 m_3 \underset{\cdot}{m}_4 m_5} \equiv \tilde{M}^{\ m_2 m_3\ m_5}_{m_1\qquad m_4} \quad .$$

That is, upper indices are written as lower, and lower indices are also written as lower, but with a dot underneath, this dot having no relation to the dots of $x^{\dot{m}}$ and $x_{\dot{m}}$.

The only properties of the Toller M-functions stated here are the invariance and covariance conditions. Other properties such as crossing, TCP, Reggization, etc. will be discussed elsewhere.[16]

The statement of Lorentz invariance in terms of Toller M-functions is very simple:

$$M_{m_1 m_2 m_3 m_4 m_5}(aa_1, aa_2, aa_3, aa_4, aa_5) = M_{m_1 m_2 m_3 m_4 m_5}(a_1, a_2, a_3, a_4, a_5). \tag{B.2}$$

This invariance condition, immediately evident from the definition (B.1) since the operators U(a) are unitary, states that a Toller M-function transforms as a Lorentz scalar. The equation is the same for all types of spinor indices as long as both sides match.

In addition to the above overall invariance condition, the

Toller M-functions have a covariance condition on each particle, e.g.,

$$M_{m_1 m_2 m_3 m_4 m_5}(a_1, a_2, a_3, a_4 g, a_5) = \sum_{m_4' = -s_4}^{s_4} M_{m_1 m_2 m_3 m_4' m_5}(a_1, a_2, a_3, a_4, a_5)\, D^{s_4}_{m_4' m_4}(g) \qquad (B.3)$$

where g is any rotation. The covariance conditions are also obvious from Eq. (B.1), given that the rest states $|\tilde{p}^m)$ transform in the same way under rotations as the usual $|\tilde{p}, m)$ states, while the states $|\tilde{p}^m]$ transform as D^*.

Toller extends his covariance condition to include parity, rotations and parity comprising the complete little group H_+ of a rest 4-vector. This matter is discussed further in Section (3).

To verify the counting of variables, one finds for the general n-point Toller amplitude:

$n \times 6$	each a_i = 6 variables
$-n \times 3$	covariances
-6	invariance
-4	δ^4(ext)
$3n - 10$.	

Finally, the Toller M-functions are related to the momentum-space M-functions (spinorial amplitudes) of Taylor[13] (Stapp[12]) by

$$M_{m_1 m_2 m_3 m_4 m_5}(a_1, a_2, a_3, a_4, a_5) = M'_{m_1' m_2' m_3' m_4' m_5'}(p_1, p_2, p_3, p_4, p_5) \prod_{i=1}^{5} D^{(o,s_i)}_{m_i' m_i}(a_i) \quad , \qquad (B.4)$$

where $D^{(o,s_i)}$ are certain spinor representation functions[13,16] of SL(2,C), and $p_i = L(q_i)\tilde{p}_i$.

Toller has shown that the n-point function $M_{m\ldots}(a\ldots)$ is analytic in $[SL(2,C) \times SL(2,C)]^n \approx$ [complex Lorentz group]^n, the only singularities being reflections via $p_i = L(a_i)\tilde{p}_i$ of the positive-α Landau singularities which are the only singularities in the p_i of the Stapp M-functions (e.g., normal thresholds, poles, triangles); kinematic singularities and constraints are not present. However, when the $M_{m\ldots}(a,\ldots)$ are confined to certain surfaces within $[SL(2,C)^2]^n$, as by using the standard frames of Section (5), these kinematic singularities reappear. This is obvious when one realizes, e.g., that the Toller 4-point function, when written as a function of $g \in O(3)$, is an ordinary helicity amplitude.

APPENDIX C

THE HELICITY POLE EXPANSION FORMULA

In Ref. 9 we have derived a certain "alternative" second-kind generalized-Legendre addition theorem and have proved its convergence. This formula, Eq. (2.11) of Ref. 9, when converted from the $\mathcal{Q}$ to the q functions of Eq. (A.13), becomes

$$e^{-\mu\xi}\, q^{j}_{\mu\mu'}(z)e^{-\mu'\xi'} = -2\sum_{m-j=1}^{\infty} (-1)^{m-j}\, e^{-m\alpha}$$

$$\times \frac{\Gamma(j+1+m)}{\Gamma(-j+m)}\, q^{j}_{m\mu}(z_1)\, q^{j}_{m\mu'}(z_2) \quad . \qquad \text{(C.1)}$$

The relation between variables (ξ,z,ξ') and (z_1,α,z_2) is given by Eqs. (2.8) and (2.9) of Ref. 9. We now make the following set of changes on Eq. (C.1):

$$\begin{aligned} \xi &\to -i\mu & \xi' &\to -i\nu \\ z_1 &\to ishf & z_2 &\to -ishh \\ \mu &\to -m & \mu' &\to -r \\ \alpha &\to \xi & m-j &\to n+1 \\ & & z &\to ch\tilde{\xi} \quad . \end{aligned} \qquad \text{(C.2)}$$

Taking $j \to -j-1$ in the equation which results from these changes leads to

$$e^{-im\mu}\, q^{-j-1}_{mr}(ch\tilde{\xi})e^{-ir\nu} = +2\sum_{n=0}^{\infty} \frac{(-1)^n}{n!}\, \Gamma(-2j+n)$$

$$\times\; e^{\xi(j-n)}\, q^{-j-1}_{j-n,m}(ishf)\, q^{-j-1}_{j-n,r}(-ishh) \;, \qquad \text{(C.3)}$$

which converges when $\mathrm{Re}(\xi) > 0$. However, from the discussion in Appendix E of Ref. 9 it can be shown that $\xi \to -\xi$ is compensated in

Eq. (C.3) by $(\mu,\nu) \to (-\mu,-\nu)$. After making these changes in (C.3), one may then take $(m,r) \to (-m,-r)$ to get an equation identical to (C.3) except that m,r and ξ are replaced by their negatives on the right side, and this new equation converges for $\mathrm{Re}\{\xi\} < 0$. Both equations can be written simultaneously by introducing an index κ,

$$e^{-im\mu}\, q^{-j-1}_{mr}(\mathrm{ch}\tilde{\xi})e^{-ir\nu} = +2\sum_{\kappa=\pm}\theta(\kappa\xi)\sum_{n=0}^{\infty}\frac{(-1)^n}{n!}\,\Gamma(-2j+n)$$

$$\times\; e^{|\xi|(j-n)}\, q^{-j-1}_{j-n,\kappa m}(\mathrm{ish}f)\, q^{-j-1}_{j-n,\kappa r}(-\mathrm{ish}h)\ , \tag{C.4}$$

now valid for $-\infty < \xi < \infty$. As the last step, the q function on the left side of (C.4) is replaced with its e-function equivalent [see Eq. (A.16)] so that, upon defining

$$F^{j}_{n,\kappa m}(f) \equiv \left[\frac{2\Gamma(-2j+n)(-1)^n\, H^{-j-1}_{m}}{n!}\right]^{\frac{1}{2}} q^{-j-1}_{j-n,\kappa m}(\mathrm{ish}f)\ , \tag{C.5}$$

Eq. (C.4) becomes

$$E^{-j-1}_{mr}(\mu,\tilde{\xi},\nu) = E^{-j-1}_{mr}(g) = (+i)^{m-r}\sum_{\kappa}\theta(\kappa\xi)$$

$$\times\sum_{n=0}^{\infty} F^{j}_{n,\kappa m}(f)\; e^{|\xi|(j-n)}\, F^{j}_{n,\kappa r}(-h)\ . \tag{C.6}$$

Setting $j = \alpha$, then putting a subscript "2" on all variables yields the result quoted in Eq. (6.1).

From Eqs. (2.8),(2.9) of Ref. 9 and (C.2) above, the relation between the BCP (Bargmann) variables $(\mu,\tilde{\xi},\nu)$ and the Fig. 15 variables (f,ξ,h) may be found:

$$\mathrm{ch}\tilde{\xi} = \mathrm{sh}f\ \mathrm{sh}h + \mathrm{ch}f\ \mathrm{ch}h\ \mathrm{ch}\xi\ , \tag{C.7}$$

$$e^{+i\mu} = \frac{[\mathrm{sh}h\ \mathrm{ch}f + \mathrm{sh}f\ \mathrm{ch}h\ \mathrm{ch}\xi + i\,\mathrm{ch}h\ \mathrm{sh}\xi]}{\mathrm{sh}\tilde{\xi}} , \tag{C.8}$$

and an expression for $e^{i\nu}$ given by $h \leftrightarrow f$ in Eq. (C.8).

APPENDIX D
THRESHOLD KINEMATICS

In Section (5) we studied the left- and right-side loop equations of Fig. 14 in order to compute the Misheloff rotation. Here we examine instead the lower loop equation of Fig. 14, namely

$$\theta_1^{-1}\nu_1\theta_2 = h_1 q_1 f_2 \quad . \tag{D.1}$$

Analysis of (D.1) in the manner of Appendix E of Ref. 9 shows that

$$\mathrm{ch}f_2 = \sin\theta_1 \frac{\mathrm{sh}\nu_1}{\mathrm{sh}q_1} \ ,$$

$$\mathrm{ch}h_1 = \sin\theta_2 \frac{\mathrm{sh}\nu_1}{\mathrm{sh}q_1} \ ,$$

where, as found in Section (5),

$$\sin\theta_1 = \frac{k_1}{(-t_1)^{\frac{1}{2}}} \tag{5.18}$$

$$\sin\theta_2 = \frac{k_2}{(-t_2)^{\frac{1}{2}}} \tag{5.21}$$

$$\mathrm{sh}q_1 = \frac{[\Delta(s_1,t_1,t_2)]^{\frac{1}{2}}}{2(-t_1)^{\frac{1}{2}}(-t_2)^{\frac{1}{2}}} \tag{5.1}$$

$$\mathrm{sh}\nu_1 = \frac{[\Delta(-k_1^2,-k_2^2,p_1^2)]^{\frac{1}{2}}}{2k_1k_2} \quad . \tag{5.19}$$

Therefore, as $k_1 \to 0$,

$$\mathrm{ch}f_2 = \frac{(p_1^2+k_2^2)}{2(-t_1)^{\frac{1}{2}}\,\mathrm{sh}q_1 k_2} = const.$$

$$\mathrm{ch}h_1 = \frac{(p_1^2+k_2^2)}{2(-t_2)^{\frac{1}{2}}\,\mathrm{sh}q_1 k_1} = \mathrm{const.} \times k_1^{-1} \ ,$$

and as $k_2 \to 0$,

$$chf_2 = \frac{(p_1^2 + k_1^2)}{2shq_1(-t_1)^{\frac{1}{2}}k_2} = \text{const.} \times k_2^{-1}$$

$$chh_1 = \frac{(p_1^2 + k_1^2)}{2shq_1(-t_2)^{\frac{1}{2}}k_1} = \text{const.}$$

These last four equations are used in Section (10) to find the threshold behavior of the kernel.

APPENDIX E

THE CROSS-CHANNEL CONTINUATION

In order to carry the kinematic structure of Fig. 15 from the multiperipheral region to the physical cross channel where $t > 0$, one must analytically continue in the Mandelstam invariants to appropriate new values and perform a complex Lorentz transformation. Our main purpose in describing this procedure is to show that the peculiar group variables appearing in Fig. 15 are simply continuations of the familiar variables one would use to describe the large-t Regge limit.

Consider, instead of Fig. 15, the single ladder rung shown in Fig. 14. The invariants t_i, t_i', t and s_1 are defined by

$$t_1' = (k_1')^2 \qquad t_2' = (k_2')^2$$

$$t_1 = (k_1)^2 \qquad t_2 = (k_2)^2$$

$$Q = (k_1 + k_1') = (k_2 + k_2') \quad , \qquad t = Q^2$$

$$p_1 = (k_2 - k_1) = (k_1' - k_2') \quad , \qquad s_1 = p_1^2 \; .$$

Our goal is to start in the multiperipheral region of the Reggeon process $1 + 2 \to 1' + 2'$, where

$$Q, k_i, k_i' = \text{spacelike}$$

$$\Delta(t, t_i, t_i') = \text{negative}$$

$$p_1 = \text{future timelike}$$

$$\text{central level} = \text{bws frames}$$

and wind up in the cross channel physical region for $2 + 2' \to 1 + 1'$, where

$$Q, k_i, k_i' \;=\; \text{future timelike}$$

$$\Delta(t, t_i, t_i') \;=\; \text{positive}$$

$$p_1 \;=\; \text{spacelike}$$

$$\text{central level} \;=\; \text{cms frames} \quad ,$$

Bws (cms) means brick wall system (center of mass system).

The first step is to continue all the t's. Figure 40 shows a "movie" of this continuation, and Table 1 describes the movie. Including t_2 and t_2' one may conclude that

$$\begin{aligned} (-t_i)^{1/2} &\to i(t_i)^{1/2} \\ (-t_i')^{1/2} &\to i(t_i')^{1/2} \\ (-t)^{1/2} &\to i(t)^{1/2} \\ (+s_1)^{1/2} &\to -i(-s_1)^{1/2} \quad . \end{aligned} \tag{E.1}$$

The branch point detours were chosen in the same way for all variables.

What effect do these changes have on the equations of Section (5)? First of all, Eqs. (5.1) become

$$\begin{aligned} \mathrm{sh}v_1 &= (s_1 + t_1 - t_2) / 2(-s_1)^{1/2}(t_1)^{1/2} \\ \mathrm{sh}\sigma_2 &= (s_2 + t_2 - t_1) / 2(-s_1)^{1/2}(t_2)^{1/2} \\ \mathrm{ch}q_1 &= (t_1 + t_2 - s_1) / 2(t_1)^{1/2}(t_2)^{1/2} \quad , \end{aligned}$$

which are now the correct BCP boost formulas for a 2-timelike/1-spacelike vertex.

More interestingly, Eqs. (5.3) and (5.5) become

$$\cos\theta_{22'} = (t - t_2 - t_2') / 2(t_2)^{\frac{1}{2}}(t_2')^{\frac{1}{2}}$$

$$\cos\theta_{22'} = \mathrm{sh}\sigma_2\ \mathrm{sh}\sigma_2' + \mathrm{ch}\sigma_2\ \mathrm{ch}\sigma_2'\ \cos X_1 \quad .$$

But now $\cos(\theta_{22'}) > 1$ which implies $\cos(X_1) > 1$, so we define

$$\cos\theta_{22'} = \cosh\eta_{22'}$$

$$\cos X_1 = \cosh\tilde{\xi}_1$$

to get

$$\mathrm{ch}\eta_{22'} = (t - t_2 - t_2') / 2(t_2)^{\frac{1}{2}}(t_2')^{\frac{1}{2}}$$

$$\mathrm{ch}\eta_{22'} = \mathrm{sh}\sigma_2\ \mathrm{sh}\sigma_2' + \mathrm{ch}\sigma_2\ \mathrm{ch}\sigma_2'\ \mathrm{ch}\tilde{\xi}_1 \quad .$$

From these expressions one recognizes that $\eta_{22'} = -i\theta_{22'}$ is the usual rapidity boost parameter connecting the rest frames of the (now) incident particles k_2 and k_2', and that $\tilde{\xi}_1 = -iX_1$ is the Regge variable of the $O(2,1)$ link (μ_1,ξ_1,ν_1) on the now spacelike line p_1 (recall that μ_1,ν_1 were set to zero).

To complete the above description, we now construct a figure like Fig. 14 in which the parameters $\eta_{22'} = -i\theta_{22'}$ and $\tilde{\xi}_1 = -iX_1$ appear explicitly as frame-connecting boosts. The frames in this new figure (which we do not draw) form a sort of shadow cabinet for the frames of Fig. 14 in exactly the sense of Fig. 21, except that the s' of Fig. 21 is now replaced by this complex Lorentz transformation

$$T = B_z\left(-i\,\frac{\pi}{2}\right) \quad .$$

The operator T, given in the 4-vector space as

$$T = \begin{bmatrix} 0 & 0 & 0 & -i \\ 0 & 1 & 0 & 0 \\ 0 & 0 & 1 & 0 \\ -i & 0 & 0 & 0 \end{bmatrix} \quad ,$$

turns timelike vectors into spacelike and vice versa so that, e.g., k_2 (in one of its spacelike rest frames)

$$k_2 = (0,0,0,\sqrt{-t_2}) = (0,0,0,i\sqrt{t_2})$$

becomes

$$Tk_2 = (\sqrt{t_2},0,0,0) \equiv \tilde{k}_2 \quad ,$$

where $\tilde{k}_2$ is the vector appearing in the new figure.

According to the rules of Eq. (E.1), the bws versor magnitudes k_i of Eq. (5.7) become

$$k_i = \frac{[\Delta(t,t_i,t_i')]^{\frac{1}{2}}}{2(t)^{\frac{1}{2}}} \quad ,$$

which are now the initial and final channel cms vector magnitudes. The z_i of Eq. (5.13) is now imaginary

$$z_i = \frac{i(t+t_i-t_i')}{2(t)^{\frac{1}{2}}} \equiv iE_i$$

as desired, since k_2 in one of its bws frames

$$k_2 = (0,k_2,0,z_2) = (0,k_2,0,iE_2)$$

becomes

$$\tilde{k}_2 = Tk_2 = (E_2,k_2,0,0) \quad ,$$

which is the normal form of a standard cms 4-vector, except $\tilde{k}_2$ points in the x-direction instead of the z-direction [see Eqs. (5.10) through (5.12)].

Our imaginary new figure can be completed very simply by examining the action of T on the Lorentz generators (see Appendix A of Ref. 9):

$$\begin{array}{ccc} \underline{G} & & \underline{T^{-1}GT} \\ J_x & \longrightarrow & iK_y \\ J_y & \longrightarrow & -iK_x \\ J_z & \longrightarrow & J_z \\ K_x & \longrightarrow & -iJ_y \\ K_y & \longrightarrow & iJ_x \\ K_z & \longrightarrow & K_z \end{array} \qquad (E.2)$$

so that, e.g.,

$$R_y(\theta_{22'}) = e^{-i\theta_{22'}J_y} \to e^{-i\theta_{22'}(-iK_x)} = B_x(-i\theta_{22'}) = B_x(\eta_{22'}) ,$$

lending credence to the above remarks concerning the variables θ and X.

Finally, consider the central level boost parameters ξ_i and ν_i which were so important for the diagonalization of Section (9). According to (E.2), the combination

$$B_y(\xi_1)\ B_x(\nu_1)\ B_y(\xi_2)$$

which surrounds the cluster p_1 in Fig. 15, becomes in the new picture

$$R_x(\phi_1)\ R_y(\beta_1)\ R_x(\phi_2) \quad .$$

where

$$\phi_1 = i\xi_1 \qquad \beta_1 = -i\nu_1 \qquad \phi_2 = i\xi_2 \qquad (E.3)$$

are the Euler angles which characterize this rung in the physical cross channel (β_1 is the scattering angle, $\hat{k}_1\cdot\hat{k}_2 = \cos(\beta_1)$), except that, as already noted, the azimuthal rotations happen to come out being x-rotations instead of z-rotations.

We conclude with a short comment about helicity. Equations (E.3) show that the central level ξ_i boosts of Fig. 15 are the continuations

(to the imaginary axis) of the cross channel azimuthal rotations of the process $2 + 2' \to 1 + 1'$. Therefore, the variable conjugate to ξ_1, namely μ_1, is the analytic continuation of the variable conjugate to ϕ_1, which happens to be the channel helicity $m = m_1 + m_1'$. This justifies our characterization of the μ or λ variables as complex helicities.[36]

APPENDIX F
REATTACHMENT OF THE END-RUNGS

How does one obtain from the solution of Eq. (10.8) the physical discontinuity for particles rather than Reggeons? One way is to continue the Reggeon discontinuity A in the masses, spins, and helicities to the desired physical points. Unfortunately, the 4-Reggeon discontinuity A appearing in Eq. (10.8) is not a standardized Toller M-function (see Fig. 29), so that one may conclude only that the continuation of A will be proportional to the physical amplitude.

An alternative and more conventional way to obtain the physical amplitude is to add the "end-rungs" back onto the multiperipheral ladder. As this involves the special end-rung kinematic configurations which we have omitted from Section (5), we simply state the answer with a few comments. In the energy plane, the end-rungs are reattached according to

$$T_{ab}(g) = \sum_{1,2} \int dg_1 \int dg_2 \; P_a(\phi_1) K_{a1}(\eta_1) \tilde{A}_{12}(\xi_2, \nu_2, \xi_3) K_{2b}(\eta_3) P_b(\phi_3) \; . \tag{F.1}$$

$\tilde{A}$ is the sum of all contributions of the form (10.1), $K_{aI}(\eta_1)$ is the left end-rung, and $P_a(\phi_1)$ is the conventional helicity propagator associated with the (a,a') channel, i.e.,

$$P_a(\phi_1) = e^{-i\phi_1(m_a + m_a')} \; . \tag{F.2}$$

Variable ϕ_1 senses the channel helicity $m = m_a + m_a'$ of the two-particle system (a,a'). The variables η_i appearing in (F.1) are like the ν_i appearing in (10.1), but not quite because the end-rungs are always in a mixed-basis configuration[9] which causes $z = ch(\nu)$ to be twisted into $z = i\, sh(\eta)$.

The diagonalized version of (F.1) is

$$T^{j}_{mm'}(a,b) = \sum_{1,2} \int \frac{d\mu}{i\pi} \int \frac{d\mu'}{i\pi} \; P_m(a) K^{j}_{m\mu}(a,1) P_\mu(1) A^{j}_{\mu\mu'}(1,2)$$

$$\times \; P_{\mu'}(2) K^{j}_{\mu' m'}(2,b) P_{m'}(b) \qquad \text{(F.3)}$$

where

$$P_m(a) = \int_0^{2\pi} \frac{d\phi}{2\pi} \; e^{-im\phi} \; P_a(\phi) = \delta_{m,m_a+m'_a} \quad . \qquad \text{(F.4)}$$

In Fig. 26 we schematize the procedure for reattaching the end-rungs to get the physical amplitude. Once one has solved the integral equation (10.8) for $A^{j}_{\mu\mu'}$ and computes the $T^{j}_{mm'}$ as in (F.3), the absorptive part $T_{mm'}(s,t)$ in the energy plane may be found from the usual inversion of the Jacob-Wick expansion. However, one may return directly to the energy plane without reattaching the end-rungs by means of an expansion formula which is in effect the inverse of the projection (9.4):

$$\tilde{A}_{12}(\xi,\nu,\xi') = \int \frac{d\mu}{i\pi} \int \frac{d\mu'}{i\pi} \int_C \frac{dj(2j+1)}{i}$$

$$\times \; [S^{j}_{\mu'\mu}]^{-1} \; Q^{-j-1}_{-\mu,-\mu'}(g) \; [P_\mu(1) A^{j}_{\mu\mu'}(1,2) P_{\mu'}(2)] \qquad \text{(F.5)}$$

where

$$S^{j}_{\mu\mu'} \equiv \frac{\sin\pi(2j)}{\sin\pi(j-\mu')\sin\pi(j+\mu)} \quad . \qquad \text{(F.6)}$$

The contours in (F.5) run up vertically to the right of all singularities of the integrand However, the j contour C contains, in addition to this vertical piece, clockwise loops around the integers and half-integers to the left of the vertical component. Formula (F.5)

can be derived from a completeness relation [q defined in Eq. (A.13)]

$$\delta(x-y) = +i\int_C dj\,(2j+1)\csc\pi(2j)\; q^{-j-1}_{\mu\nu(x)}\; q^{j}_{\mu\nu}(y)$$

$$(x,y > 1) \qquad \text{(F.7)}$$

which in turn can be derived by the techniques of Ref. 9, Appendix G.1.

Finally, it should be noted that the projection (9.4) is precisely the continuation of the usual Regge theory Froissart-Gribov projection to imaginary and in general complex helicities. Formula (F.5) is (the discontinuity of) the Mandelstam-Sommerfeld-Watson transform, the discrete-helicity version of which was used to get Eq. (2.2) with (2.4).

ACKNOWLEDGMENTS

I would like to thank Evelyn Grant, Deberah Olson, Candy Voelker and Dessa Bucksbaum for invaluable technical assistance in producing this report; my parents for their constant moral support, the U.S. Government and the Lawrence Berkeley Laboratory for paying the bills, Jaime Millan, Jean-Pierre Sursock and Dr. Henry Stapp for useful and interesting discussions, Ms. Georgella Perry for her constant surveillance, and George Weissmann for continually reminding me that there are other aspects of life at least as interesting as particle physics. I wish also to thank the professors of the Berkeley Physics Department for their excellent teaching, in particular Professors Gene Commins and J. D. Jackson, and also Ms. Teri Doizaki for being so nice.

Finally, and most importantly, for an exhilarating educational experience I am indebted beyond measure to Professor Geoffrey F. Chew whose civility, sharp insight, and infinite patience I will try my best to emulate.

The work cited in this Thesis has been done under the auspices of the U.S. Department of Energy.

REFERENCES

1. A. H. Mueller and I. J. Muzinich, Ann. Phys. (N.Y.) 57, 20 (1970).
2. A. H. Mueller and I. J. Muzinich, Ann. Phys. (N.Y.) 57, 500 (1970).
3. M. Ciafaloni, C. DeTar and M. N. Misheloff, Phys. Rev. 188, 2522 (1969).
4. M. Ciafaloni and C. DeTar, Phys. Rev. D1, 2917 (1970).
5. M. Ciafaloni and H. J. Yesian, Phys. Rev. D2, 2500 (1970).
6. N. Mukunda, J. Math. Phys. 14, 2005 (1973);
   J. Pasupathy and B. Radhakrishinan, Ann. Phys. (N.Y.) 83, 186 (1974).
7. G. F. Chew and C. Rosenzweig, Physics Reports (to be published).
8. H. P. Stapp, "Ordered S-Matrix Approach to the Topological Expansion for Baryons and Mesons," LBL-6735 (August 16, 1977).
9. P. Lucht, "The Generalized-Legendre Addition Theorems, SU(1,1), and the Diagonalization of Convolution Equations," LBL-5527 (October 11, 1976).
10. C. Rosenzweig and G. F. Chew, Phys. Letters 58B, 93 (1975);
    G. F. Chew and C. Rosenzweig, Phys. Rev. D12, 3907 (1975).
11. M. Toller, Rivista del Nuovo Cimento 3, 403 (1969);
    M. Toller, Nuovo Cimento 62A, 341 (1969);
    M. Toller, Nuovo Cimento 53A, 671 (1968), Section 2;
    M. Toller, Nuovo Cimento 54A, 295 (1968), Section 10;
    C. Cosenza, A. Sciarrino and M. Toller, Nuovo Cimento 57A, 253 (1968), Section 3.
12. H. P. Stapp, J. Math. Phys. 9, 1548 (1965);
    H. P. Stapp, in H. E. Phys. and Elem. Part., ICTP, Trieste (1965), p.3;
    H. P. Stapp, Phys. Rev. 125, 2139 (1962).

13. J. R. Taylor, J. Math. Phys. 7, 181 (1966).

14. S. Mandelstam, Ann. Phys. (N.Y.) 19, 254 (1962);
N. Drechsler, Nuovo Cimento 53A, 115 (1968);
C. Cronström, Ann. Phys. (N.Y.) 78, 340 (1973).

15. M. Toller, Nuovo Cimento 54A, 295 (1968), equation (6.8).

16. P. Lucht, (in preparation).

17. H. P. Stapp, Phys. Rev. 128, 1503 (1962).

18. M. N. Misheloff, Phys. Rev. 184, 1732 (1969).

19. R. J. Eden, P. V. Landshoff, D. I. Olive and J. C. Polkinghorne, The Analytic S-Matrix (Cambridge University Press, 1966).

20. N. F. Bali, G. F. Chew and A. Pignotti, Phys. Rev. 163, 1572 (1967);
N. F. Bali, G. F. Chew and A. Pignotti, Phys. Rev. Lett. 19, 614 (1967).

21. L. Serterio and M. Toller, Nuovo Cimento 33, 413 (1964), p.418.

22. G. F. Chew, N. L. Goldberger and F. E. Low, Phys. Rev. Lett. 22, 208 (1969).

23. Ya. I. Azimov, Sov. J. Nucl. Phys. 4, 469 (1967).

24. J. D. Jackson and G. E. Hite, Phys. Rev. 169, 1248 (1968).

25. C. Rosenzweig and G. Veneziano, Phys. Letters 52B, 335 (1974).

26. J. R. Freeman and Y. Zarmi, Nucl. Phys. B112, 303 (1976).

27. J. Finkelstein and J. Koplik, Phys. Rev. D14, 1437 (1976).

28. G. F. Chew and A. Pignotti, Phys. Rev. 176, 2112 (1968).

29. J. R. Freeman, Y. Zarmi and G. Veneziano, Nucl. Phys. B210, 477 (1977);
J. R. Freeman and C. E. Jones, "Toward a General Proof of the Planar Pole Bootstrap," Nebraska preprint (to be published in Phys. Rev. D);
J. R. Freeman and C. E. Jones, Criteria for Good FMSR for Reggeon

Amplitudes," Nebraska preprint (to be published in Phys. Rev. D); J. R. Freeman, "The Cylinder ... ," Nebraska preprint (submitted for publication.

30. Ref. 26, page 320.

31. B. Nicolescu, "Evidence for Baryonium Exchange in Medium and High Energy Scattering," to be published in Nucl Phys. B, also published as Lawrence Berkeley Laboratory Report LBL-6701.

32. A. D. Martin and T. D. Spearman, Elementary Particle Theory (North-Holland, Amsterdam, 1970).

33. M. Andrews and G. Gunson, J. Math. Phys. 5, 1391 (1964).

34. Ref. 9, Appendix H.16.

35. Bateman Manuscript Project, A. Erdelyi et al (McGraw-Hill, New York, 1953), Vol. 1.

36. P. Goddard and A. R. White, Nuovo Cimento 1A, 645 (1971); C. E. Jones, F. E. Low and J. E. Young, Phys. Rev. D4, 2358 (1971); C. E. DeTar, C. E. Jones, F. E. Low, J. H. Weis and J. E. Young, Phys. Rev. Lett. 26, 675 (1971); C. E. DeTar and J. H. Weis, Phys. Rev. D4, 3141 (1971); C. E. Jones, F. E. Low, J. E. Young, Phys. Rev. D6, 640 (1972); H. D. I. Abarbanel and A. Schwimmer, Phys. Rev. D6, 3018 (1972); J. H. Weis, Phys. Rev. D6, 2823 (1972).

37. R. C. Brower, C. E. DeTar and J. H. Weis, Physics Reports 14C, 257 (1974).

38. A. R. White, "The Analytic Foundations of Regge Theory," CERN Report TH.2136-CERN (February 16, 1976); Proceedings of the Les Houches Institute of Theoretical Physics (June 1975).

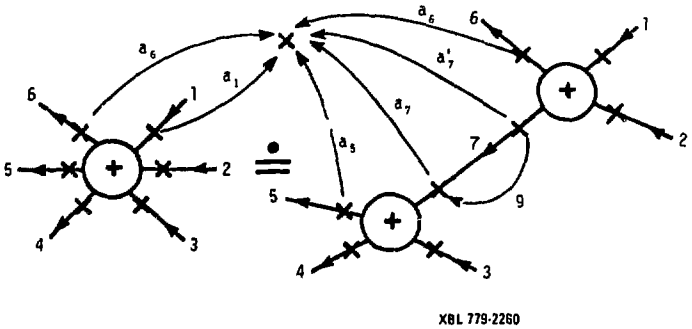

Fig. 1. A particle pole term contained in the 6-point function.

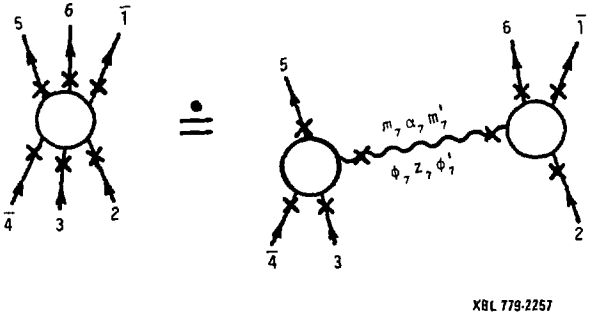

Fig. 2. A Regge pole contribution to the 6-point function.

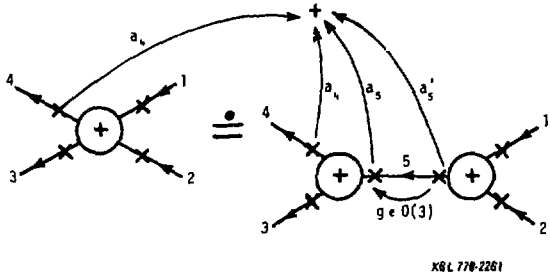

Fig. 3. A particle pole term contained in the 4-point function.

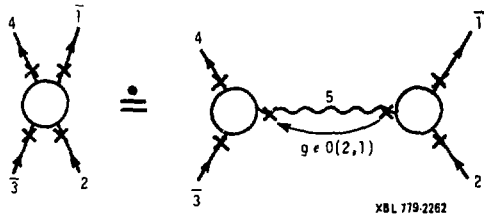

Fig. 4. A Regge pole contribution to the 4-point function.

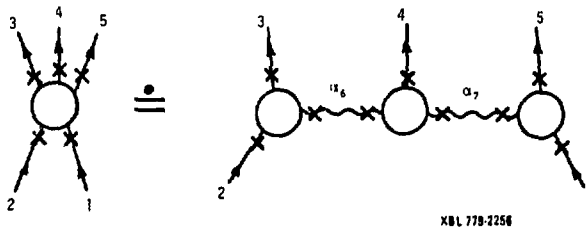

Fig. 5. A double-Regge contribution to the 5-point function.

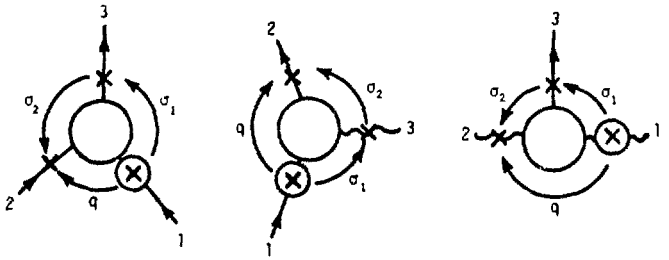

XBL 779-2265

Fig. 6. The standard Toller vertex in no-Regge, single-Regge, and double-Regge configurations.

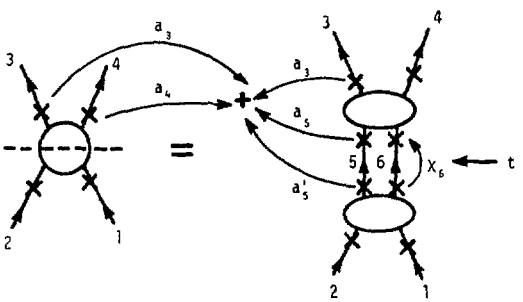

XBL 779-2253

Fig. 7. Elastic unitarity; X_6 is the Misheloff rotation for particle 6.

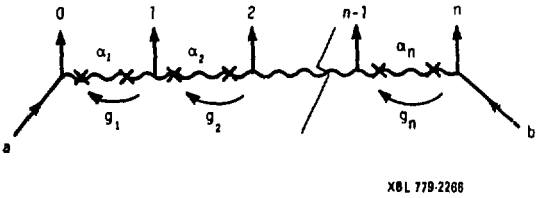

Fig. 8. Multi-Regge production amplitude.

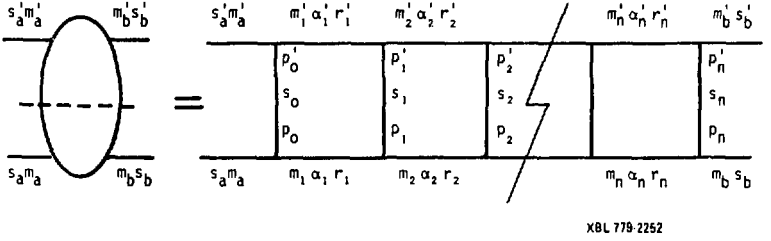

Fig. 9. Spin and helicity labeling for multiperipheral unitarity product. Upper variables are primed versions of lower variables.

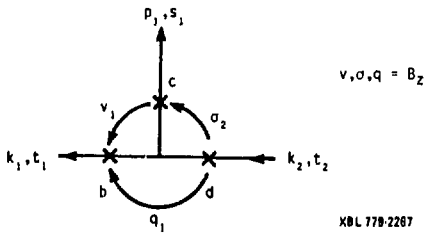

Fig. 10. The BCP frame triad for a production vertex.

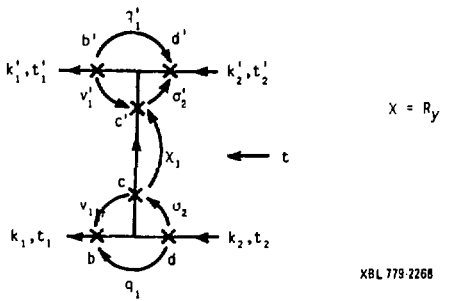

Fig. 11. Two vertices combined to make one rung.

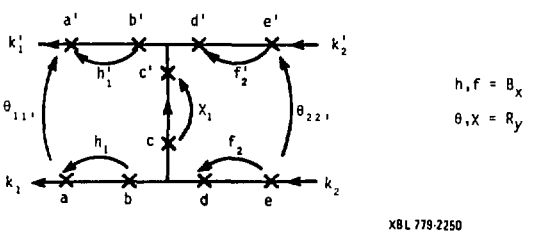

Fig. 12. Four new frames added to the rung.

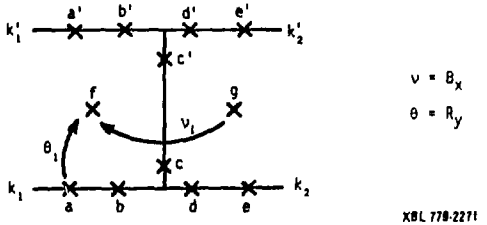

Fig. 13. Central level frames f and g added to the rung.

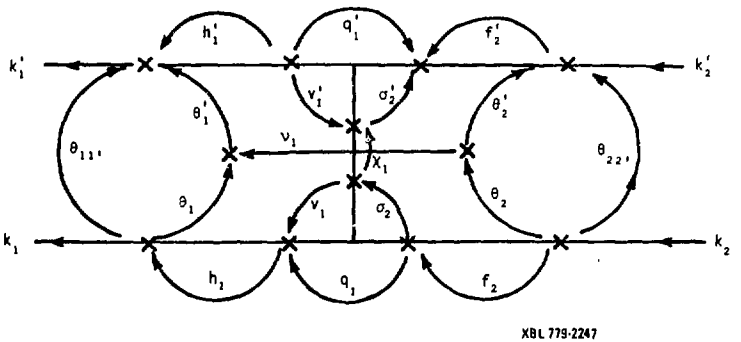

Fig. 14. Complete 12-frame system describing one rung.

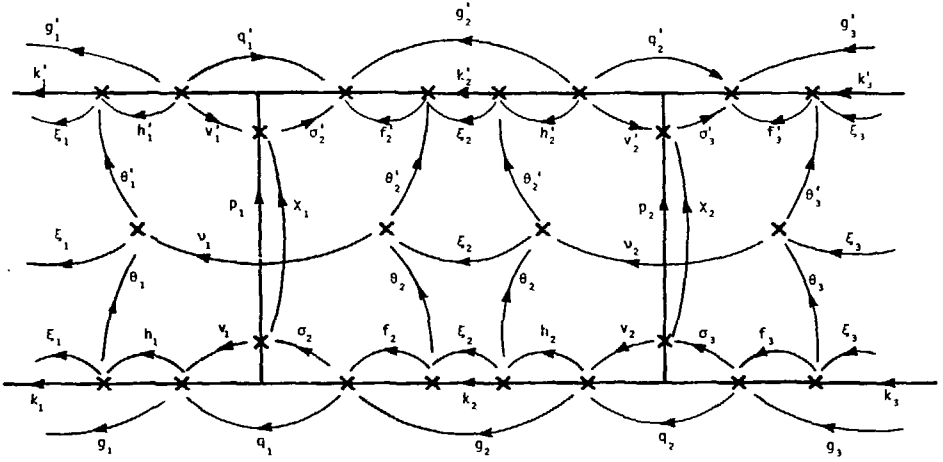

Fig. 15. Multiperipheral ladder formed by combining rungs of Fig. 14. Rungs are separated by y-boosts ξ_i. Legend indicates meaning of labeled parameters. XBL 779-2246

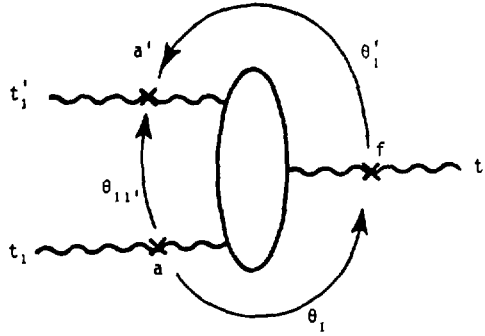

XBL 779-2251

Fig. 16. Standard frames for triple-Regge vertex in its spacelike configuration, $\Delta(t,t_1,t_1') < 0$.

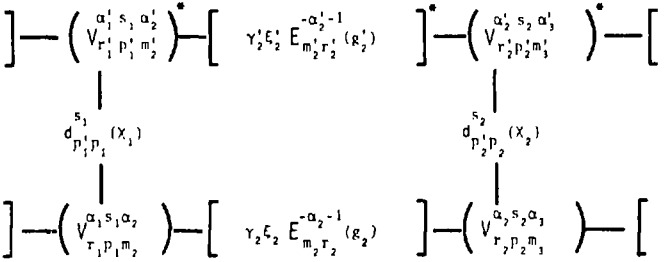

XBL 779-2270

Fig. 17. Functional structure of the multiperipheral ladder, after Mandelstam trick.

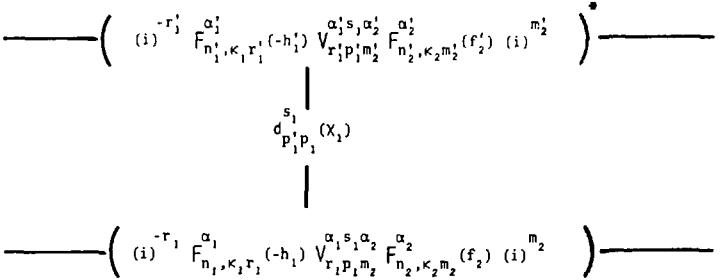

Fig. 18. When E-functions of Fig. 17 are helicity-pole expanded, residual functions F are grouped to the rungs to form kernels. This is the kernel K_{12}. XBL 779-2248

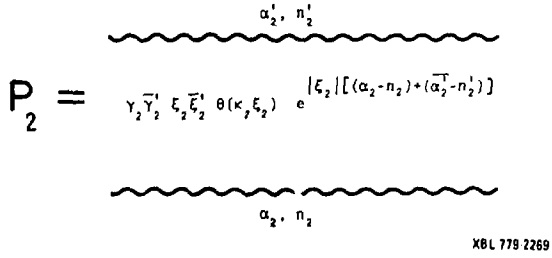

Fig. 19. The helicity-pole propagator.

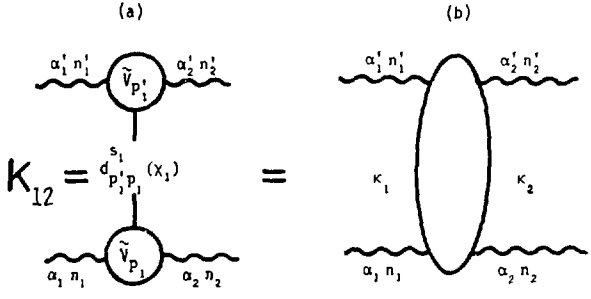

Fig. 20. The kernel.

XBL 779-2249

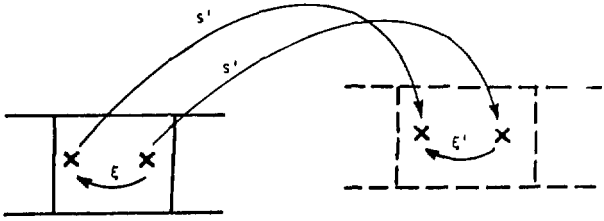

XBL 779-2264

Fig. 21. Dotted figure shows segment of multiperipheral ladder in parity-inverted world. In that world, frames shown are connected by $\xi' = -\xi$.

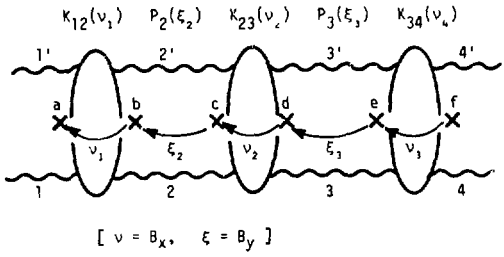

XBL 779-2254

Fig. 22. The 3-particle or 3-cluster contribution to the 4-Reggeon amplitude.

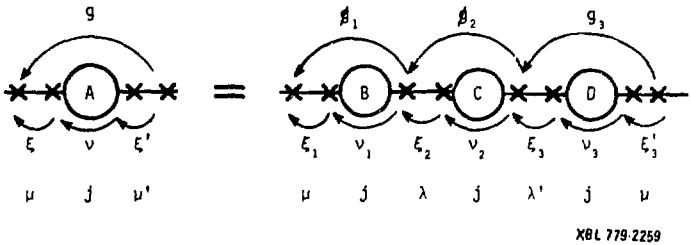

Fig. 23. Functions B, C, D are convoluted to give function A. The variables on the bottom line are conjugate to the boost parameters as shown. The diagonal variable j is angular momentum, variables μ and λ are helicities.

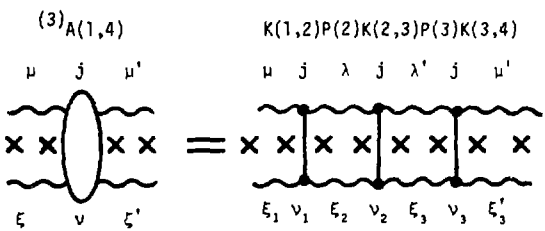

Fig. 24. The 3-particle/cluster contribution to the 4-Reggeon amplitude, in both energy-plane and j-plane.

XBL 779-2258

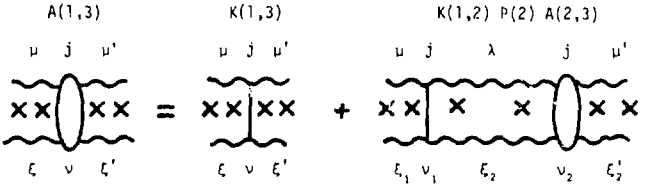

Fig. 25. The bootstrap equation in both energy- and j-planes.

XBL 779-2263

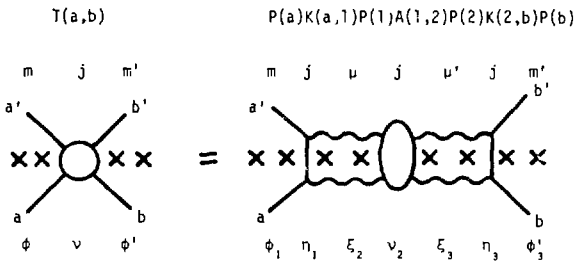

Fig. 26. The reattachment of the end-rungs (see Appendix F).

XBL 779-2255

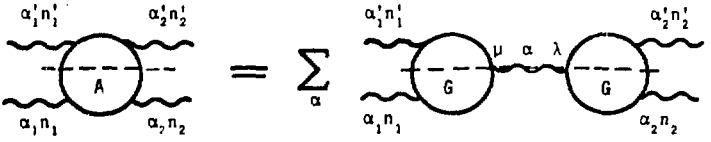

Fig. 27. The Regge-pole expansion of the unnormalized 4-Reggeon ring discontinuity. XBL 779-2312

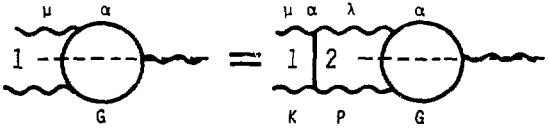

Fig. 28. The vertex bootstrap. XBL 779-2313

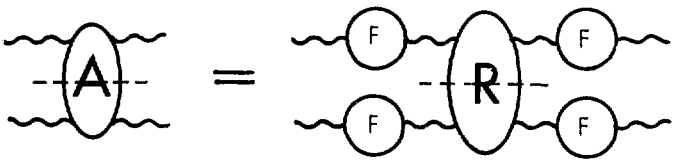

Fig. 29. Relation between discontinuity A and the Toller-normalized 4-Reggeon ring discontinuity. The R-notation is that of Ref. 7. XBL 779-2318

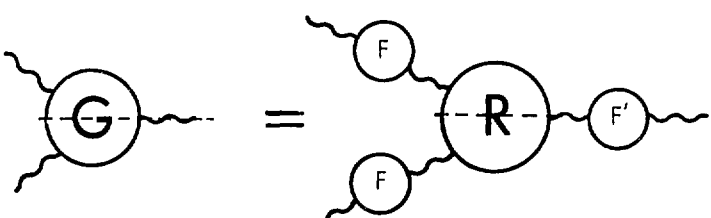

Fig. 30. Relation between the cut vertex G and the Toller-normalized ring function R. XBL 779-2319

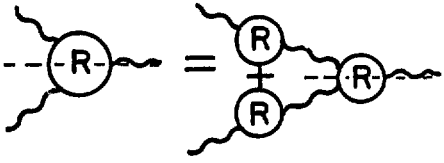

XBL 779-2316

Fig. 31. Highly schematic bootstrap for the 3-Reggeon ordered amplitude.

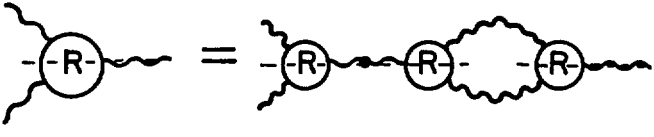

XBL 779-2317

Fig. 32. Vertex bootstrap with "dotted Reggeon" replacing the single produced particle of Fig. 31.

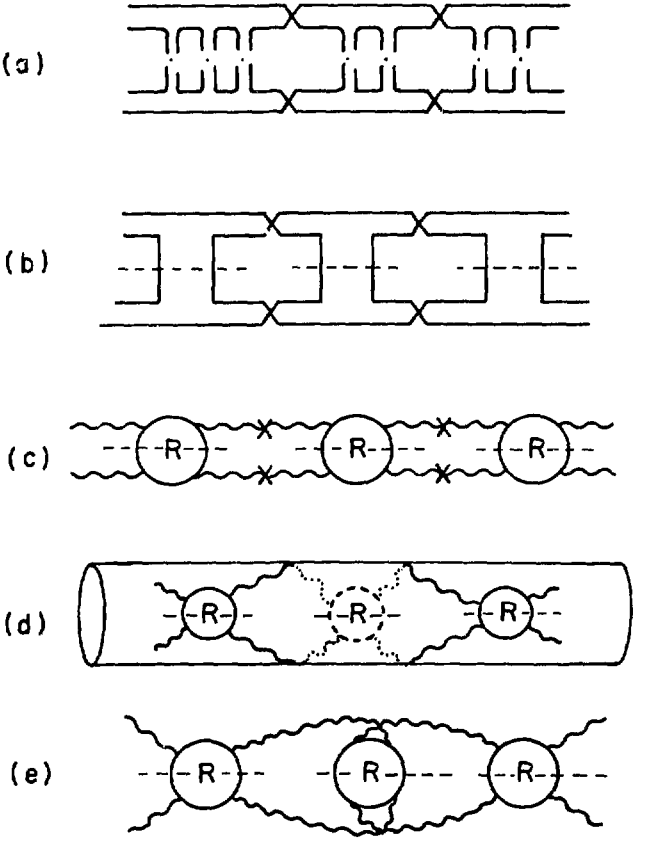

Fig. 33. The two twist-pair contribution to the cylinder in various notations (see text). XBL 779-2314

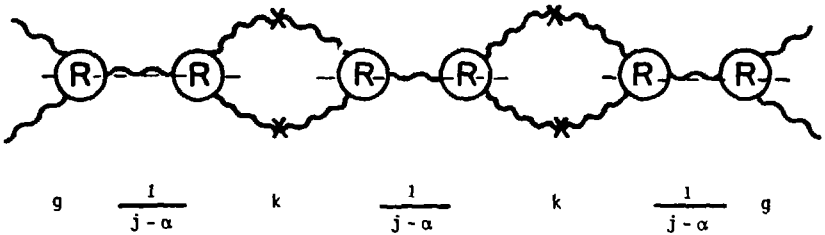

Fig. 34. The diagonalized two twist-pair cylinder term near $j = \alpha$.

XBL 779-2320

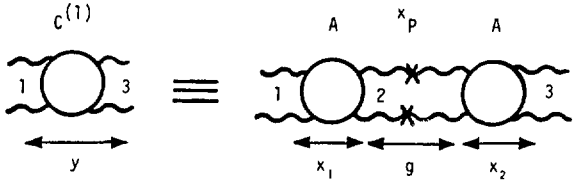

Fig. 35. The $C^{(1)}$ cylinder term in the rapidity model.

XBL 779-2321

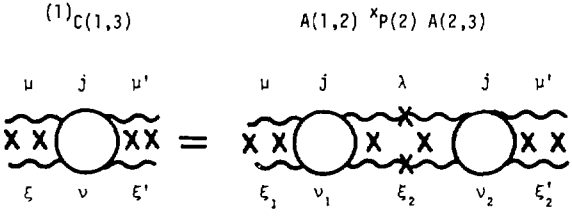

Fig. 36. The $C^{(1)}$ cylinder term with exact kinematics.

XBL 779-2322

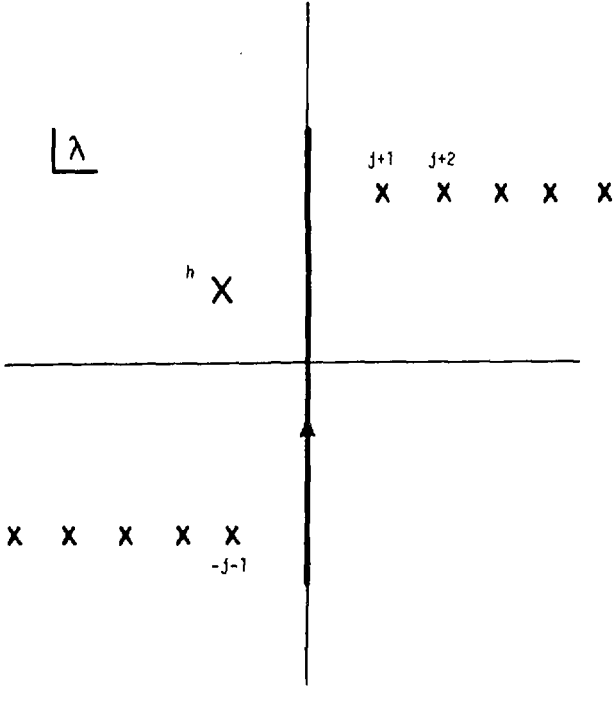

XBL 779-2315

Fig. 37. The complex helicity plane for Eq. (11.26) or (11.27). If helicity pole h is in the right half-plane, contour should be deformed to the right. The other poles may or may not be present depending on nonsense zeros.

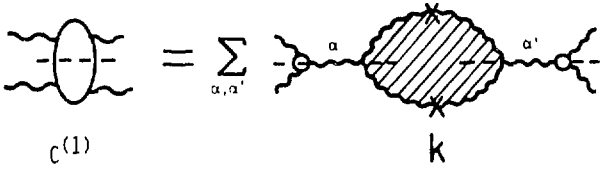

XBL 779-2323

Fig. 38. $C^{(1)}$ may be expressed as a double Regge sum involving the complete twisted Reggeon loop k. The cross-hatch indicates that the loop has been summed over all helicity poles of all possible Reggeon pairs.

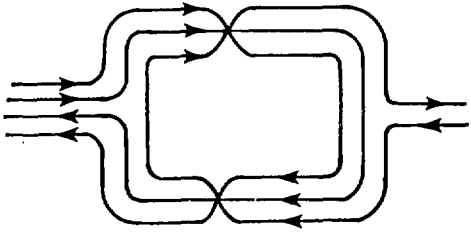

Fig. 39. Quark line structure of twisted Reggeon loop coupling meson to baryonium. Since loop Reggeons are fermions, ϵ-factors in propagator are set to one-half. XBL 779-2324

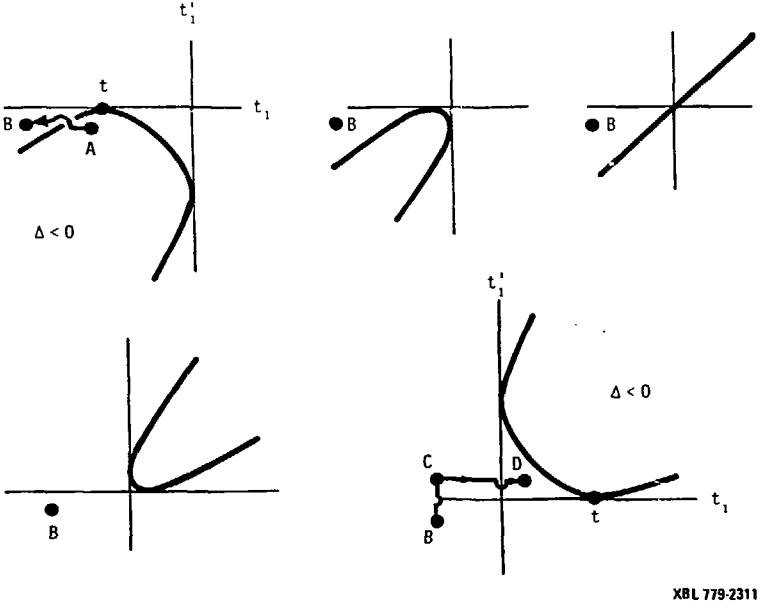

Fig. 40. Five frames of a movie showing the kinematic continuation of a segment of the multiperipheral ladder from the multiperipheral region A where $t < 0$ to the cross channel physical region D where $t > 0$. Heavy line is equation $\Delta(t, t_1, t_1') = 0$. Frames of movie are described in Table 1 (next page).

TABLE 1.

A	$(-t_1)^{\frac{1}{2}}$	$(-t_1')^{\frac{1}{2}}$	$-\Delta(t,t_1,t_1')^{\frac{1}{2}}$	$(-t)^{\frac{1}{2}}$	$(+s_1)^{\frac{1}{2}}$
B	$(-t_1)^{\frac{1}{2}}$	$(-t_1')^{\frac{1}{2}}$	$+i(+\Delta)^{\frac{1}{2}}$	$(-t)^{\frac{1}{2}}$	$(+s_1)^{\frac{1}{2}}$
B	$(-t_1)^{\frac{1}{2}}$	$(-t_1')^{\frac{1}{2}}$	$+i(+\Delta)^{\frac{1}{2}}$	$+i(t)^{\frac{1}{2}}$	$(+s_1)^{\frac{1}{2}}$
C	$(-t_1)^{\frac{1}{2}}$	$+i(t_1')^{\frac{1}{2}}$	$+i(+\Delta)^{\frac{1}{2}}$	$+i(t)^{\frac{1}{2}}$	$(+s_1)^{\frac{1}{2}}$
D	$+i(t_1)^{\frac{1}{2}}$	$+i(t_1')^{\frac{1}{2}}$	$+i(+\Delta)^{\frac{1}{2}}$	$+i(t)^{\frac{1}{2}}$	$(+s_1)^{\frac{1}{2}}$
D	$+i(t_1)^{\frac{1}{2}}$	$+i(t_1')^{\frac{1}{2}}$	$+i(+\Delta)^{\frac{1}{2}}$	$+i(t)^{\frac{1}{2}}$	$-i(-s_1)^{\frac{1}{2}}$